

Inaugural dissertation
for
obtaining the doctoral degree
of the
Combined Faculty of Mathematics, Engineering and Natural
Sciences
of the
Ruprecht-Karls-University
Heidelberg

Presented by
Christina Maria Schlagheck, M.Sc.
born in Wesel, Germany
oral examination: 27.06.2025

Organoid-based studies on the fundamental rules of retinal
tissue self-organization and patterning

Referees: Prof. Dr. Joachim Wittbrodt
Prof. Dr. Steffen Lemke

Abstract

The formation of an organ during development is a complex, highly regulated process that involves a variety of signals provided by the organismal context. In contrast, in culture, stem cells self-organize into 3D tissues, which recapitulate certain aspects of tissue architecture and cell composition seen *in vivo*. These organoids provide a valuable tool for analyzing tissue formation under controlled biochemical or biomechanical conditions.

In this study, I employed retinal organoids grown from blastula cells of medaka fish (*Oryzias latipes*), which recapitulate aspects of early retinal development but fail to undergo the characteristic morphogenesis of the retina to the double-layered cup-shape, nor form cells of the ciliary margin zone (CMZ). Using this system, I investigated how mechanical cues instruct retinal cell type specification in retinal organoids and explored the self-organization of retinal cells in different environments.

Specifically, I examined the effect of mechanically-induced tissue bending on CMZ formation in retinal organoids, revealing that artificial imposition of tissue shape alone was not sufficient to induce CMZ. However, spontaneous emergence of CMZ-tissue within retinal organoids that contain both retinal and non-retinal tissue suggests the importance of tissue boundaries for establishing the different retinal domains.

Further, I investigated the formation of the neural retina (NR) in the medaka organoids. I show that NR cell types differentiate and form clusters of recurring composition and arrangement. Contrasting with the stratified NR formed in the embryo, the cluster formation poses a striking alternative patterning of retinal cells, which is reminiscent of the compound eyes of insects. Supplementation of the organoid culture with Laminin enabled the establishment of NR cell layering.

The results presented in this thesis provide insight into basic patterning processes employed by medaka retinal cells in reduced environments. Considering these features of organoids in future studies may help to understand evolutionary transitions between different organ phenotypes across species.

Zusammenfassung

Bei der Entwicklung von Organen ist eine Vielzahl von Faktoren involviert, die im organismischen Umfeld in komplexer zeitlicher und räumlicher Präzision zusammenspielen. Im Gegensatz dazu bilden Stammzellen in 3D-Kultur selbstständig Gewebe (Organoide), die in ihrer Zellkomposition und Gewebsarchitektur einige Charakteristika von *in vivo* Organen aufweisen, diese jedoch nicht in ihrer Gänze imitieren können. In dieser kontrollierten biochemischen und biomechanischen Umgebung kann die Formierung von den Organ-ähnlichen Geweben iterativ analysiert werden. In dieser Studie verwendete ich Retina-Organoiden aus Medaka (*Oryzias latipes*) Blastulazellen, welche einige Aspekte der frühen Retinaentwicklung durchlaufen, jedoch weder die charakteristische Morphogenese der Retina zu einer doppelschichtigen becherförmigen Struktur, noch Zellen der ciliaren Randzone (CMZ) bilden. Basierend auf diesen Retina-Organoiden untersuchte ich den Einfluss von mechanischen Signalen auf die Spezifizierung von Retinazelltypen, sowie die Selbstorganisation von Retinazellen in verschiedenen Umgebungen.

Ich untersuchte wie mechanisches Biegen des differenzierenden Retinagewebes die Entstehung der CMZ beeinflusst. Die künstliche Änderung der Gewebemorphologie allein war nicht ausreichend für die Bildung der CMZ. Die spontane Entstehung von CMZ-Gewebe in Retina-Organoiden, die sowohl retinales als auch nicht-retinales Gewebe enthalten, weist auf die Bedeutung von Gewebe-Grenzen für die Bildung der verschiedenen Retinadomänen hin.

Weiterhin untersuchte ich die Bildung der neuronalen Retina (NR) in späteren Stadien der Organoidkultur. Ich zeige, dass Zelltypen der NR differenzieren und sich in Clustern formieren. Diese Cluster bestehen aus allen NR-Zelltypen in wiederkehrender Zusammensetzung und Anordnung. Im Gegensatz zum geschichteten Aufbau der NR im Medaka Embryo stellt die Clusterbildung eine herausstechende Alternativorganisation von NR-Zellen dar, die eher an jene der Facettenaugen von Insekten erinnern. Durch die Ergänzung der Organoid-Kultur mit Laminin konnte ich zeigen, dass die Schichtung des Retinagewebes etabliert werden kann.

Die Ergebnisse dieser Arbeit geben Einblick in die Selbstorganisation von Retinazellen in einem nicht-embryonalen Kontext. Die Analyse solcher grundlegenden Mechanismen der Gewebsbildung in Organoiden kann zukünftig wertvolle Erkenntnisse liefern, die potentiell Einblicke in unterschiedliche Organphänotypen im evolutionären Kontext bieten kann.

Table of Contents

Abstract.....	I
Zusammenfassung.....	III
Abbreviations	IX
1 Introduction	1
1.1 Tissue patterning and complexity of factors in organs and organoids	1
1.2 Retinal cell complexity and tissue morphology in embryonic retina and retinal organoids	3
1.2.1 Teleost retina – a multi-layered tissue with stereotypical microarchitecture	3
1.2.2 Medaka retinal organoids – simple architecture and reduced complexity with controllable environment	4
1.3 Retinal tissue morphology and retinal cell layer specification.....	6
1.3.1 Morphogenesis in retinal development.....	6
1.3.2 CMZ establishment in the medaka retina is not yet understood	7
1.3.3 Medaka retinal organoids do not undergo stereotypic retinal morphogenesis	8
1.3.4 Medaka retinal organoids as a model to study the mechanical impact on CMZ formation ..	10
1.4 Neuroretina: cell specification and pattern formation.....	12
1.4.1 Neuroretina establishment in distinct temporal and spatial order.....	12
1.4.2 Neural retina forms as a stratified epithelium	13
1.4.3 Alternative retinal patterning: periodic pattern formation in <i>Drosophila melanogaster</i>	17
1.4.4 Neuroretinal cell differentiation and patterning in the early medaka retinal organoid	18
Aims and objectives.....	19
2. Results	21
2.1 Retinal tissue shape and CMZ fate	21
2.1.1 Tissue morphology and retinal specification – Hypothesis.....	21
2.1.2 Experimental design and tools for tissue bending and cell fate read-out.....	22
2.1.3 Rectangular shape restriction of retinal tissue pre-RPC formation does not induce CMZ formation	28
2.1.4 CMZ formation in organoids cannot be correlated to mechanical impact generated on tissue	30
2.1.5 Increased complexity of mechanical input does not induce CMZ formation	32
2.1.6 Epithelial and curved morphology in spontaneously formed CMZ regions	34
2.1.7 Tissue polarity in day 1-treated organoids differs from day 2 treated organoids	35
2.1.8 Conclusion: tissue bending and CMZ formation.....	37

2.2 Neural retinal differentiation and maturation in organoids.....	38
2.2.1 Retinal ganglion cells are maintained within day 7 retinal organoids	38
2.2.2 Otx2-positive cells display striking cellular patterning beyond day 4.....	40
2.2.3 Retinal cell types are differentiating in late retinal organoids and pattern in clusters.....	42
2.2.4 Retinal clusters have a shared cellular composition and spacing	44
2.2.5 Cells in inter-cluster space undergo apoptosis while clusters are stable over time	47
2.2.6 Retinal clusters show tight association visible in ultrastructure	49
2.2.7 Reorganization of neural retina going along with loss of global tissue polarity	50
2.2.8 Clusters are formed by several unrelated progenitors.....	52
2.2.9 Pattern formation is impacted by Notch-signaling	53
2.2.10 Layering of cell types in presence of Laminin.....	56
2.2.11 Organoids cultured without Matrigel establish non-inverted epithelial tissue regions	58
3. Discussion	61
3.1 Epithelial bending and its impact on CMZ formation	61
3.1.1 Tissue polarization, mechanics, dimension and limitations within the experimental set-up.	62
3.1.2 CMZ morphology and its connection to cell shape	64
3.1.3 Dependency of CMZ induction on tissue-tissue and tissue-ECM interactions	66
3.2 Retinal patterning in late medaka organoids	69
3.2.1 Neuroretinal cell types differentiation in late retinal organoids	69
3.2.2 Retinal cell cluster as a minimal structural unit of retinal organization	71
3.2.3 Mechanism of retinal cluster formation	72
3.2.4 Higher-level of tissue organization in the organoids.....	76
3.2.4 Impact of Laminin on retinal patterning	77
3.2.5 Patterning transition from an array of clusters to a continuous epithelium as an evolutionary innovation.....	79
3.2.5 Organoids as a tool to study conservation, basic patterning principles and developmental robustness	80
4. Conclusion.....	83
5. Materials and Methods.....	85
5.1 Materials	85
5.1.1 Organisms.....	85
5.1.2 Consumables	85
5.1.3 Chemicals, reagents and kits.....	87
5.1.4 Solutions and buffers	90
5.1.5 Antibodies	91
5.1.6 Equipment and Instruments.....	92
5.1.7 Software	94

5.2 Methods	95
5.2.1 Fish husbandry	95
5.2.2 Medaka retinal organoid generation	95
5.2.3 Stamp and mould fabrication	96
5.2.4 Whole mount staining of medaka organoids and medaka embryos.....	97
5.2.5 Cryosectioning	97
5.2.6 Light microscopy imaging and image processing	98
5.2.8 Electron microscopy Sample Preparation and Ultramicrotomy	100
5.2.9 Electron Microscopy and Image Processing	100
6. Appendix	101
References	112
Publications during PhD	129
Acknowledgements	131
Declaration	133
List of figures	135
List of tables	139

Abbreviations

AB	antibody
AC	amacrine cells
Ath5	ADP-ribosyltransferase 5
Atoh7	<i>Atonal BHLH Transcription Factor 7</i>
BMP	bone morphogenic protein
BP	bipolar cell
CMZ	ciliary margin zone
Cndp1	<i>Carnosine Dipeptidase 1</i>
CO₂	carbon dioxide
°C	degree Celsius
DAPI	4',6-Diamidino-2-Phenyindole, Dilactate
DAPT	N-[N-(3,5-difluorophenacetyl)-l-alanyl]-s-phenylglycine-butyl ester
dpf	days post fertilization
DMSO	Dimethyl sulfoxide
Dpp	decapentaplegic
Drosophila	<i>Drosophila melanogaster</i>
ECM	extracellular matrix
EGFR	epidermal growth factor receptor
ERM	embryo rearing medium
FBS	fetal bovine serum
FGF	fibroblast growth factor
g	gravitational force equivalent
GFP	green fluorescent protein
HC	horizontal cell
Hh	hedgehog
IGF	insulin growth factor
IPL	inner plexiform layer
INL	inner nuclear layer

KDE	kernel density estimate
mCherry	monomeric red fluorescent protein
medaka	<i>Oryzias latipes</i>
MG	Müller glia cell
n	sample number
NR	neural retina
OC	optic cup
o.n.	over night
ONL	outer nuclear layer
OPL	outer plexiform layer
OS	outer segments
OV	optic vesicle
Otx2	Orthodenticle homeobox 2
PBS	phosphate-buffered saline
P/S	penicillin-streptomycin
PFA	paraformaldehyde
PKC-alpha	protein kinase C alpha
PKC-zeta	protein kinase C zeta
Prox1	Prospero homeobox protein 1
PTW	phosphate-buffered saline with tween
RGC	retinal ganglion cell
RGL	retinal ganglion cell layer
RPC	retinal progenitor cell
RSC	retinal stem cell
PR	photoreceptor cell
r.t.	room temperature
RPE	retinal pigmented epithelium
Rx(2)	Retinal homeobox transcription factor (2)
Shh	sonic hedgehog

TUNEL	terminal deoxynucleotidyl transferase dUTP nick end labeling
ubi	ubiquitous
UHD	Heidelberg University
v.	version
wt	wild type
zebrafish	Danio rerio
2D	two dimensional
3D	three dimensional

1 Introduction

1.1 Tissue patterning and complexity of factors in organs and organoids

Organoids have drastically transformed the way we study organ development and function (reviewed in Tang et al., 2022; reviewed in Lan et al., 2024; reviewed in Zhao and Yan, 2024; reviewed in Chakrabarty et al., 2024). Immediate, direct accessibility of the developing tissue, as well as control over external biochemical or biomechanical cues facilitate targeted interventions and continuous monitoring. However, the growth of tissue in isolation, including the absence functionally connected tissues, vascularization and the immune system, poses fundamental challenges for the aspired applications. While significant advances have been made in optimizing culture protocols for organoid generation, gaps in the current understanding about essential developmental cues hinder the ability to fully emulate the tissue architecture and cell type diversity of native organs (reviewed in Pan et al., 2020; Jensen and Little, 2023; O'Hara Wright et al., 2020; among others).

In the naturally evolved, embryonic context, a variety of physical and biochemical signals instruct cell type induction in space and time, such as gradients of signaling molecules, direct contact of neighboring cells and tissues and mechanical cues resulting from tissue morphogenesis (reviewed in Heller and Fuchs, 2015, reviewed in Sutlive et al., 2022, among others). Understanding how individual factors affect tissue formation in living organisms can be difficult, especially when addressing mechanical forces and the three-dimensional (3D) context of tissues within an organ and relative to other organs. Interdependence of different cues and the limited accessibility for precise experimental mechanical intervention within organisms complicate experimental procedures. In *in vitro* culture systems, however, iterative approaches probing for the effect of single cues or combinations of signals can be done more easily. At the same time, insights gained in respect to the requirement of signals can help to improve culture conditions for the tissue of interest. Yet, it still remains an open question to which extent organoid cultures accurately reflect *in vivo* biology and how closely they can replicate the composition and structure of organs.

Nevertheless, tissues grown in organoids reflect the extent to which cells of a given tissue-type can organize autonomously. Studying the tissues emerging can therefore provide valuable insights into fundamental biological processes employed by cells to govern self-organization. Organoid systems can hence complement our understanding of the autonomy of tissue organization and unveil alternative pathways employed based on a given environment.

While fundamental principles of organ development are conserved across species, each species has evolved distinct strategies for patterning and structuring organs. The retina, as the photosensitive tissue enabling vision, has evolved in many different ways (reviewed in Schwab, 2018). It shares basic functional and patterning similarities with retinal tissues across organisms. Retinal organoids, forming retina-like structures, have been established from mammalian and medaka fish (*Oryzias latipes*) cells (Eiraku, 2011, Nakano, 2012, Zilova et al., 2021). While mammalian culture systems have achieved remarkable progress in replicating retinal tissue structure and cellular composition, several limitations remain. These include the variability between individual organoids, incomplete functional connections between cells and, and light sensitivity (O'Hara Wright et al., 2020, Cowan et al. 2020, among others). The medaka retinal organoid system, has so far been less explored. Early stages of retinal development were characterized and the successful establishment of retina-fated progenitor cells and the onset of neuroretinal (NR) cell differentiation were shown (Zilova et al., 2021). In terms of tissue morphology and cell type diversity, the medaka retinal organoids appear to obtain a reduced complexity compared to the *in vivo* retina, and pose the possibility to study signals for retinal pattern formation and cell type induction. Its fast developmental speed as in the embryo, and stable tissue formation make it an attractive model for exploring the mechanism that govern retinal patterning (Zilova et al., 2021).

Within the study, I aim to explore basic principles that are involved in the patterning process in retinal organoid tissue. In the following, I will focus on the patterning processes and instructiveness of cues found in medaka fish retinal organoids. I will address the significance of morpho-mechanical processes for the establishment of the ciliary marginal zone (CMZ) and the patterning of the neural retina (NR) in the retinal organoid system.

1.2 Retinal cell complexity and tissue morphology in embryonic retina and retinal organoids

1.2.1 Teleost retina – a multi-layered tissue with stereotypical microarchitecture

The retina of teleosts shares many features with other vertebrate retinæ. It assumes a cup-shaped tissue morphology with distinct, stereotypic organization of retinal cell types (Figure 1.1). The neural retina (NR), which is containing the neural cell types of the retina, is forming the central, most distal portion of the cup-shaped tissue. The NR is surrounded by a single layer of stretched, pigmented cells called the retinal pigmented epithelium (RPE). The RPE provides nutritional support and stability to the NR (reviewed in Wang et al., 2023). The peripheral interface of these two layers converges at the rim of the cup and is harboring a specialized niche of cells termed the ciliary marginal zone (CMZ). Within teleosts, retinal stem cells (RSCs) and retinal progenitor cells (RPCs) are harbored in the CMZ and give rise to differentiated retinal cell types in the post-embryonic retina (Raymond et al., 2006, Miles and Tropepe, 2021, Centanin et al., 2011).

The NR consists of three major (nuclear) cell layers containing all neural cell types vital for the detection, computation and propagation of visual information. The outer nuclear layer (ONL) hosts cone and rod photoreceptor cells (PRs) shaping the light sensitive cell layer of the retina. Within the inner nuclear (INL) layer, the nuclei of horizontal cells (HC), bipolar cells (BP), and amacrine cells are positioned in a distinct layered arrangement. The third layer, which is positioned closest to the lens, harbors retinal ganglion cells (RGC) whose axons are forming the optic nerve projecting to the optic tectum in the brain (Figure 1.1). The synaptic connections between adjacent cell soma layers are established in plexiform layers, the outer plexiform layer (OPL) and the inner plexiform layer (IPL). Synapses between PR, BP and HC are located in the OPL. The IPL contains connections between BP, AC and RGCs. Visual information is received, converted and processed by the PR and propagated to the cells of the INL. HC, BP and AC compute the information and transmit to the RGCs, which finally send the information towards the brain. This stereotypical composition is important for the retinal signaling axis (reviewed in Schiller, 2010; Kitambi and Malicki, 2008; Meister

and Berry, 1999). The Müller glia (MG), a glial cell type, stretch through the cell layers, providing structural support to the retina. Moreover, MG are important for neuronal cell maintenance, synaptogenesis and regeneration (Bernardos et al., 2007; Lust and Wittbrodt, 2018; Tworig and Feller, 2022). In medaka, the retina is forming within 5 days of development, and maturing to functionality until the hatching of the fish at day 9 (Kitambi and Malicki, 2008).

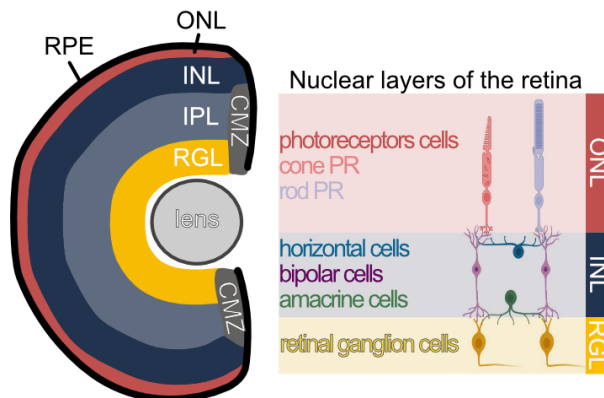


Figure 1.1: Medaka retinal architecture. Scheme of the cup-shaped teleost retina with distinct cellular arrangement and schematic display of cellular morphology and layering in the NR. NR composed of ONL, OPL, INL, IPL, and RGL containing neuroretinal cell types. RPE surrounding the NR adjacent to IPL and CMZ positioned in the distal hinge of retinal cup. Lens positioned adjacent to RGL. RPE – retinal pigmented epithelium, CMZ- ciliary marginal zone, NR – neural retina, ONL – outer nuclear layer, INL – inner nuclear layer, IPL – inner plexiform layer, RGL – retinal ganglion cell layer, PR – photoreceptor

1.2.2 Medaka retinal organoids – simple architecture and reduced complexity with controllable environment

Medaka retinal organoids can be formed from aggregates of primary pluripotent embryonic stem cells isolated from blastula stage (stage 11) Medaka embryos (Iwamatsu, 2004; Zilova et al., 2021). Isolated blastula cells aggregate and under specific culture conditions differentiate into retinal tissue. The developmental progress of the tissue grown under *in vitro* conditions reflects the developmental speed of the medaka embryo.

The retinal organoids show a more basic tissue morphology and reduced cell type diversity as compared to the embryonic retina. In minimal input conditions, exclusively cells contributing to the NR are formed along with non-retinal cells in the central

organoid. RPE cells and RSCs, inhabiting the CMZ, are not established spontaneously alongside to the differentiating NR cells. To date, medaka retinal organoids were characterized until early stages of retinal development and differentiation (day 4), and therefore the successful generation of the full NR cell type diversity has not been reported yet.

Structurally, the retinal organoid obtains a spherical shape after aggregation and maintains this spherical shape throughout the differentiation process. Retinal tissue is covering the circumference of the organoid. The retinal cell types arrange in the outer layer of the organoid with RGCs being at the circumference and BP/PR precursors more medially in the organoid. The HC precursors position in-between the PR and BP precursors. This layering appears to be inverted in comparison to the embryonic retina and to what was reported for retinal organoids from mouse and human (Zilova et al., 2021; Eiraku et al., 2011; Nakano et al., 2012).

Occasionally, non-retinal tissue emerges on the organoid surface next to retinal tissue, which can impact the tissue complexity and morphology of the organoid. The induction of NR tissue, however, is the main structure forming under stable culture conditions. Short developmental time frames, as well as the accessibility of the tissue pose the retinal organoids from medaka cells as a valuable platform to address cell fate decisions and pattern formation of retinal cells in *in vitro* conditions. The availability and usage of genetically encoded reporter systems is an advantage for studying cell differentiation and diversity. From the embryonic offspring of fish lines carrying such reporter, blastula cells can be used for organoid generation and cell identities can be followed up on in real time in the retinal organoid.

The reduced Incomplete cell type composition compared to the embryonic retina raises questions about the necessary cues to achieve the generation of the missing cell types. Is the simple tissue morphology of the organoid as a sphere connected to the absence of CMZ and RPE? Can the retinal organoids establish a mature NR in later stages and does it obtain an inverted cell layering as suggested by the day 4 organoid?

In the following, I will summarize the literature on the establishment of the cup-shaped retina in connection with the formation of the CMZ (chapter 1.3). Subsequently, I will describe the process of NR patterning described for vertebrates and an invertebrate (*Drosophila melanogaster*) to introduce different paths of retinal pattern formation (chapter 1.4).

1.3 Retinal tissue morphology and retinal cell layer specification

1.3.1 Morphogenesis in retinal development

The development of the vertebrate retina involves complex morphological changes leading to the formation of a cup-shaped retina harboring RPE, NR, and CMZ. In teleosts, like Medaka and zebrafish (*Danio rerio*), eye development begins with the establishment of the eye field in the anterior neural plate. The morphogenesis of the retina commences with the evagination of the optic vesicle (OV) (Heermann et al., 2015; Kwan et al., 2012). The cells within the OV form a pseudostratified epithelium (neuroepithelium) (Kitambi and Malicki, 2008). The neuroepithelium is build up by tightly packed columnar cells with clear membrane polarity. The apical side of the epithelium is proximal, while the basal surface is distal (Herder et al., 2013).

Invagination of the distal OV leads to a cup-shaped structure, called optic cup (OC) (Figure 1.2). During the formation of the OC, neuroepithelial cells migrate from the proximal layer of the OC to the distal layer. This process termed as 'neuroepithelial flow' positions cells from the proximal OC in the future NR and CMZ areas (Heermann et al., 2015; Nicolás-Pérez et al., 2016; Sidhaye and Norden, 2017; Sokolova, 2019). In the double-layered OC, multipotent retinal progenitor cells (RPCs) pose the common pool of cells giving rise to all the retinal cell types of the NR, CMZ and RPE (Turner and Cepko, 1987; Holt et al., 1988; Wetts and Fraser, 1988). Within the cup-shaped tissue, the retinal cell layers are establishing in their distinct locations and subsequent proliferation and cell shape adaptation is leading to the final shape of the retina (Figure 1.2).

The Inward folding of the tissue during OC formation is accompanied by morphogenetic changes on the cellular level. Progenitors in the central part of the OC are reducing the basal cell surface by actomyosin constriction while the apical side expands (Martinez-Morales et al., 2009; Nicolas-Perez et al., 2016; Sidhaye and Norden, 2017; Bogdanovic et al., 2012). At the same time, cells at the future hinge position between NR and RPE are constricting (Sokolova et al., 2023) (Figure 1.2). These cellular constrictions are likely involved in enabling the tissue bending to form the OC (Eiraku et al., 2011; Eiraku et al., 2012; Okuda et al., 2018). Mechanical forces within OC formation are further generated by NR proliferation causing tissue tension,

the flattening of RPE cells and the differential growth rates of the retinal tissue layers (Moreno-Marmol et al., 2021). Studies performed on mouse retinal organoids (Eiraku et al., 2011; Eiraku et al., 2012; Okuda et al., 2018) triggered a relaxation-expansion hypothesis, which is based on the rigidity of RPE and the flexibility of NR tissue along with the constriction at their rim to support epithelial folding during OC formation. How the mechanical impact within OC formation is instructing the retinal cell layer specification in medaka remains to be explored.

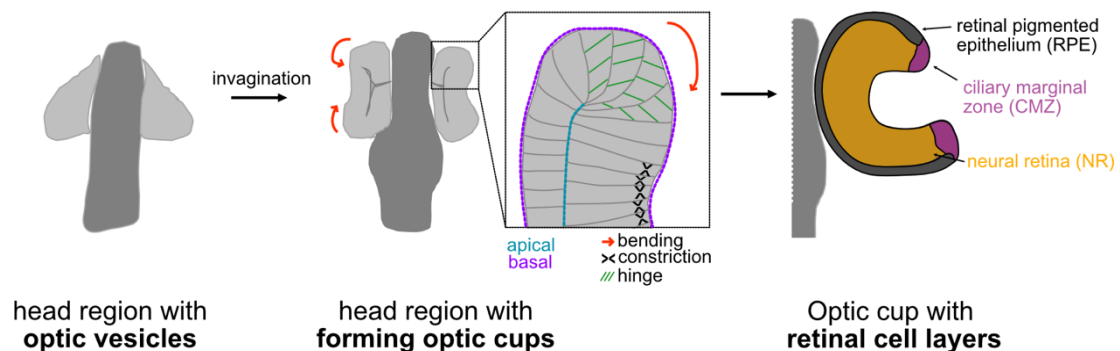


Figure 1.2: Morphogenetic steps in retinal development. Depiction of morphological changes during retinal development of Medaka. Optic vesicles (Ovs) contain a neuroepithelium with retina committed cells. Invagination of the OV leads to optic cup (OC) formation. Inward bending (red arrow) of the distal OV is enabled by cell shape changes in the hinge region (green dashes) and basal constriction (black arrow heads) in the central OC. Apical side of the tissue marked in blue, basal side marked in purple. Within forming OC, retinal progenitor cells are established. Once OC is fully formed, three main retinal cell layers are specified, neural retina (NR), ciliary margin zone (CMZ) and retinal pigmented epithelium (RPE).

1.3.2 CMZ establishment in the medaka retina is not yet understood

Descriptions of the OC formation could not yet explain the establishment of the CMZ in the prominent hinge region between RPE and NR. The epithelial flow during OC formation leads to the positioning of cells, originating from the dorsal OC, in the region that will later form the CMZ. The specification of the RSCs in the CMZ was proposed to not be pre-defined but coinciding with the retinal morphogenesis, due to onset of the RSC marker *cndp1* expression during OC formation (Sokolova, 2023). The plasticity of RPCs enabling them to contribute to any cell type of the retina, suggests a connection of their specification towards RSC fate and their position within the OC at the retinal hinge region. This could be connected to several aspects accompanying

OC formation, as the mechanical impact of tissue bending, the ECM surrounding the niche, interaction with neighboring tissues or potential signaling cues. To date, CMZ induction could not yet be connected to a signaling cue. From studies in mouse, however, Wnt/ β -catenin signaling poses as a candidate as its activation in retinal cells was connected to an expansion of the ciliary margin (Liu, et al., 2007). Generally, the balance of the activity of the FGF (fibroblast growth factor) family and Wnt/ β -catenin signaling is important for the specification of the NR and RPE in mouse (reviewed in Heavner and Pevny, 2012). Due to the position of the ciliary margin between the NR and RPE, the impact of Wnt/ β -catenin signalling could therefore be relevant for its specification. Dissecting and identifying the individual significance of differential cues on CMZ establishment is challenging due to the complex interplay of factors acting on the tissue simultaneously within the embryonic context.

The Intricate morphological architecture of the retina and the *in vitro* OC formation in mouse and human retinal organoids (Eiraku, 2011; Nakano, 2012) suggests a tight link between the morphological event and cell type induction. Mechanical cues playing a role in OC formation are difficult to dissect in the embryonic context and reported changes to morphogenetic processes usually required the mutation of genes, which ultimately impacted on more than just the mechanical aspect. To specifically manipulate mechanical cues, the retinal organoid system poses as a suitable platform.

1.3.3 Medaka retinal organoids do not undergo stereotypic retinal morphogenesis

In medaka retinal organoids no substantial morphogenetic events, similar to those observed in embryonic medaka retinae, can be observed. After seeding of the isolated pluripotent embryonic stem cells (day 0), the cells form a spherical aggregate (Figure 1.3A, B). Within a media void of substantial signaling factors and low concentration of serum-like solutions (Differentiation media), the aggregated cells commit to retinal fate by day 1. To induce epithelialization, the ECM supplement Matrigel is added to the organoid culture. On the second day after seeding, the organoid contains multipotent RPCs organized in a continuous epithelium in the outermost layers of the organoid. The organized rim structure is phenotypically visible by a more transparent tissue on

the edge of the organoids by day 2 of culture (Figure 1.3B). The RPCs are hereafter giving rise to RGC precursors by day 3, and precursor cells for BP, PR and HC (Zilova et al., 2021). The retinal tissue does not form Ovs or Ocs as the embryonic retinal tissue under standard conditions.

This is contrasting the formation of OC-like structures in mouse and human organoid cultures (Eiraku et al, 2011; Nakano et al., 2012). In these systems, the formation of RPE, ciliary margin and NR were seen alongside the adaption of specific cell shapes: columnar cells in the RPE, wedge shaped cells in the CMZ, and pseudo-stratified epithelium in NR (Eiraku, 2011; Nakano, 2012). This was achieved in the absence of lens and surface ectoderm (Hasegawa et al., 2016). The differentiation protocol for medaka retinal organoid culture mimics that of the mouse retinal organoid culture, yet it was adapted to the species-specific developmental timing (Eiraku et al, 2011). However, the culturing conditions suitable for mouse retinal organoids do neither support OC morphogenesis, nor differentiation of RPE and a CMZ in the medaka retinal organoid system. The medaka retinal organoid system appears to require additional cues for the morphogenetic processes and retinal cell differentiation than provided in standard mammalian conditions.

Morphogenesis poses a challenge in many organoid systems, including retinal organoid cultures performed by other researchers and intestinal organoids. Epithelial bending and the resulting morphology and cell type diversity cannot always be replicated (Völkner et al., 2016; Wang et al., 2022). The ventral NR was proposed as the default path within retina formation (Hasegawa, 2016). This suggests that for the formation of CMZ and RPE inductive cues are missing.

Even though only NR cell types are forming spontaneously in the basic culture conditions in the medaka retinal organoid by day 4, the RPCs generated in the retinal organoids have the capability to give rise to RPE and the cells of the CMZ under inductive conditions, marked by cell pigmentation and the expression of a CMZ-reporter construct. The timed treatment of the organoids before or during RPCs stage with a Wnt-agonist, allowed to induce both RPE and CMZ cells (Zilova et al., 2021, unpublished data from Lucie Zilova). This opens up the possibility to explore the cues impacting the retinal specification and CMZ formation. The obvious missing substantial morphological change in the organoid and the absence of the CMZ suggest a possible

impact of the geometrical arrangement of the tissue and the mechanical forces connected to it.

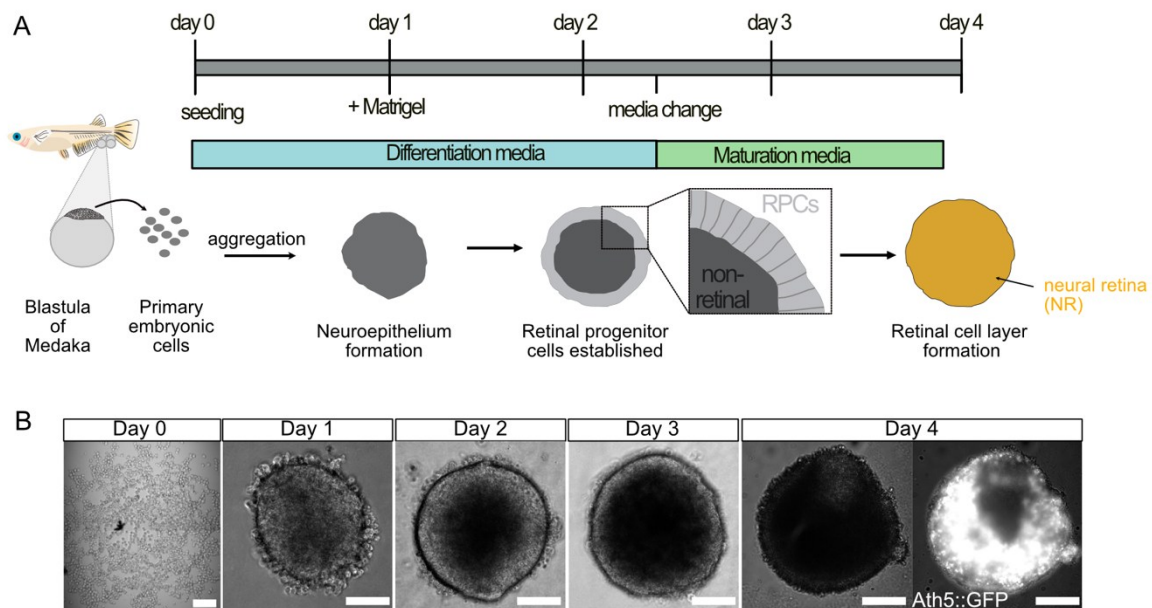


Figure 1.3: Medaka retinal organoid maintain spherical morphology throughout differentiation progress. (A) Scheme of organoid preparation and culture protocol for the course of 4 days. Primary embryonic cells are isolated from blastula staged medaka embryos and seeded in differentiation media for aggregation. A spherical organoid is formed and neuroepithelium is established by day 1. Matrigel is supplemented to the culture by day 1. By day 2, RPCs are formed in the organoid, which are arranged in an epithelium in the outermost layer of the organoid tissue. More centrally, the organoid contains non-retinal cells. The media is changed for maturation media on day 2. By day 3, neural retinal cell differentiation is starting. (B) Representative images of organoids in the course of 4 days. Single cells in culture well on day 0 (scale 200 μ m) and the aggregated organoid on day 1. By day 2, tissue at organoid rim appears to be transparent. RGC- reporter Ath5::GFP expression in day 4 organoid shows NR fate. Scale 100 μ m for images day 1- day 4.

1.3.4 Medaka retinal organoids as a model to study the mechanical impact on CMZ formation

The CMZ of medaka is a reservoir for RSC (Chow and Lang, 2001; Sinn and Wittbrodt, 2013). Due to their ability to give rise to retinal cell types post-embryonically, the formation of the CMZ is of interest for regenerative research. The prominent morphological distinction of the of NR, RPE and CMZ domains, suggest a function of the overall tissue architecture in defining the layering. The formation of the stem cell niche in the hinge region, as the region with the most tissue tension, has not yet been

understood. The question arises whether the tissue architecture itself has an impact on the establishment of the stem cell niche in the retina.

Mechanical cues have been found to induce cellular signaling processes and to be involved in stem cell positioning. Mechanical stresses resulting from cell shape changes and arrangement can enhance compartmentalization of gene expression, such as Sox9, which promotes stem cell positioning in developing organs (Villeneuve et al., 2024). Muncie et al. (2020) reported the activation of Wnt/ β -catenin signaling in human ESC cell culture that were subjected to mechanical tension. Also, epithelial bending was shown to induce beta-catenin signaling (Di Meglio, 2022). This suggests that the bending of the cells themselves can be important for Wnt/ β -catenin signaling activation in the OC and the establishment of the different cell types. For studying such processes, fish-derived retinal organoids would represent a valuable model as opposed to mouse and human retinal organoids due to the absence of OC formation in the fish organoid system. Forces on the organoid tissue can be applied by an active mechanical stimulus or passively, by physically constraining the three-dimensional (3D) environment of the organoid. To provide the mechanical input alongside the developmental process, a prolonged culture with the intervention can be desired, which favors the passive intervention. In *in vitro* tests, Okuda et al. (2018) could show that gross mechanical input on the epithelium has a long-term impact on intracellular tension. The basis for the cell to maintain their architecture is the constant adaptation of the cytoskeleton and it balancing out external forces and internal tension (Singh, 2018). Mechano-sensory pathways activate downstream signaling that can lead to the change of cellular behavior by promoting differentiation or proliferation (Erlach, 2018; Muncie, 2020). These studies clearly show the influence of cell shape on cell fate. On tissue and organismal level, however, such investigations are difficult to be conducted because of the inaccessibility of the tissue in the embryo.

Addressing the open question of how neuroepithelial tissue bending affects CMZ induction in the organoid system enables the isolated investigation of a single component within the broader developmental process, separate from other signaling influences. In the organoid culture, full control over the biochemical, but also the biophysical environment opens new options to study cellular and tissue behavior. Factors can be assessed independently of the numerous influences provided by the

surrounding tissue within the embryo, and will thus provide unprecedented insights into the instructiveness of the morphological event during CMZ formation. I will address in this study the impact of tissue shape changes on the specification of the RPC towards the CMZ.

1.4 Neuroretina: cell specification and pattern formation

1.4.1 Neuroretina establishment in distinct temporal and spatial order

The NR is composed of seven neural cell types and one glial cell type, arranged in a distinct spatial order. These cell layers are formed in a temporal order across the layers and progresses gradually from central to peripheral (Kitambi and Malicki, 2008). The neural retinal cell differentiation in medaka starts at stage 26 (2 dpf, Iwamatsu, 2004) with RGCs differentiating as the first neurons in the retina. The RGC layer is formed by stage 29 (3 dpf, Iwamatsu, 2004), and the axons of the RGCs form the optic nerve (Kitambi, and Malicki, 2008). The expression of the transcription factor *Atoh7* (Atonal Homolog 7) is marking the differentiation of RPCs towards RGCs (Kay et al., 2001; Pérez Saturnino et al., 2018).

From the *Atoh7* positive progenitors also PR, AC and HC are forming, while maintained *Atoh7* expression itself is crucial for retaining the RGC fate (Kay et al., 2001, Ma et al. 2004). In the postembryonic retina, it was found that a contrasting group of precursors forming BP, AC and MG are defined by the expression of Notch. In this case Notch is negatively regulating the expression of *Atoh7* and therefore, the presence of Notch is inhibiting the establishment of the *Atoh7* driven cell types (Pérez Saturnino et al., 2018). The same separation between Notch and *Atoh7*-driven progenitor pools has been shown for the embryonic retina in *Xenopus laevis* (Mills and Goldman, 2017).

Both, INL and ONL are specified by stage 30 (3 dpf) in the central retina and by stage 34 (5 dpf), all NR cell layers (RGC layer, INL, and ONL and two plexiform layers) are differentiated and cover the full NR (Kitambi and Malicki, 2008). Retinal progenitors differentiating towards BP and PR share the expression of *Otx2*. Specific interaction

with transcription factors, as *Prdm1* and *Vsx2*, restrict *Otx2*-expressing precursors to either photoreceptor or bipolar fates, respectively (Koike et al., 2007; Nishida et al., 2003; Fossat et al., 2007; Glubrecht et al., 2009)

BP can be detected by PKC-alpha (Hauk, 2018; Greferath et al., 1990), HC by *Prox1* (Dyer et al. 2003), AC by *Meis1* (Mrstakova and Kozmik, 2024). AC and RGC share the expression of *HuC/D* (Park et al., 2000; Ekström and Johansson, 2003; Lyu et al., 2023).

The maturation of PR is gradual, with double cone PR being first detected in the central retina at stage 33 (4.5 dpf) by the expression of *Zpr1* (Kitambi and Malicki, 2008). Markers for the rod PR, as rod opsin, the light-insensitive protein component of rhodopsin (not yet bound to 11-cis-retinal) (reviewed in Hofmann and Palczewski, 2015), are expressed at stage 35 (5.5 dpf) in the central retina. By stage 39 (9 dpf), the complete retina shows rod marker (rod opsin) expression, but with varying intensities in different areas (Kitambi and Malicki, 2008). The development of the PR is concluding with the differentiation of outer segments, an essential part of the PR for photosensitivity. The outer segment is a highly specialized sensory cilium, composed of tightly stacked membrane discs which harbor the light sensitive opsins of the PR (reviewed in Xu et al., 2024). The differentiation of outer segments is becoming evident by stage 39 (9 dpf) and gets most prominent in adult eyes.

1.4.2 Neural retina forms as a stratified epithelium

The layered organization of retinal cells depends on maintaining proper epithelial tissue structure which is supported by the ECM surrounding the NR. When the OC is established, distal cells in the forming NR elongate to form a pseudostratified neuroepithelium (Nicolas-Perez et al., 2016). The tissue maintains the apico-basal polarity through OV and OC stages and along cellular proliferation in the NR, with the apical side of the NR facing the RPE and the basal side facing the lens (Avanesov and Malicki, 2010). Within the stratified epithelium, the cells are oriented in a perpendicular axis and organize in the described cell type specific order.

The proliferation of RPC within the forming NR is localized at the apical side of the tissue. In the course of asymmetric divisions, differentiation of cell types is induced. For zebrafish, cells were described to occupy the layer corresponding to their differentiated cell type by active migration (Avanesov and Malicki, 2010). The loss of tissue polarity in this process leads to mis-organization and the loss of layering (Malicki et al., 1996).

Vertebrate retinogenesis has been described within different organisms and by diverse methods, as fixed samples or live imaging. The model proposed by Barton and Fendrik (2015) suggests to combine the longstanding suggestion of different competence states within RPCs allowing for the differentiation of specific cell types and the observation of a stochastic offspring generated by RPCs (Figure 4A).

For zebrafish, the differentiation of cells from RPCs to the different retinal cell types has been suggested to happen rather stochastic and not in a uniformly ordered manner (Almeida et al., 2014; He et al., 2012). It was observed that clones give rise to a variable number of differentiating cells and also a diverse combination of cell types (He et al., 2012). Almeida et al. (2014) described that different retinal cell types differentiate simultaneously in confined regions of the NR. They hypothesized that the cells, being interdigitated at first, migrate apically or basally into their respective layer, likely orientating in relative space to each other. The cell type generated within the NR formation was suggested to depend on a “competence state” of the RPCs which seems to be time dependent and results in a limited number of cell fates (Livesey and Cepko, 2011). This predisposition of the RPCs was described as collectively defined by internal transcription factors and external signaling cues (Avanesov and Malicki, 2010).

The Influence of several signaling factors on retinal cell patterning have been described. IGFs (insuline-like growth factor) and Wnts have been found to be important for RPC proliferation (Stenkamp, 2007; Masai et al., 2005), FGF for nasal-temporal patterning of the retina (Picker and Brand, 2005) and the initiation of retinal neuron production (Martinez-Morales et al., 2005). Notch signaling is important for the maintenance of proliferating progenitors in the NR and glial differentiation (Livesey and Cepko, 2001; Del Bene et al., 2008). In absence of Notch signaling within the

retina, MG do not differentiate, the retinal cell number is reduced, cell death is increased and pattern formation is impacted (Bernardos et al., 2005).

In vertebrates, the retinal cell patterning processes has also been connected with coordinated cell death of neurons. During retinal development in zebrafish, cell death was observed during OV evagination and across all cell layers within the NR (Schmitt and Dowling, 1994; Li et al., 2000; Biehlmaier et al., 2001). Cell death within all cell layers of the retina was reported in rats (Galli-Resta and Ensini, 1996; Vogel and Möller, 1980), as well as in the RGC layer of humans (Provis et al., 1985).

To maintain the epithelial organization of the NR, structural support is provided by the surrounding ECM. The retinal ECM is comprised by a complex combination of proteins including collagens, proteoglycans, and glycoproteins as fibronectin and laminin. (reviewed in Prieto-Lopez et al., 2024). ECM is involved in biochemical signal propagation and also provides mechanical cues (stiffness, strain, compressive, shear, tensile forces) (reviewed in Frantz, 2010; Prieto-Lopez, 2024). The rigidity/stiffness of ECM is important for development for correct cell layering, cell differentiation and maturation (Yi et al., 2022; Miller et al., 2017; Reinhard et al., 2015). Further, the presence of basement membranes formed by ECM is crucial for epithelia in the ectoderm lineage to create tissue polarization (Varshney et al., 2015). The ECM surrounding the retina is partially regulated by MG cells (Reinhard, 2015; Song et al., 2021), which are themselves essential for the maintenance of the retinal structure by providing tensile support (Bachleda et al., 2016; Wohl et al., 2017).

Referencing basic processes between species can help to understand patterning processes that are encountered in isolated systems, like organoids. Insights from organisms with simpler retinal structures have shed light on various aspects of retinal patterning in vertebrates. Patterns like the striking cone photoreceptor arrangement forming a mosaic pattern in tangential plane in the retina of teleosts, as well as general cell fate determinators and neurogenesis have been attempted to describe based on knowledge gained from other species (reviewed in Avanesov and Malicki, 2010; Stenkamp and Cameron, 2002). For reference, the periodic pattern formation in the *Drosophila melanogaster* retina will be described below.

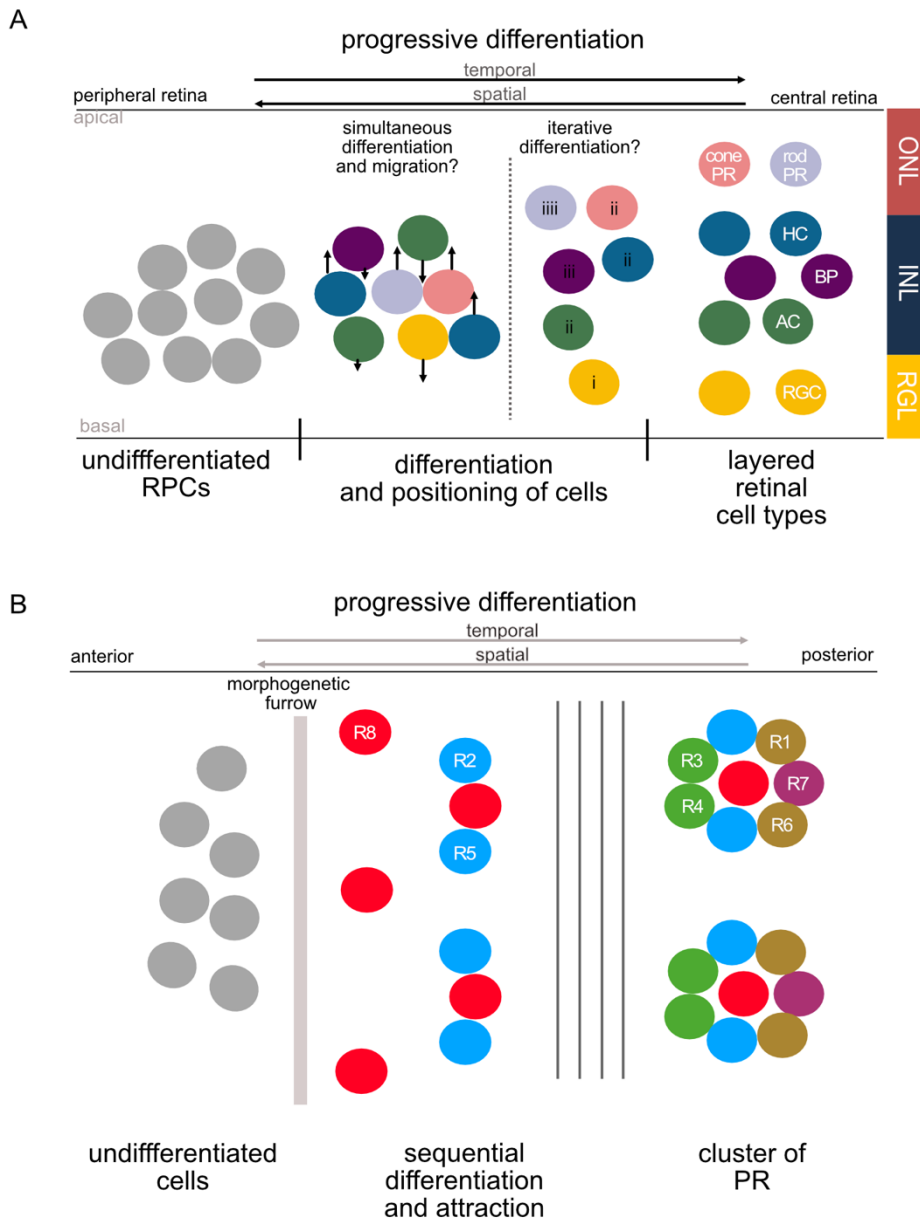


Figure 4: Current understanding of retinal patterning process in teleosts and *Drosophila melanogaster*. (A) Scheme depicting neural retinal cell differentiation from retinal progenitor cells (RPCs) to differentiated retinal cell types in a stratified epithelium. Nuclear layers (ONL, INL, RGL) indicated by colored bars on the right. Apical side of the epithelium on top, basal side on the bottom. Temporal progress of differentiation from RPCs (left) to established cell layers (right). Spatially, differentiation of retinal cell types progresses from the central retina (right) to the periphery (left). Proposed modi for differentiation and positioning of retinal cells into the cell layers in NR include regional differentiation and active cell migration (marked by black arrows) into layers and iterative differentiation from RGL to IPL marked by i-iiii within a region. (B) Scheme depicting cell differentiation and patterning process in retinal development of *Drosophila melanogaster*. A progressive differentiation and pattern formation within the optic disc is described from posterior (right) to anterior (left). Initiation of differentiation is induced by the progression of the morphogenetic furrow (light grey bar). Gradual specification of PR (R1-R8) results in the formation of a retinal cell cluster. The first cell specified is R8 in recurrent distance to the next like-cell (R8 PR). In the course of several steps (not depicted, gap indicated by parallel dark grey bars) PR cell clusters are formed in stereotypic distance.

1.4.3 Alternative retinal patterning: periodic pattern formation in *Drosophila melanogaster*

Which alternative arrangements, other than layering of photosensitive neurons exist in the animal kingdom forming a functional eye? In *Drosophila melanogaster* (subsequently referred to as *Drosophila*), retinal cell types are organized in clusters, called ommatidia, which are arranged in a periodic pattern throughout the retina (reviewed in Warren and Kumar, 2023). An ommatidium forms a structurally and functionally independent unit. During the retinal development in *Drosophila*, the eye imaginal disc, a monolayer epithelium, is specified by the combination of signaling factors spreading along with the movement of a linear wave of mitosis, called the morphogenetic furrow (Figure 4B). Hedgehog (Hh) signaling and the activity of Decapentaplegic (Dpp), the equivalent to bone morphogenic protein (BMP) in vertebrates, are involved in priming cells to become the central organizing PR (R8). Both are central for the correct retinal patterning in the *Drosophila* retina. The R8 PRs, the first cell of a forming ommatidium, are defined in a regularly spaced distance to the next R8, outlining the pattern of ommatidia spacing. The selection of the central PR is defined by Notch-dependent suppression of the neighboring cells to selectively remain with one organizing PR per forming ommatidium. The absence of Notch signaling during the pattern formation causes abnormal spacing between ommatidia, with the R8 being positioned closer than usual. Further, the activity of EGFR signaling is important for PR specification and recruitment of the other PR cells forming the ommatidium, and long-range distance refinement of the R8 PR. The R8 PR is expressing *atonal*, whose homologues are also found to be involved in driving retinal development in vertebrates. (reviewed in Warren and Kumar, 2023). In total, 14 cells are forming an ommatidial unit, eight PR and six accessory cells. Between ommatidia, the interommatidial lattice is formed, which is made of secondary and tertiary pigment cells. The juxtacrine signaling pathway Notch is especially involved in boundary formation, the establishment of planar polarity and cell fate specification (Fanto and Mlodizik, 1999; Bao, 2014). Within the patterning process, cell death of lattice cells and some cells per ommatidium are recurrent (Cordero et al., 2004; Brachmann and Cagan, 2003).

1.4.4 Neuroretinal cell differentiation and patterning in the early medaka retinal organoid

Many aspects of early medaka retina formation can be recapitulated in medaka organoids, and until day 4, the differentiation of RGCs, Otx2-positive cells, likely progenitors for BP and PR, and Prox1-positive cells, likely representing horizontal cells, have been described (Zilova et al., 2021). An inverted layer arrangement has been suggested, with the RGCs positioning in the outermost layer of the organoid and the Otx2- and Prox1- positive cells position more centrally. Yet so far, further retinal cell differentiation and patterning of the NR has not been reported. The developmental timing of the retinal organoids is close to the embryonic development, with a delay of a few hours, and thus the differentiation of retinal cell types and their spatial organization need to be studied in retinal organoids cultured beyond day 4.

In other retinal organoid systems using human and mouse embryonic stem cells (ESCs), organoids successfully generate all retinal cell layers and Müller glia, as well as their correct layering in ONL, INL, RGC-layer and the outer and inner plexiform layers (Nakano et al., 2012; Cowan et al., 2020; Wahle et al., 2023; Eiraku et al., 2011; Völkner et al., 2016). Also, the formation of Ribbon synapses in PR was observed. On a functional level, however, only in some retinal cells a weak neuronal activity could be reported (Cowan et al., 2020). Despite recent improvements, still significant variability in differentiation efficiency and organoid composition are reported, also between different cell lines (reviewed in O'Hara-Wright and Gonzalez-Cordero, 2020). Engineering approaches complementing the organoid culture with intracellular or extracellular cues might help to approach the desire to obtain retina-like organoids to study development, identify disease mechanisms, and facilitate drug discovery (Zhao and Yan, 2024, Afting et al., 2024).

Many factors need to be effectively orchestrated to create a functional tissue. Within this study, I will explore the differentiation and patterning of NR cell types in the maturing retinal organoid and address the principles employed for pattern formation in the *in vitro* system.

Aims and objectives

Patterning of tissues is a complex process crucial for the proper functionality of the organ. Understanding the impact of single cues on tissue specification and the architecture of the organ is essential to unveil underlying principles of pattern formation. The basic understanding of cues shaping the organ during development provides further foundation for organoid-engineering approaches aiming towards physiological tissue compositions. Organoid systems with defined biochemical and biomechanical environments allow to consecutively test the impact of single cues on tissue formation and patterning. In my two objectives, I overall explore the limits of tissue self-organization in late retinal organoids and address the effect of its 3D environment. Rather than aiming to approach the full complexity of the retina, this aids to understand the internal capacities of cells in respect to tissue formation and to address questions to the patterning process.

Objective I

This study addresses the influence of forces on tissue specification *in vitro*. Making use of the medaka retinal organoid system, I study the influence of epithelial bending on retinal cell differentiation. By physically constraining the 3D environment for the spherical organoid during specific developmental stages, I impose a diverging shape on the developing retinal organoid. With this approach, I explore the effect of tissue bending forces imposed on the retinal organoid and its instructiveness for the formation of a CMZ-like structure.

Objective II

Further, I study the formation of neuroretinal tissue in the late retinal organoid beyond the described initial stages. I investigate retinal cell type differentiation, tissue structure and neuroretinal patterning within the medaka organoid system. I strategically test for pathways employed in the pattern formation of the *in vitro* retinal tissue to understand the mechanisms driving tissue formation in the absence of the embryonic environment. Additionally, I address how the transition between different patterning mechanisms is impacted by ECM.

2. Results

2.1 Retinal tissue shape and CMZ fate

2.1.1 Tissue morphology and retinal specification – Hypothesis

Medaka retinal organoids obtain a simple spherical tissue shape and give rise to one retinal cell layer, the neural retina (NR), in standard culture conditions (Figure 2.1 A1, A4). Within embryonic retinal development, retinal tissue undergoes a distinct morphogenesis forming a cup-shape and the three retinal cell layers, NR, RPE and CMZ, are established (Figure 2.1 A2, A3, A5). The formation of the OC includes the bending of the neuroepithelium along the apical side of the tissue approaching a 180° angle (Figure 2.1 A6). Within the hinge region of the bend tissue, the CMZ is established. The lack of morphogenetic tissue bending within the retinal organoid and the absence of the CMZ poses the question whether the mechanical impact during OC morphogenesis is involved in CMZ formation.

As the common progenitor cells for all three retinal cell layers, RPCs, are formed in the retinal organoid system but only the NR is differentiating, it can be supposed that the inductive cues for CMZ differentiation are missing. The spherical shape of the organoid is the energetically least costly structure. It suggests the need for external mechanical cues to induce morphological changes to the *in vitro*-grown retinal tissue. Connecting these aspects, the application of external mechanical forces to the retinal organoid tissue could fill the missing gap for CMZ induction in the organoid system. Based on this, I hypothesized that bending of the retinal tissue formed in the organoid pre-onset of NR differentiation can induce CMZ fate.

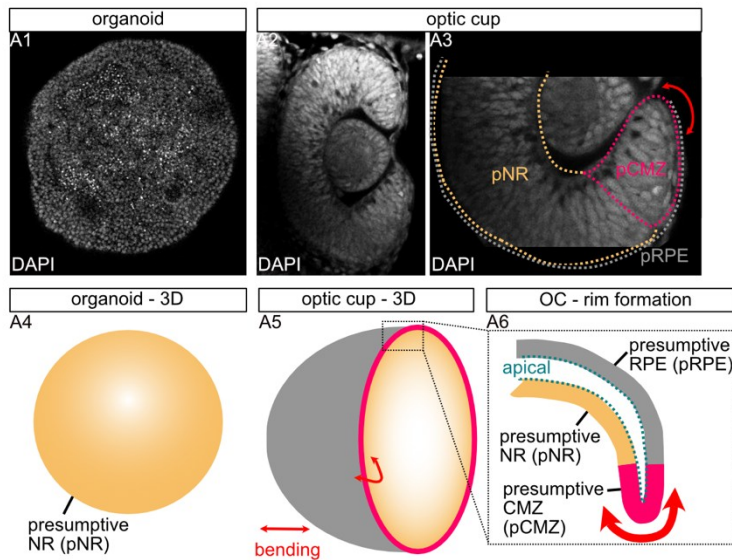


Figure 2.1: Retinal organoids display a reduced tissue complexity in comparison to the embryonic. (A) DAPI stained tissue showing central section of retinal organoid (A1) and embryonic OC (A2,A3). Cell layers forming in OC are outlined by colored dashed lines, orange marking presumptive NR (pNR), pink marking presumptive CMZ (pCMZ) and grey marking presumptive RPE (pRPE). Red arrow indicating tissue bending within OC formation. Scheme of organoid (A4) and OC (A5) in 3D. In the spherical organoid pNR is established. The cup-shaped OC with zoom in on the OC rim (A6) shows a bending (red arrow) along the apical side of the tissue and the distinct positions of the retinal cell layers forming.

2.1.2 Experimental design and tools for tissue bending and cell fate read-out

2.1.2.1 Fluorescent reporter line to read-out retinal fates live

To be able to approach the question whether tissue shape instructs cell fate or tissue patterning of the retina, I decided to focus on the induction of the CMZ. The CMZ is formed at the peripheral rim of the folding OC and tissue bending or folding is preceding or coinciding its specification. I therefore set out to design a set-up to induce tissue bending to the retinal organoids and culture the organoids within a constraining environment. To do this, the proper tools needed to be established.

For the faithful and fast recognition of a successful induction of the CMZ, I employed a reporter line generated by Dr. Lucie Zilova, which expresses two reporter constructs, for the neural retina (Rx2::H2B_GFP) and the stem cells in the CMZ (Cndp1::ONTR_mCherry) (Figure 2.2). Using this reporter line to generate organoids

offers the opportunity to screen the expression of the reporters live on the day of analysis (Figure 2.2 B). It also serves as a control for the retinal fate of the organoid by expression of Rx2::H2B_GFP on day 2 and day 4. The CMZ in the fish retina is established by day 3 and can be detected by the overlaying expression of Rx2::H2B_GFP and Cndp1::mCherry (2.2 A). Within the organoids, CMZ-reporter positive tissue can be chemically induced by the addition of a Wnt-agonist on day 2 (not shown, data by Dr. Lucie Zilova). Upon induction, the expression of Cndp1::mCherry is visible by late day 3/day 4 of culture. Therefore, I defined day 4 of organoid culture to score for a successful induction of CMZ.

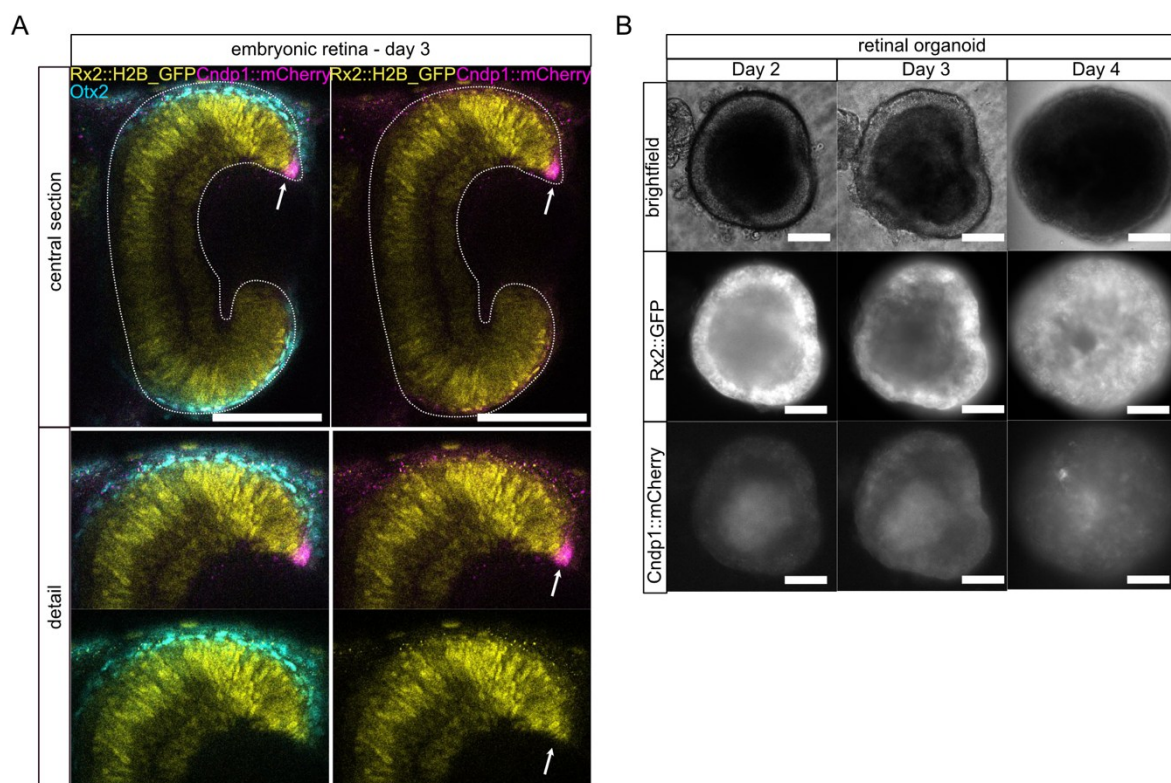


Figure 2.2: Fluorescent reporter line allows for live tissue recognition in embryo and organoid. (A) Fluorescent images of day 3 embryonic retina showing the tissue stained by the reporter Rx2::H2B_GFP (yellow) for the NR and Cndp1::mCherry (magenta) for the CMZ. Central section shown as well as zoom-in on upper half of retina. Otx2-label marking RPE (cyan). Clear architectural separation of CMZ to NR and RPE visible marked by arrow. Cndp1::mCherry expressing cells co-express nuclear Rx2::H2B_GFP reporter. Scale 100µm. (B) Expression of reporter constructs in retinal organoid from day 2 to day 4. Expression of Rx2::H2B_GFP marker across all days, no expression of Cndp1::mCherry. Scale 100µm.

2.1.2.2 Moulds for simplified tissue bending

Recreating the invagination of the OC within the spherical organoid would require an indentation of the tissue by a pin, pressing the organoid into a cup shape. This approach is technically challenging, since it requires an active movement of such pin. Alternatively, the morphology of the organoid can be changed by limiting its 3D environment in space and hereby forcing the tissue into a pre-determined shape. Technically this approach presented itself as more suitable, because organoids can be easily transferred to a new environment after aggregation. Therefore, I decided to transfer retina-fated organoids into space constraining moulds to impose tissue bending.

For the mould design, optical and physical accessibility, organoid integrity and the suitability for prolonged culture needed to be considered. To ensure both optical and physical accessibility, I outlined shapes in 2D (x-y) and extruded these in perpendicularly (z) to create a 3D mould. The upper and lower side of the shape are open and display the 2D outline of the shape. The mould is accessible for organoid mounting and the tissue bending is impacting at the upper and lower rim of the organoid which is accessible by microscopy. To approach the tissue deformation with reduced complexity, I chose a simple shape of a rectangle, which forms a cuboid in 3D, to restrict and deform the organoid tissue (Figure 2.3 A). The design of such mould was tailored towards constraining the spherical organoids with a diameter of 300-450 μm , but ensure the integrity of the tissue with a sufficient space for the organoid to remain intact. As a control, a round shape was designed to compare the space-unrestricted culture within the same material and media environment with the shape-restricted organoids. To create the mould, I chose agarose as a suitable material. Agarose is water-based and rigid in high concentrations, which allows the organoids to constantly be in contact with the culturing media. Agarose is further non-toxic and molecularly not interacting with the cells. I defined 2% agarose in 1x PBS as suitable and stable over days at 26°C in the incubator.

To cast the agarose gel, a negative structure of the intended shape can be inserted into the liquid phase of the agarose and imprint the mould by displacing the material. Therefore, I decided to design stamps with the shapes of choice which can be removed

after solidification and leave the imprinted positive within the agarose. Further, the shapes were designed to be conical, since the casting process includes the removal of the stamp from the solidified state of the chosen material. This also allows to restrict organoids with minor size variation in the same moulds. The mould design and fabrication were done by 3D printing together with Gero Hofmann. The stamps to create the moulds were designed to fit a 6cm culture dish as well as in a 1 well dish in 96 well format (Figure 2.3 A, Figure 6.1).

Forcing organoids into a cuboid (rectangular shape), a pressure impact on the organoid and a compression of the central tissue is imposed. The edges of the organoid facing the mould are bent along the agarose wall in a 90° angle (Figure 2.3 B). With the simple rectangular shape, the induction of a tissue bending at the epithelial rim is combined with compression of tissue regions within the organoid as a whole. It also creates a differential exposure of the tissue within the organoid to the named forces and can therefore be scored in relation to the position across the different treatments (Figure 2.3 B). The round shape creating a cylinder mould, does not restrict the organoid in space and does not impose a tissue bending.

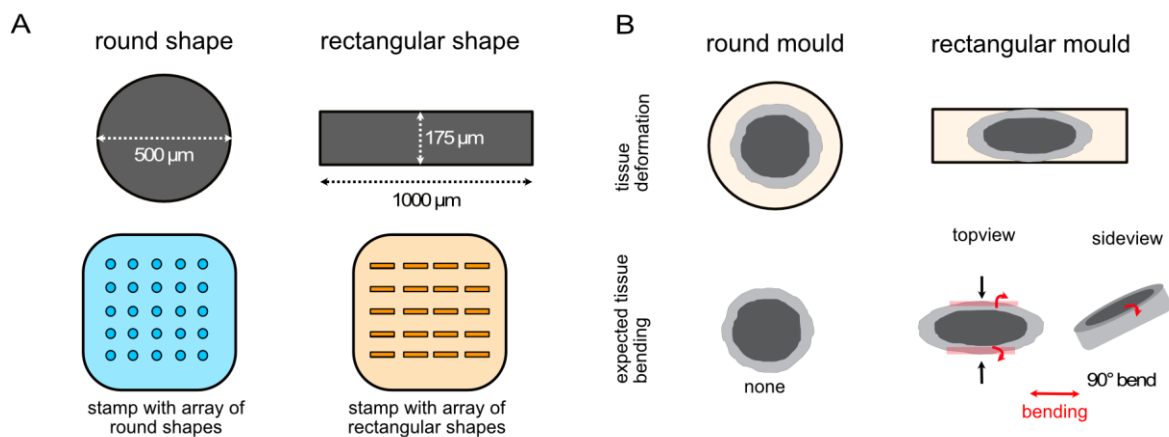


Figure 2.3: Mould design and expected bending impact on tissue. (A) Scheme of shape negatives of round and rectangular shape. Array of shapes were 3D printed in a stamp format. (B) Scheme of tissue deformation and tissue bending imposed on organoid due to physical restriction in shapes.

2.1.2.3 Experimental outline

The time point to start the mechanical input was estimated based on the retinal fate establishment in the organoid, by the time window for the chemical induction of the CMZ with Wnt-agonists and the morphological changes in the embryonic retinal development. After aggregation of the organoids, retinal fate is established by day 1 and multipotent RPCs are formed by day 2 (Zilova et al., 2021). The chemical induction of CMZ by Wnt/ β -catenin signaling was shown when organoids were treated on day 2. Therefore, the RPCs arranged in the epithelial structure are competent to adopt CMZ fate. To test the ability of enforced tissue bending to induce CMZ, I transferred organoids at day 1 and day 2 after aggregation. These timepoints cover pre- and post-RPC fate establishment (Rx2-expression) in the organoids, respectively, and therefore include the early and late impact of tissue shape on cell differentiation (Figure 2.4 A). Organoids can be removed from the Matrigel environment after 6h of Matrigel treatment and adapt retinal fate, as described for RPE induction experiments by Zilova et al. (2021).

Agarose moulds were prepared on the day of usage in a 1-well plate. The 1-well plate allowed to imprint several arrays of both round and rectangular shapes in the same culture well. Mounting of the organoids into the moulds was done by transferring the organoids using a pipet, and then pushed into the mould using a needle. Due to the swelling of the water-based agarose, the mould diameters were increasing in comparison to the designed negatives. However, the physical impact on the organoid tissue was created and therefore the swelling effect was considered negligible. The organoids were incubated until day 4. Read-out of the acquired cell fate on day 4 was done by fluorescent imaging of the Rx2::H2B_GFP and Cndp1:mCherry reporter with the Acquirer imaging machine (Figure 2.4 B). Rx2::H2B_GFP signal alone reporting NR fate while overlapping expression of both reporter fluorophores within a cell shows the presence of cells adopting CMZ fate. The imaging of the organoids from the bottom of the well captures the tissue at the rim of the organoid facing the agarose, here vertical, which is bending along the agarose wall.

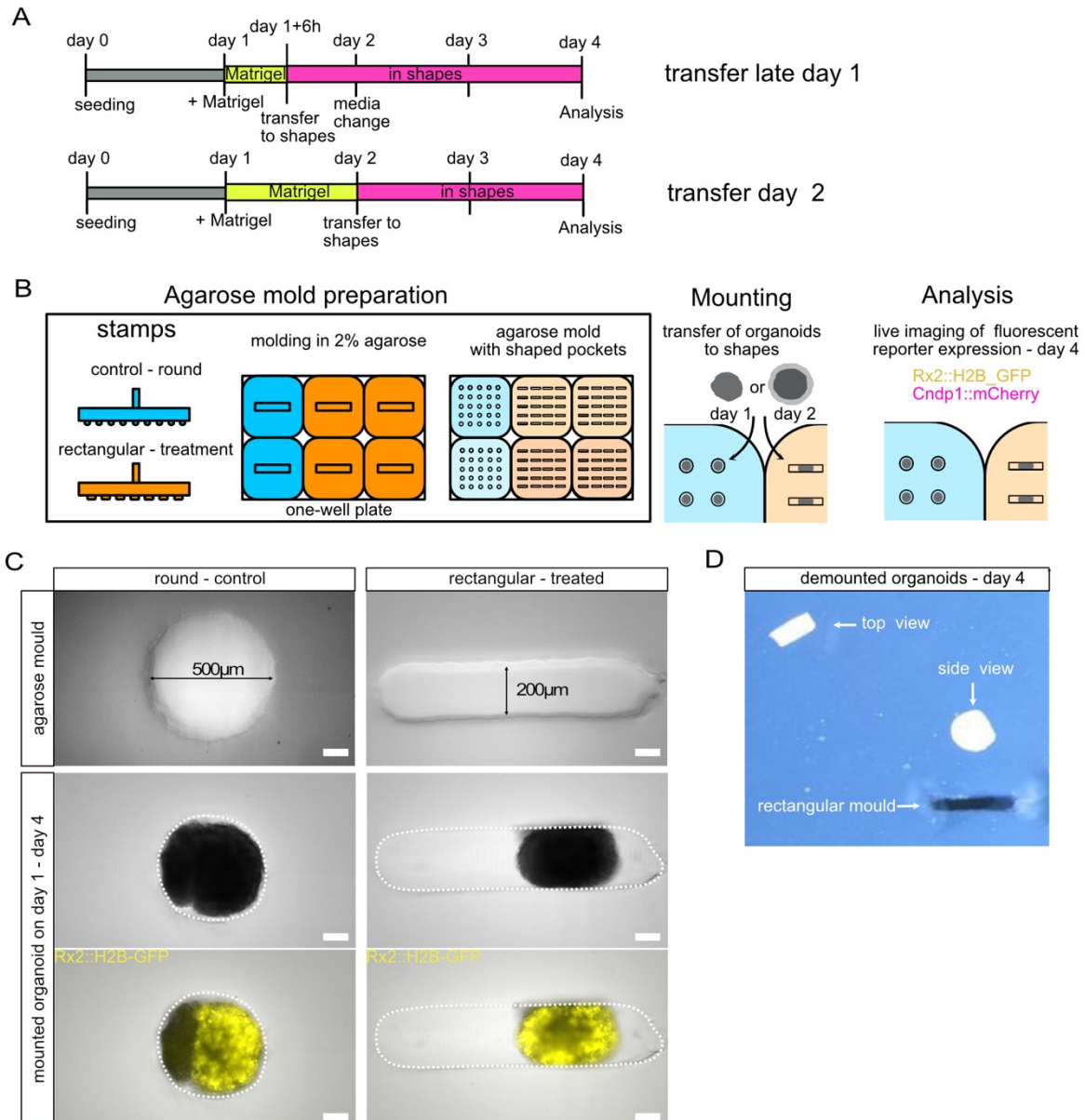


Figure 2.4: Mould design and shape expectation preparation for morphological shape induction for organoids. (A) Scheme showing time frames of exposure to Matrigel and mounting in shapes until analysis for organoids mounted on day 1, 6h after Matrigel application, or on day 2. (B) Scheme of experimental outline for mould preparation and organoid culture and in moulds. Stamps with round and rectangular shapes for imprinting into agarose are placed into 1-well plate filled with liquid agarose (2% in PBS). Stamps are removed after solidification and moulds are imprinted into agarose. Organoids are mounted on either day 1 or day 2 and after culture within moulds analyzed for retinal cell type reporter expression on day 4. (C) Agarose moulds imaged in brightfield. Mounted organoids express Rx2::H2B_GFP in round and rectangular mould after culture in moulds for 3 days. Scale 100µm. (D) Demounted organoids after culture in rectangular shape have coin shape. Organoid in top view and organoid in side view are shown on agarose.

To test that the chosen set-up allows for the culture of organoids and the differentiation of retinal tissue, I analyzed the expression of the Rx2::H2B_GFP reporter on day 4

within organoids transferred on day 1 to agarose shapes. Expression of the Rx2::H2B-GFP reporter was reliable for both conditions (Figure 2.4 C). Therefore, the set-up could be used for the intended experiments. For the analysis of cell differentiation with immune staining, the organoids can be fixed and demounted from the moulds. The organoids adopt a coin-shape within the rectangular mould which is kept after removal from the moulds (Figure 2.4 D).

2.1.3 Rectangular shape restriction of retinal tissue pre-RPC formation does not induce CMZ formation

To test the impact of tissue bending before the establishment of the RPC containing epithelium on retinal cell differentiation, the organoids were mounted into the described moulds on late day 1. By day 4, the samples were analyzed for the expression of the retinal reporters live in the moulds (Figure 2.5 A). Only batches with a retina-tissue only control samples (round shape) were considered for shape-induction analysis (Figure 2.5 B; Figure 6.2). Due to high autofluorescence of the organoids and the epifluorescence set-up of the Acquirer imaging machine, the fluorescent CMZ reporter (Cndp1::mCherry) signal was normalized by the autofluorescence value captured from non-reporter wild type organoids in the same set-up (Figure 2.5 C). As a second way to resolve a potential Cndp1::mCherry signal, I used rolling ball background subtraction with a radius of 15 pixels (Figure 2.5 C).

Maximum projection of the same number of z-slices for the control and shape-induced organoids, described background subtraction and overlay of all the samples was done to estimate whether a common region within the organoid was induced to form CMZ (Figure 2.5 D). Within 59 organoids imaged in live, as well as 10 in detail with immune histochemistry (Figure 2.5 D; Figure 6.3), no induction of Cndp1-expression could be detected. Notably, no obvious signs of pigmentation were visible, therefore no induction of RPE in this set-up was found.

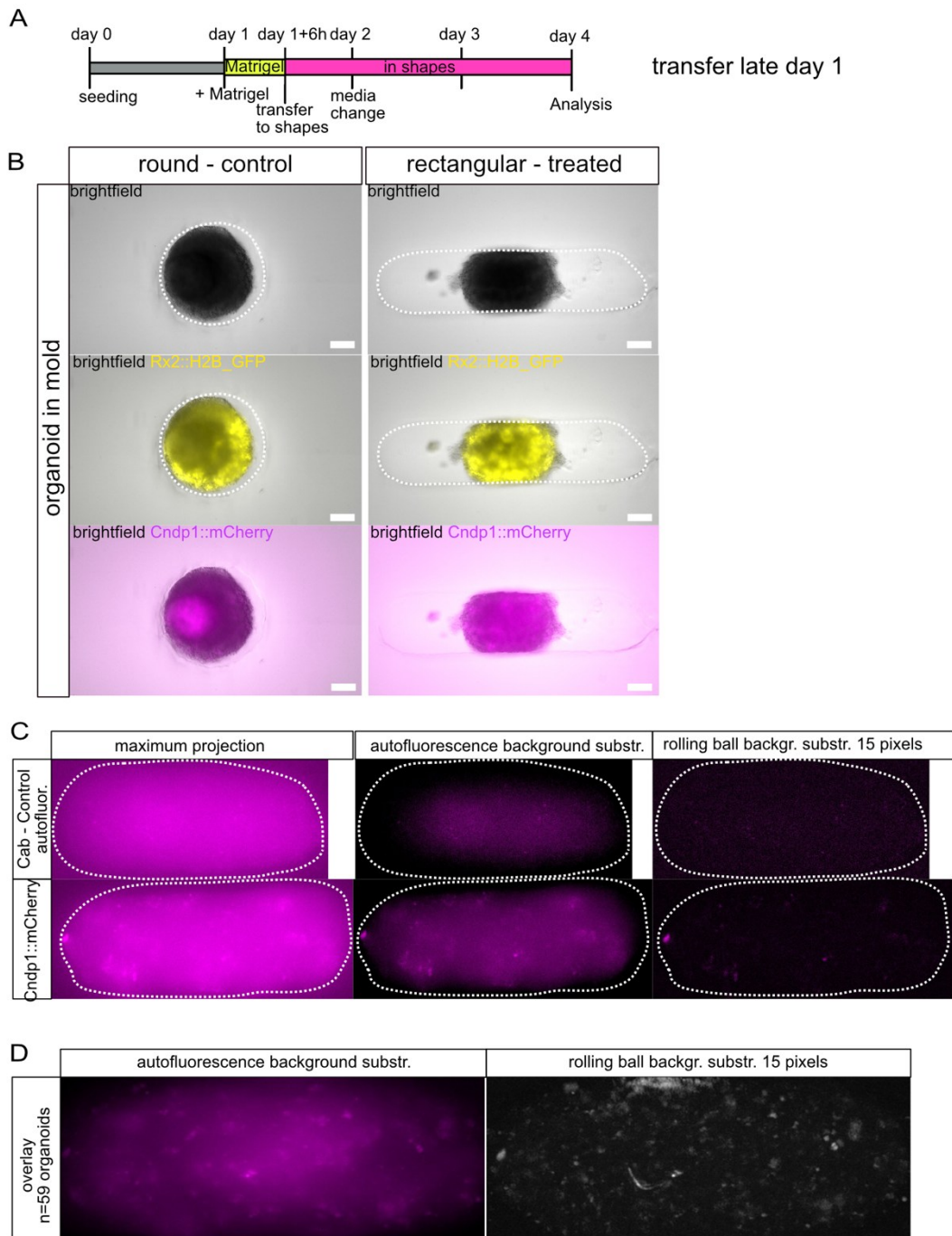


Figure 2.5: Organoids mounted in rectangular moulds on day 1 show no CMZ induction by day 4. (A) Scheme showing time frames of exposure to Matrigel and mounting in shapes until analysis for organoids mounted on day 1, 6h after Matrigel application. (B) Fluorescent reporter signals overlaid with brightfield of organoids mounted in shapes on day 4 imaged with Acquirer imaging machine. Scale 100 μ m. (C) Maximum projection of z-slices imaged in from one organoid with no red fluorophore (Cab – Control) and *Cndp1::mCherry* reporter carrying organoids. Outline of organoids marked by dashed line. Cab-Control sample used for autofluorescent background control. Background subtraction estimated by averaging signal intensity of 5 Control samples for both Control and reporter-carrying organoid. Alternative background subtraction done by rolling ball background subtraction algorithm with 15 pixels radius using Fiji. (D) Overlay of 59 maximum projections of reporter-carrying organoids mounted in rectangular shape after autofluorescence background subtraction or rolling ball background subtraction (15 pixels). Overlay done by morphing all organoids to the same width and length. Images acquired within two independent experiments.

2.1.4 CMZ formation in organoids cannot be correlated to mechanical impact generated on tissue

To test whether the mechanical impact of tissue bending can instruct established RPCs to adapt CMZ fate, I transferred the organoids to the restrictive shape on day 2 of culture (Figure 2.6 A). In the course of three independent experiments of mounting organoids on day 2 into the control and restrictive shape, complex organoids harboring NR-tissue and CMZ- tissue, but also non-retinal tissue emerged in both conditions (Figure 2.6 B, Figure 6.4). The emergence of complex organoids with retinal and non-retinal tissue poses a variability in the organoid culture. This variability can be influenced by several factors as cell isolation and critical steps in the first days of organoid culture, which remained in this case unresolved. To be able to comment on the effect of the shape induction, only organoid batches with a retina-only phenotype, seen by the expression of the retinal marker Rx2::H2B_GFP all around the organoid in the control condition, can be considered. Hereby, the influence of cell differentiation cues provided by neighboring tissues (e.g. via signaling, creation of a transitioning zone) can be separated from the influence of the mechanical input.

Within the organoids transferred on day 2, spontaneous formation of Cndp1::mCherry positive tissue regions could be seen, which could not be associated with the imposed mechanical treatment.

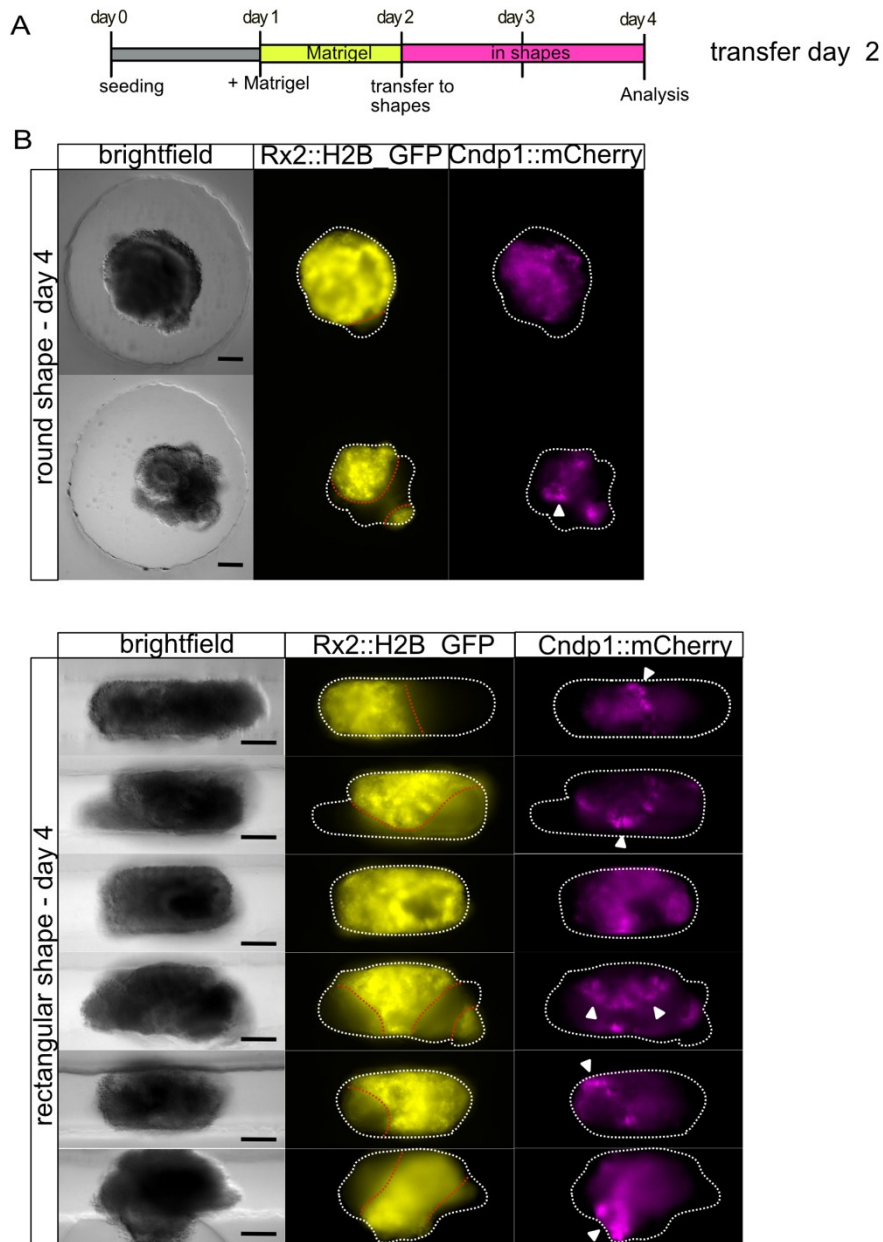


Figure 2.6: Organoids mounted in rectangular moulds on day 2 with complex tissue composition cannot be scored for shape-induction causality. (A) Scheme showing time frames of exposure to Matrigel and mounting in shapes until analysis for organoids mounted on day 2. (B) Fluorescent reporter signals overlaid with brightfield of organoids mounted in shapes on day 4 imaged with Acquirer imaging machine. White dashed lines outlining organoid shape. Red dashed lines outlining Rx2::H2B_GFP reporter positive areas vs. reporter negative areas. White arrowheads pointing at Cndp1::mCherry reporter positive tissue. Scale 100 μ m.

2.1.5 Increased complexity of mechanical input does not induce CMZ formation

The simple tissue bending along one axis within the rectangular shapes could not be causatively connected to CMZ induction. To further approach the complexity of the morphological tissue shape and therefore the mechanical impact in the optic cup, I designed shapes with a second axis of bending. I outlined a shape with a curved mould, here called “C-shape”, resulting in an extruded sickle shaped mould. A second shape creating multiple tissue bending points, here called “X-shape”, resulting in an extruded dumbbell-shaped mould was designed (Figure 2.7 A,B).

When designing the shapes, the desired tissue deformation, but also sustained tissue integrity and accessibility for manipulation and media were considered. Both, the C-shape and X-shape create an inversion of the tissue curvature from convex to concave, with an opening angle of 120° in x-y direction in addition to the 90° bending in z-direction (Figure 2.7 B). Along with the curvature inversion to concave, several points of tissue bending were induced by the restrictive pins from the side (Figure 2.7 B). For the C-shape, several minor different designs were used, but due to their overlap in outline, the results were grouped under “C-shape” (Figure 6.5) The mould design was done in collaboration with Gero Hofmann and the negatives were 3D nano-printed by Frederik Mayer (AG Wegener, KIT) and Philipp Mainik (AG Blasco, UHD). To handle the 3D nano-printed structures, Gero Hofmann built a holder, which in combination with the nano-printed shapes can be used as a stamp. The stamp outline was customized to fit a multi-well coverslip and produce agarose moulds within each well. To be able to detect the reporter expression for the retinal fates, in the context of imposed shapes using live imaging, or enhanced by immune staining, the culture set-up was transitioned to a multiwell-coverslip with 8 separate wells. The multiwell-coverslip has a glass bottom enabling the direct read-out of fluorescence expression at the inverted confocal microscope (Figure 6.6). Further, the small chambers allow for the fixation and immune staining of the organoids within the constriction. This increases the reliability of detecting the fluorophore expression. The set-up was employed to treat both states of retinal development, day 1 and day 2 (Figure 2.7 C).

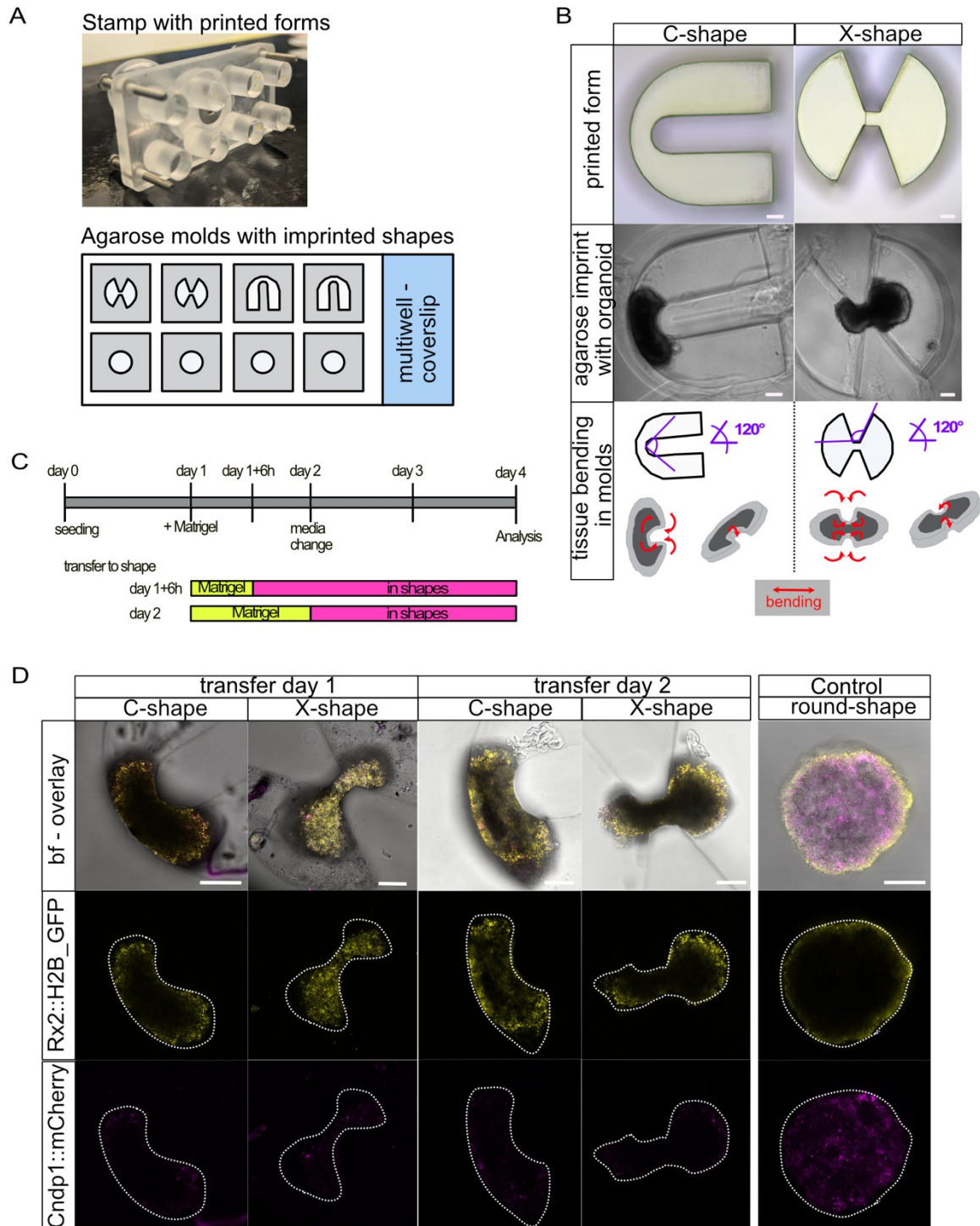


Figure 2.7: Tissue bending along two axes on day 1 and day 2 does not instruct CMZ formation. (A) Stamp with nano-printed complex shapes for imprinting agarose moulds into multiwell-coverslips. Scheme of agarose moulds with imprinted shapes. (B) C-shape and X-shape structures printed with Nanoscribe printer by Philipp Mainik (AG Blasco, UHD). Agarose moulds with imprinted shapes and mounted organoids. Scale 100 μ m. Tissue bending experienced by tissue in agarose moulds. (C) Scheme showing time frames of exposure to Matrigel and mounting in shapes until analysis for organoids mounted on day 1, 6h after Matrigel exposure, or on day 2. (D) Organoids (day 4) fixed and immune stained in moulds after culture for 3 day (transfer day 1) or 2 days (transfer day 2) in agarose moulds. Reporter fluorophores enhanced by immune labelling against fluorophores. White dashed line outlining organoid shape. Scale 100 μ m.

No Induction of Cndp1-expression could be connected to the tissue shape induction (day 1, C-shapes (25 organoids, thereof 12 immune stained); X-shape (10 organoids, thereof 5 immune stained); day 2, C-shapes (33 organoids, thereof 13 immune stained), X-shape (8 organoids, thereof 4 immune stained)) (Figure 2.7 D).

The more complex tissue shape employed here, induction including bi-axial tissue bending and the enforcement of concave tissue curvature, did not lead to CMZ induction.

2.1.6 Epithelial and curved morphology in spontaneously formed CMZ regions

While the spontaneous establishment of CMZ in the previous experiment was not suitable for an association with the shape induction, the tissue shape and context compatible with CMZ formation can be observed within these samples. The Cndp1::mCherry-positive regions in the complex organoids showed that the reporter positive tissue regions have a structured and epithelial organization (Figure 2.8). In 78% of cases these tissue regions are positioned at the rim of the organoid and have a curved morphology (n=35 domains). To extract the tissue context in which the CMZ-tissue is forming, the tissues flanking the mCherry expressing cells were scored. In all cases CMZ formed next to NR tissue (35/35), in 11% (4/35) it was framed by NR and pigmented tissue representing RPE and in 17% (6/35), it was flanked by non-retinal tissue and NR. No exclusive tissue context for the formation of Cndp1-positive tissue could be determined, but the direct neighborhood with the NR on at least one side of the CMZ-tissue was seen in all cases.

Spontaneously formed CMZ-tissue displayed an epithelial morphology and obtained tissue curvature. No selective tissue-tissue context for CMZ formation was evident from the spontaneous tissue formation.

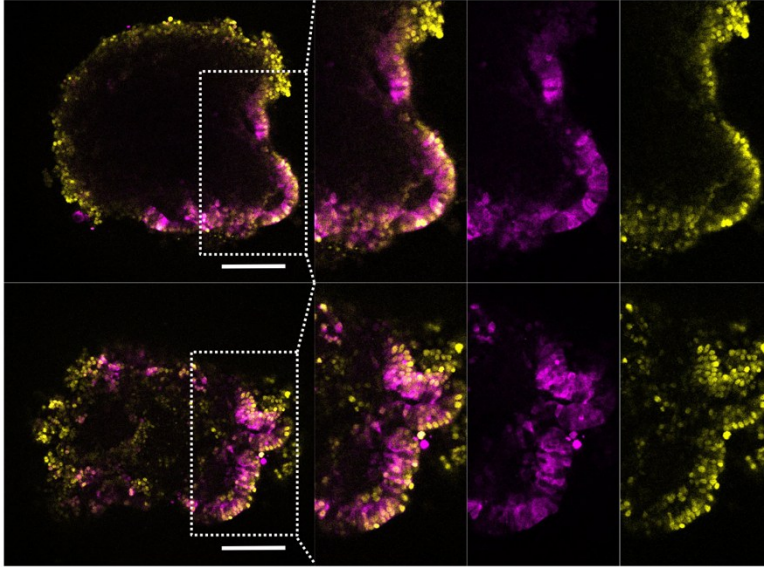


Figure 2.8: Spontaneous CMZ formation shows epithelial and curved morphology for reporter-positive tissue stretches. Day 4 organoids with Cndp1::mCherry positive regions organized in an epithelial-like fashion. Rx2::H2B_GFP positive nuclei arrange in epithelium. Cndp1::mCherry tissue stretch has with curved tissue morphology. Scale 100 μ m.

2.1.7 Tissue polarity in day 1-treated organoids differs from day 2 treated organoids

As seen before, the epithelial structure appears to be tightly connected to CMZ formation. While the retinal identity was shown to be established for organoids transferred to the shapes on late day 1 and day 2 in this study, the epithelialization of retinal organoid tissue was only shown to be established by day 2 (Zilova et al., 2021).

In context with the shape treatment from day 1, organoids are removed from the Matrigel environment after 6h. The shortened exposure to ECM proteins might hinder the organoid tissue to obtain an epithelial structure. To test this, I investigated the polarity of the tissue within organoids on day 2, when exposed to Matrigel for 6h and then mounted into the agarose moulds (d1) (Figure 2.9 A). I compared the tissue structure to the tissue organization and RPC establishment in organoids cultured without Matrigel or in standard condition (Matrigel- treatment from day 1 to day 2) on day 2 (Figure 2.9 B).

To probe for the polarization of the retinal tissue, immune labeling with an antibody against PKC-zeta was used to visualize the apical side of retinal tissue, as shown for the OC of the medaka embryo (Herder et al., 2013) (Figure 6.7). The epithelial cell arrangement can be further outlined by the arrangement of nuclei on the organoid rim visualized by DAPI staining.

Organoids transferred to the agarose moulds on day 1 harbor vertically oriented cells in the outermost cell layer (Figure 2.9 C). The apical marker PKC-zeta cannot be detected and therefore no indication for a polar tissue organization can be marked (Figure 2.9 C). In contrast, within the Matrigel-treated organoid, the epithelium is composed of several layers of vertically oriented nuclei with common cell orientation with the apical side towards the inner side of the organoid (Figure 2.9 D). The condition void of Matrigel, however, shows a non-polarized and thin epithelium (Figure 2.9 D). This morphology is more similar to the shape treated organoids. The transfer to the moulds on day 1 includes the removal from the Matrigel-environment after 6h of treatment and appears to lead to a similar tissue organization as when the organoid is not exposed to Matrigel. Since the epithelium of the constrained and non-constrained samples within the shape treatment show the same organization, the phenotype is not caused by mechanical compression but the shortened exposure to Matrigel.

While the polarity and epithelial organization appears to be different in presence and absence of Matrigel from day 1 to day 2 of culture, organoids grown in both conditions establish RPCs by day 2 and differentiating retinal cell types by day 4 (Figure 6.7). This confirms the differentiation potential of the retinal cells within each condition, which is also the case for the organoids transferred to the shapes on day 1. However, the non-polarized tissue within the day 1 treated samples compared to day 2 transferred organoids might affect their ability to form the epithelialized CMZ tissue. Taken together, the tissue bending treatments performed were impacting a polarized epithelium when mounted on day 2 and an unpolarized tissue when transferred on day 1.

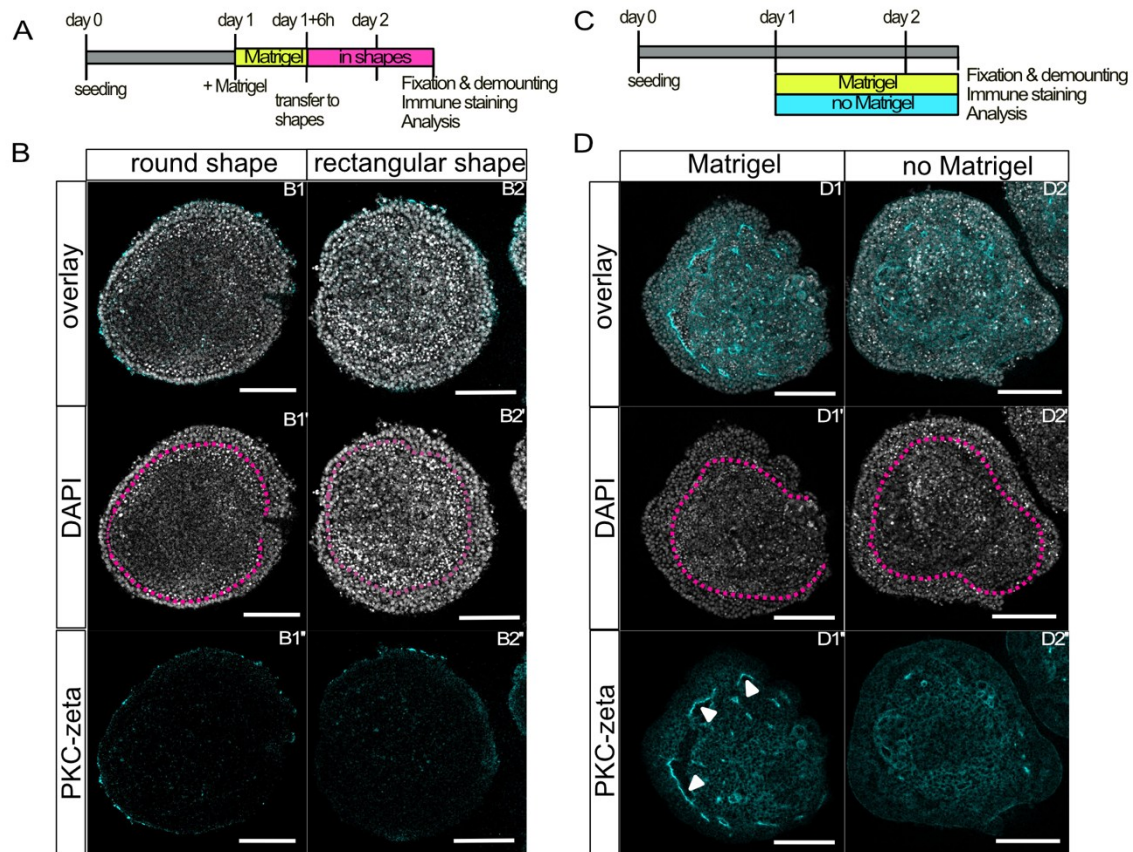


Figure 2.9: Organoids with shortened Matrigel exposure show altered epithelial make-up and polarity. (A) Scheme showing organoid culture and time frames of exposure to Matrigel and mounting in shapes until analysis for organoids mounted on day 1, 6h after Matrigel exposure. (B) Immune staining of day 2 organoids for apical marker PKC-zeta when mounted to round or rectangular shape on day 1 after exposure to Matrigel for 6h. DAPI staining nuclei. Magenta dashed line marking inner border of epithelium visible in DAPI-stained nuclei arrangement. Scale 100 μ m. (C) Scheme showing organoid culture and time frames of exposure to Matrigel until analysis on day 2. (D) Immune staining of day 2 organoids for apical marker PKC-zeta when cultured with Matrigel or without. DAPI staining nuclei. Magenta dashed line marking inner border of epithelium visible in DAPI-stained nuclei arrangement. Polarized epithelium marked by arrowheads. Scale 100 μ m.

2.1.8 Conclusion: tissue bending and CMZ formation

The forced deformation of the organoids was neither necessary, nor sufficient to induce CMZ formation. As expression of the CMZ reporter was just as common in the control organoids grown without spatial restrictions as they were in organoids with induced bending at various angles. The conclusion therefor is that the CMZ can form spontaneously, without externally applied forces, and is not induced to form by the specific conditions tested here. This does not preclude the possibility that such forces play a role in retinal formation in the embryo, but demonstrates that the process can occur without them.

2.2 Neural retinal differentiation and maturation in organoids

2.2.1 Retinal ganglion cells are maintained within day 7 retinal organoids

Primary pluripotent embryonic stem cells of medaka fish can generate retinal organoids. By day 2, RPCs form and by day 4 RGCs differentiate and an inverted pseudo-stratified retinal cell layering is assumed by day 4 (Zilova et al, 2021; Figure 2.10 A). However, the potential for further differentiation and maturation of other retinal cell types in medaka retinal organoids beyond 4 days of culture remains unexplored. *In vivo*, the development of a fully stratified retina in medaka fish occurs around 5 days post-fertilization (stage 34), with continued maturing until day 9, which also marks the day of hatching (Kitambi and Malicki, 2008; Iwamatsu, 2004). Given the developmental timeline, I focused my investigation on the establishment of retinal tissue within late retinal organoids at 7 days of culture. By this time the retinal cell types should be formed.

To investigate the progression of neural retinal cell differentiation in medaka retinal organoids, I employed the same culture conditions as used until day 4. To examine whether the RGC are maintained within the organoid up to day 7, I used an Ath5::GFP reporter line. The reporter (Ath5: old name for Atoh7) is a faithful marker for identifying RGCs in embryos (Figure 2.10 B) and can be used to track their presence and maintenance over time in the retinal organoid cultures.

To visualize individual cells and their processes within the experimental set-up, Ath5::GFP reporter-carrying cells were mixed with wild-type cells in a ratio of 1:4 during seeding. Consequently, one would estimate that approximately 20% of RGCs are labelled within each organoid. Within day 4 organoids, RGCs are distributed within the outer layers of the organoid and long axonal projections can be followed up with the cytosolic GFP labelling (Figure 2.10 C). This pattern of RGC distribution and visible axonal projections extending throughout the tissue is also seen by day 7 (Figure 2.10 C). The observed differentiation and maintenance of RGC is robust, with 100% of organoids containing RGCs from day 3 to day 7 under standard conditions (Figure 6.8).

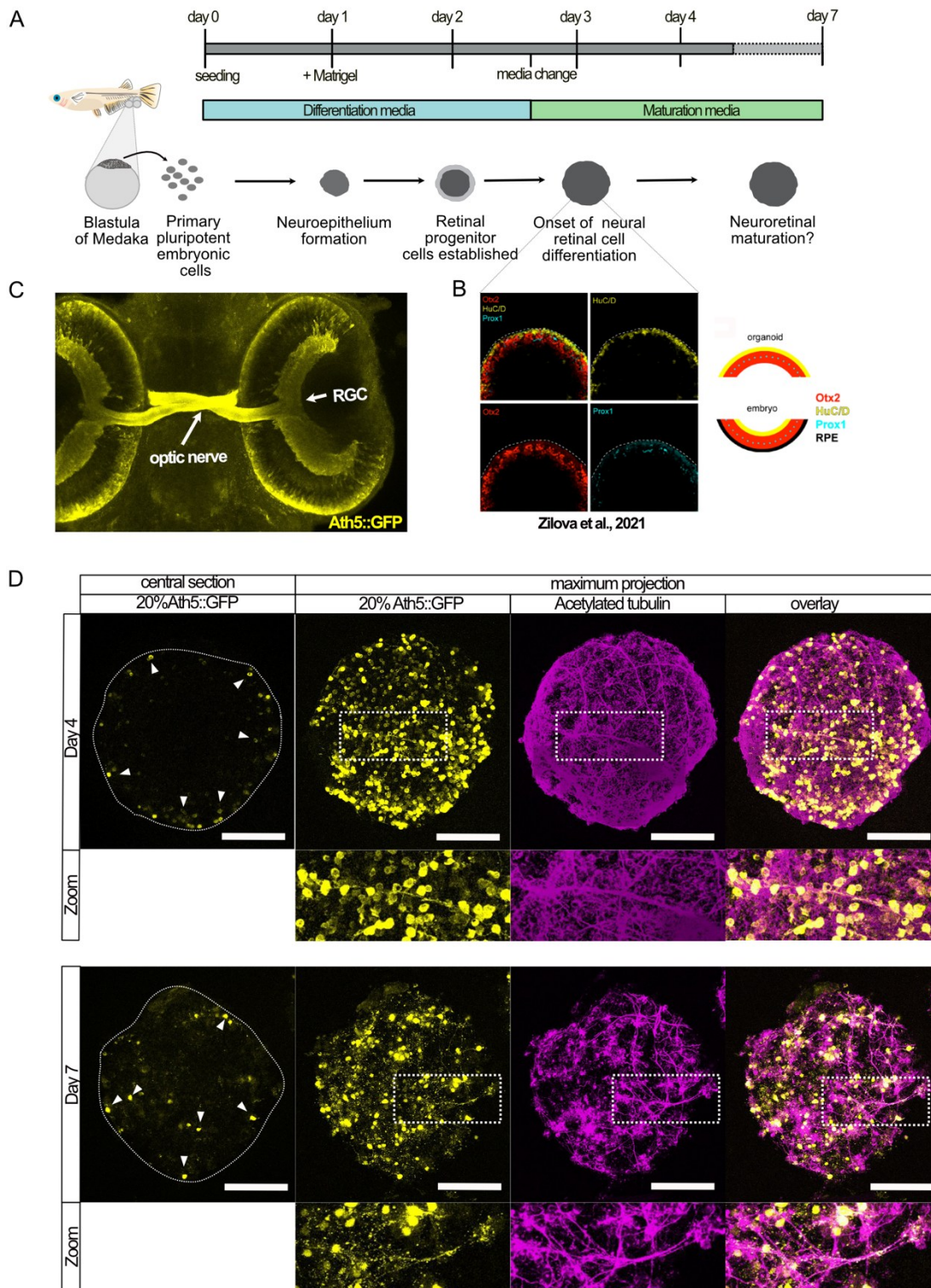


Figure 2.10: Retinal ganglion cells and long axonal projections in 7 days old retinal organoids. (A) Schematic representation of organoid generation from primary embryonic pluripotent cells from blastula staged Medaka embryos until day 4 and beyond. Cells are seeded in differentiation media and by day 1, a neuroepithelium is formed. Matrigel is added to the culture on day 1. On day 2, organoids establish retinal progenitor cells. Media is changed for maturation media and as described in Zilova, et al. (2021), by day 4 retinal layering is

indicated. The establishment of cell retinal cell types after day 4 of culture are not described yet. (B) Panel of retinal cell markers on day 4 and scheme of inverted retinal cell layering adapted from Zilova et al. (2021). Retinal cell types are stacked in the outer layers of the retinal organoid. HuC/D positive cells localize at the outermost rim, and Otx2-positive and Prox1-positive cells layer below. The presumptive layering is inverted in comparison to the embryonic retina. (C) Retinal ganglion cells and optic nerve marked by GFP expressed in Ath5::GFP reporter fish in day 4 embryo. Maximum projection of confocal images. RGCs are localized in the innermost retinal layer and axons are forming the optic nerve projecting to the optic tectum. (D) Retinal ganglion cells in day 4 and day 7 old organoids organize in the outermost layers of the organoid and project axons. 20% of cells within the organoid are derived from embryos carrying the fluorescent reporter Ath5::GFP, and 80% of cells are wild type cells. The RGC labelled represent a fraction of the RGCs present. Acetylated tubulin marking axons of neurons within the retinal organoid and partially overlay with RGC axons. Scale 100µm.

To gain a more comprehensive understanding of general neuronal presence within the organoids, I performed immunohistochemistry labelling of all axons using acetylated tubulin (Figure 2.10 C). Within the organoids at both day 4 and day 7 of culture, axonal projections spanned through the outermost layers of the organoid and created an intersected network of individual strands. However, the number of neurons and their interconnectivity decreases over time, as by day 7, axonal projections seemed to be more distinct and separated (Figure 2.10 C).

In addition to retinal neurons, non-retinal neurons and projections between tissues were also observed (Figure 6.9). The complexity of neuronal cell projections throughout the organoid suggests an environment that supports neuron differentiation and survival. The RGCs were found to be distributed throughout the organoid rather than being restricted to one layer on the organoid surface as previously reported at day 4 (Zilova et al., 2021). Having confirmed the presence of RGCs within the late retinal organoids, I next investigated the progression of the Otx2-positive progenitor cells, specifically PR and BP precursors, over time, and whether they would be present in late retinal organoids.

2.2.2 Otx2-positive cells display striking cellular patterning beyond day 4

The presence of the RGCs in the late retinal organoid suggested the differentiation of additional retinal cell types. I used the protein orthodenticle homeobox 2 (Otx2) as a

marker to investigate the presence and distribution of potential BP and PR cells and their precursors, which express Otx2 in the neural retina (Figure 2.11 B).

I examined Otx2-expressing cells in organoids on day 4 and day 7 (Figure 2.11 A) and found that Otx2-positive cells are present at both time points. The co-presence of RGC marked by Ath5 confirmed the retinal identity of the tissue (Figure 2.11 A2, A4). Between days 4 and 7, the distribution and density of Otx2-positive cells changed, with a prominent pattern emerging by day 7. Initially, at day 4, Otx2-positive cells were distributed randomly throughout the outer layers of the organoid, especially at the outermost rim (Figure 2.11 A1). However, in the central regions of the organoid morphological distinct circular clusters can be detected (Figure 2.11 A1). By day 7, the Otx2-positive cells had organized into distinct circular clusters in both the peripheral and central regions of the organoid (Figure 2.11 A3).

The sustained presence of the Otx2-positive cells in retinal context by day 7 suggests that PR and BP are present in the late retinal organoids. To further characterize the maturation of retinal organoids, I analyzed cell types present in more mature retinae.

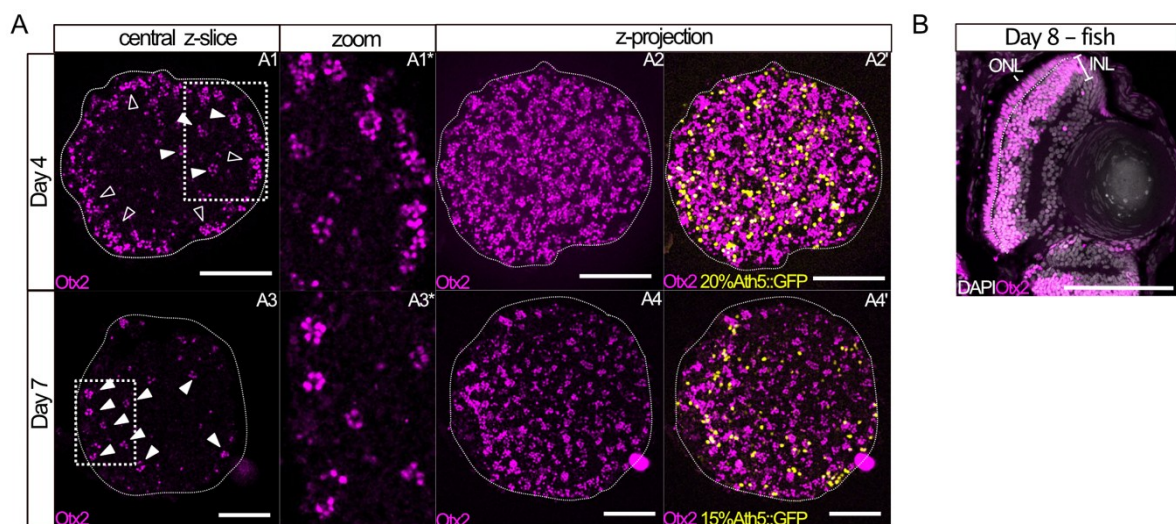


Figure 2.11: Otx2-positive cells are present in day 7 retinal organoids and form morphologically distinct clusters as the organoid matures. (A) Retinal organoids derived of wild type (wt) and Ath5::GFP reporter cells (4:1) stained for the presence of Otx2 and GFP by immunohistochemistry on day 4 (seen in n=100 organoids in N=14 independent experiments) and day 7 (seen in n=75 organoids in N=11 independent experiments). Otx2 expressing cell cluster are indicated by white filled arrow heads. Unorganized Otx2-expressing cells are indicated by unfilled white arrow heads. Zoom on central slice showing rim section in detail. Scale 100 μ m. (B) Section of embryonic retina at 8 days stained with the antibody against Otx2. PR (ONL) and BP (INL) are positive for Otx2-label. Scale 100 μ m.

2.2.3 Retinal cell types are differentiating in late retinal organoids and pattern in clusters

The neural retina (NR) exhibits a stereotypic cellular organization, comprising rod and cone PR, BP, horizontal cells (HC), amacrine cells (AC) and RGCs (Figure 2.12 B). To identify these cell types in retinal organoids, I employed immunohistochemistry to detect characteristic markers or combination of markers and compared their expression to that in the retinae of hatchlings (Figure 2.12 A).

In the embryonic retina, cone PRs are identified by co-expression of Otx2 and Zpr1, while rod PRs express both Otx2 and rhodopsin. HCs, marked by Prox1, form a layer adjacent to the PRs. BP are characterized by co-expression of Otx2 and PKC-alpha. HuC/D labels both amacrine cells and retinal ganglion cells (RGC), with RGCs specifically marked in the Ath5::GFP reporter line. The precise layering of the embryonic retina enables reliable identification of these distinct cell types based on their position and expression pattern.

In day 7 retinal organoids, all the aforementioned labels can be detected (Figure 2.12 C). Within clusters of Otx2-positive cells, Rx2-Otx2-double positive cells representing photoreceptors are positioning next to Otx2-positive only cells (Figure 2.12 C1,C2). I specifically identified cone PRs (Zpr1) (Figure 2.12 C4, C5) and rod PR (rhodopsin) within the Otx2-positive clusters (Figure 2.12 C8, C9). The remaining Otx2-positive cells that are not PR likely represent BP cells, and the BP specific cytosolic marker PKC-alpha confirmed the presence of BP (Figure 2.12 C6). HC (Prox1) are positioned adjacent to PRs (Figure 2.12 C7). Due to the lack of a specific marker, AC cannot be definitively identified. In addition to the clustering of PR, BP and HC, RGCs (Ath5) associate closely with the clusters and project axons throughout the organoid (Figure 2.12 E). Since the Ath5::GFP label only covered approximately 20% of RGCs, I labeled day 7 organoids by acetylated tubulin to capture all neuronal axons in association with the retinal clusters. This showed that axonal extensions span the distance between clusters and surround the retinal clusters and suggests a general association with of the retinal clusters with far projecting neurons (Figure 2.12 F).

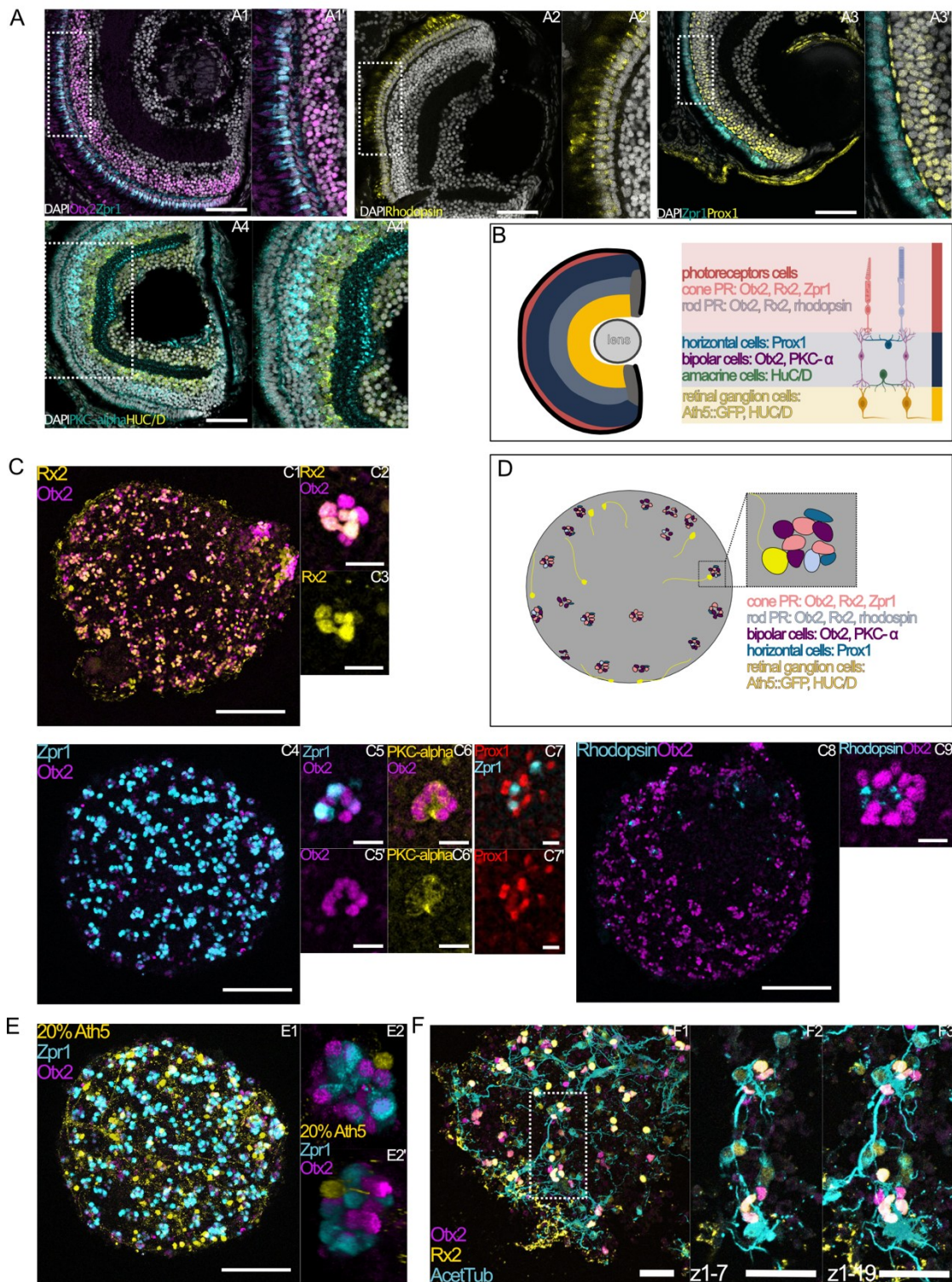


Figure 2.12: Differentiated neuroretinal cell types in late retinal organoid organize in clusters. (A) Retinal cell types stained with immune labeling in sectioned fish retina at day 8 post hatch. Otx2 labels photoreceptors (PRs) and bipolar cells (BPs), Zpr1 and Otx2 double labeling showing cone PR. Rhodopsin marking rod PR. Prox1 marking horizontal cells adjacent to Zpr1-positive cone PR. PKC-alpha marking BP and HuC/D marking amacrine cells and retinal ganglion cells (RGCs). Scale is 50 μ m. (B) Schematic representation of retinal cell layering in embryonic retina and the respective labels used to identify cell types. (C) Differentiated retinal cell types form cell clusters in the organoid by day 7. Otx2-positive cell clusters spread within organoid overlay with Zpr1-label for cone PR. Ath5::GFP positive RGCs position in-between. Otx2-positive cell clusters are formed which include Otx2- and Rx2-

double positive PR (n=16 organoids, in N=3 independent experiments), and Otx2-positive only BP. PR include Otx2- and Zpr1-positive cone PR (n=31 organoids, in N=6 independent experiments) and Otx2 – and rhodopsin-positive rod PR (n=15 in N=3 independent experiments). BP are further confirmed by PKC-alpha-staining (n=6 in N=2 independent experiments). Prox1-positive cells mark horizontal cells (n=16 organoids in N=4 independent experiments) adjacent to Zpr1-positive cone PR. RGCs are marked by fluorescent reporter Ath5::GFP, with cells projecting throughout the organoid (n=35 organoids in N=9 independent experiments). 20% of RGCs are stained due to 1:4 mix of reporter-carrying cells and wild type cells while seeding on day 0. Scale 100 μm or 10 μm . (D) Schematic summary of retinal cell types identified within retinal organoids at day 7 and their positional relation. I RGCs position adjacent to PR and BP containing clusters. Maximal projection of day 7 organoid labeled for Zpr1 (cyan), Otx2 (magenta) and GFP (20% of cells carrying Ath5::GFP reporter) and 3D reconstruction of single cluster. 3D reconstructed cluster shown from two angles, rotated by 100°. Scale 100 μm . (F) Axonal projections along retinal clusters span along several clusters. Maximum projections of organoid labeled for Zpr1 (cyan), Otx2 (magenta) and acetylated tubulin (AcetTub, cyan). Overview showing projection of 19 slices, while zoom-in on two clusters is shown for a partial stack (z1-7) and all slices (z1-19). Scale 25 μm .

I identified the presence of rod and cone PR, BP, HC and RGC organizing in a cluster arrangement. Notably, retinal cell types differentiate in the organoids but structure differently compared to the layered embryonic retina (Figure 2.12 D). To further investigate the organization of these retinal cell clusters, I next assessed the regularity of cellular composition within clusters and their positional organization relative to one another.

2.2.4 Retinal clusters have a shared cellular composition and spacing

To investigate whether the retinal cell clusters formed in late retinal organoids share a regular composition of cell types, I quantified PR and BP cells within clusters, as well as the total number of Otx2-positive cells per cluster and the spacing between the clusters (Figure 2.13 A). Using quantitative analysis of fluorescence microscopy data, I analyzed the number of cells per cluster and their corresponding markers.

Within retinal clusters, the number of Otx2-positive cells, representing PR and BP (Figure 2.13 B), ranged from 2 to 22 cells per cluster. However, the majority of clusters contained 6-9 cells as indicated by a Gaussian distribution (Figure 2.13 B). The distance between retinal clusters showed a broad distribution, ranging from approximately 20 μm to 70 μm with a double peak distribution, and an average spacing

of 45.34 μm , (Figure 2.13 C; Figure 6.10). A double peak within the minimal distance distribution could show a multiple of the single distance or hint at differential minimal distance values within organoids. Such differences might be caused by differential distances linked to the position of the cluster within the organoid, e.g. depth, but cannot be linked within this assay.

The ratio of PR and BP cells was constant and scaled with the total cell number within a cluster (Figure 2.13 D). This suggests that the cell type ratios are preserved. To further analyze this, I calculated the proportion of cell types in each retinal cluster.

Within retinal clusters, on average 67% of cells were positive for Otx2 and Rx2, identifying them as PR. The remaining 33% of cells within retinal clusters were positive for Otx2 only, determining them as BP (Figure 2.13 E). Among photoreceptor cells per cluster, Zpr1-positive cone PR represented on average 44% of cells (Figure 2.13 E). This suggests, that two-thirds of the PR within a cluster are made up of cone PR and the remaining third is made up of rod PR.

However, the presence of rod PR was not observed for every cluster (Figure 2.13 F). Due to the non-nuclear labelling of the rhodopsin marker (see Figure 2.13 C8, C9), it was not possible to clearly allocate the rhodopsin label to an Otx2-positive nucleus and consequently the number of rhodopsin label-positive cells cannot be clearly defined. Therefore, I scored for the presence of the rhodopsin label per cluster rather than per cell. On average, rod PR were present in 50% of clusters (Figure 2.13 F). This suggests that not all retinal clusters harbor both photoreceptor cell types on day 7, which might be connected to the delayed differentiation of rod PR in comparison to cone PR.

With this quantification, I could find that the ratio of cone PR and BP cells within retinal clusters is preserved. The cellular ratios are scaled with the number of cells included in the cluster and the spacing of the retinal clusters is within a minimum distance.

Having confirmed the identity of the cells contributing to the spaced clusters to be retinal, the tissue between the clusters could not be identified with the retinal markers. Therefore, I further investigated the cells covering the area between the retinal clusters.

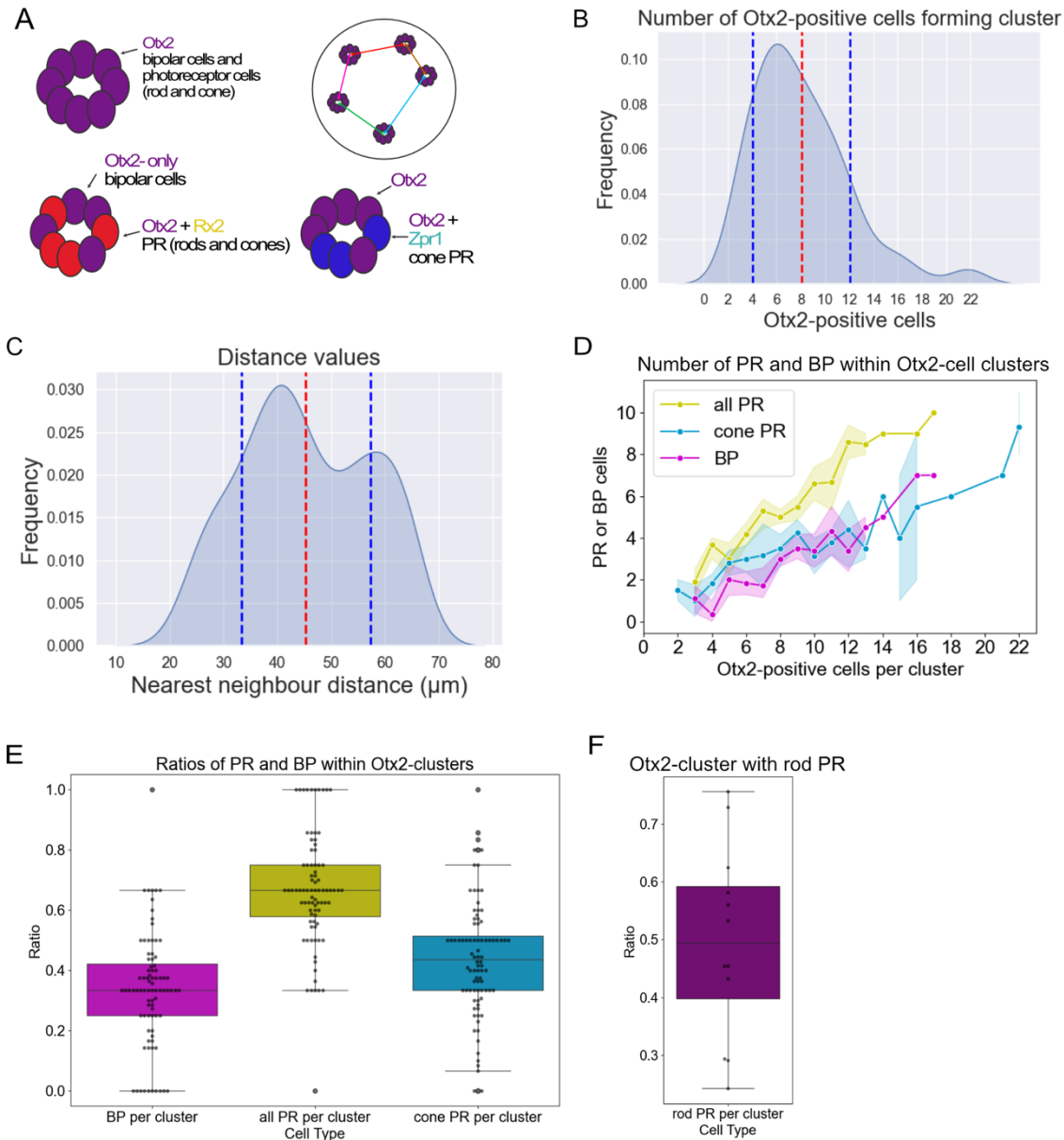


Figure 2.13: Quantification of cellular ratios and cluster distribution in day 7 retinal organoid. (A) Scheme of cell type and label association within retinal cell cluster used as base for quantifications and scheme for distance measurements of clusters within organoid. (B) Quantification of overall cell number in Otx2-clusters in day 7 organoids. Frequency of cell counts is plotted relative to Otx2-cell number counted (kernel density estimate (KDE) plot). The number of cells within one cluster ranges from 2-22 cells, the mean value is marked by red dashed line, standard deviation indicated by blue dashed lines. N=166 clusters were counted manually across N=18 organoids. (C) Distance between retinal cell clusters in direct neighborhood. Frequency of distance values between neighboring clusters plotted relative to distance in μm (KDE plot). The distance between clusters has a regularity and a minimal distance of 21 μm . Mean distance to nearest neighbor is 45.34 μm (N=10 organoids from 2 independent experiments n=159 clusters, n=279 nearest neighbor distances). Two peaks within gaussian curve indicate different minimal distance values across organoids. Description of quantification in Supplementary figure 3). (D) Number of all PR, cone PR and BP against Otx2-cell number within cluster. Number of all PR quantified by manually counting the number of Rx2-Otx2- double positive cells within an Otx2-cell cluster and from the same data sets BP were scored as Otx2 only. Within N=9 organoids from 2 independent experiments, n=78

clusters were quantified. From different samples, Zpr1-Otx2-double positive cells were scored against Otx2-cell number within respective clusters. N=9 organoids from 3 independent experiments, n=88 clusters quantified manually. I Comparison of relative contribution of cell type within cell cluster. Box plots showing ratios of BP/Otx2-cell number within cluster (median=0,33), PR/ Otx2-cell number within cluster (median=0,67) and cone PR/ Otx2-cell number within cluster (median=0,44). (F) Presence of rod PR within clusters quantified by scoring each cluster with rhodopsin label as positive (median=0,50). Across 12 organoids from 3 independent experiments, 606 clusters were scored for overlap with rhodopsin marker-staining. Ratios were made within one organoid sample and plotted.

2.2.5 Cells in inter-cluster space undergo apoptosis while clusters are stable over time

Given the previous evidence of non-retinal neurons in the organoids (see Figure 2.10 C, Figure 6.9), I investigated whether the cells between the retinal clusters were non-retinal neural cells. Immune labelling of the organoid tissue with HuC/D, a marker for post-mitotic neurons, revealed that the cells between the Otx2-clusters were not non-retinal neurons (Figure 2.14 A). Morphologically, their nuclei appeared smaller in diameter and more condensed compared to those within the Otx2-positive cell clusters, suggesting apoptosis within the cells. To test this assumption, I performed a TUNEL (Terminal deoxynucleotidyl transferase dUTP nick end labelling) assay to detect DNA fragmentation within cells on the surface of the organoid. The cells with smaller nuclei and DAPI-dense label are indeed undergoing apoptosis (Figure 2.14 B). Although the TUNEL staining was technically limited to the surface of the organoid, similar small nuclei were observed in deeper layers of the organoid tissue, suggesting that cell death may occur throughout the tissue.

Extensive cell death suggests that rather than a patterning process the retinal clusters is a result of the overall death potentially due to unsuitable culture conditions. Therefore, I extended the culture of organoids beyond day 7 to check for the maintenance and integrity of the retinal organoid. Probing for retinal markers and the presence of the cluster structure on both day 9 and day 11 confirmed the maintenance of retinal clusters containing cone PR and RGCs over at least 5 days (day 7- day 11) (Figure 2.14 C). This confirms that the formed retinal clusters are not the result of tissue death but an active patterning for the benefit of survival.

I found that the cells between the retinal clusters do not contribute to the retinal tissue and partially undergo apoptosis, whereas the retinal clusters remain stable over time. To further investigate the cellular maturation and cellular interactions within the day 7 retinal clusters, I next examined the ultrastructure using electron microscopy.

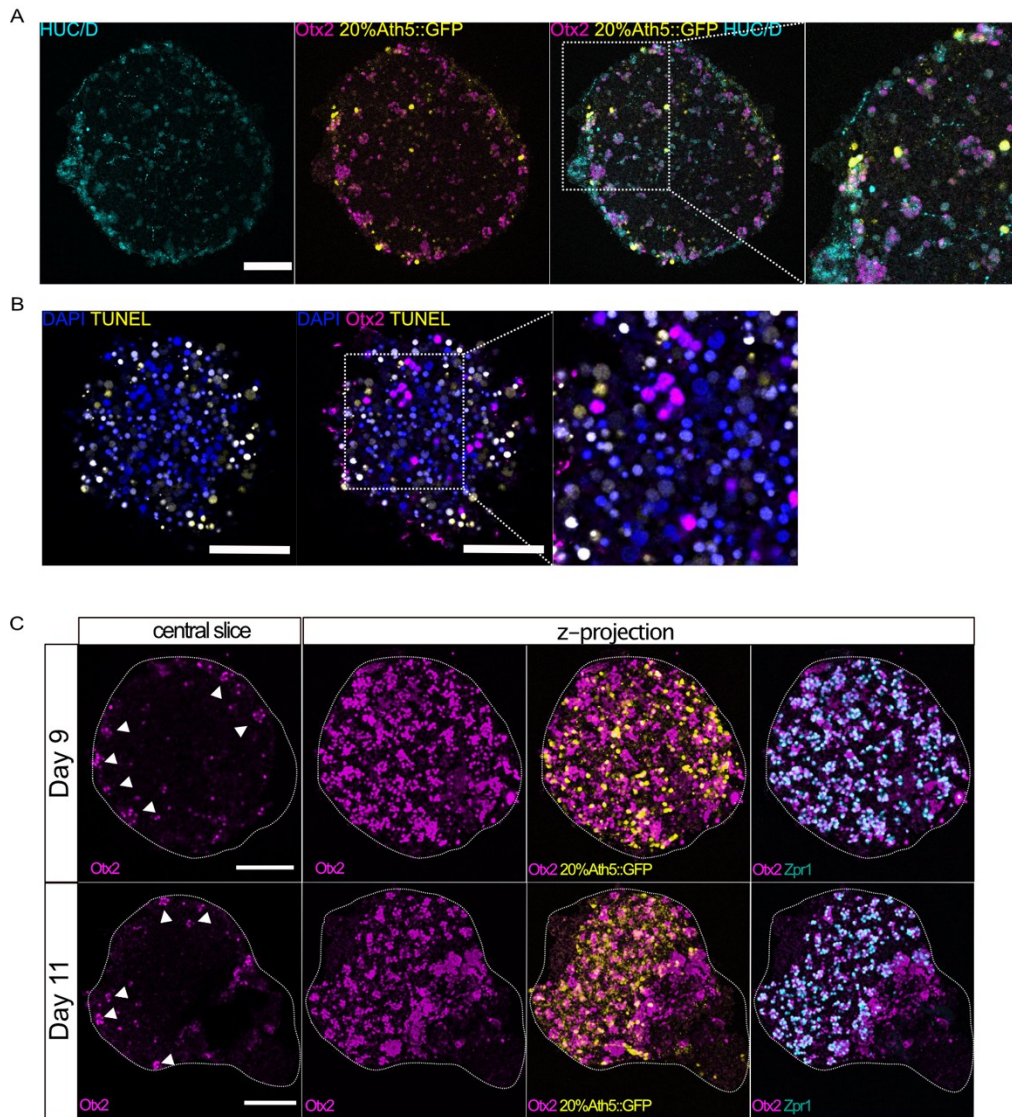


Figure 2.14: Cells between retinal clusters are dying while retinal clusters are stable until at least day 11. (A) 7 day old organoid generated from 80 % wt and 20 % Ath5::GFP reporter cells, labelled with HuC/D (postmitotic neurons) and Otx2. Scale 100µm. (B) TUNEL-assay performed with day 9 organoids to identify apoptotic cells. DAPI showing numerous nuclei with a small diameter in comparison to Otx2-positive cells. The same cells show TUNEL label on organoid surface but not in more central regions. Many cells in vicinity of Otx2-clusters are TUNEL positive. Scale 50 µm. (C) Retinal organoids derived of wild type (wt) and Ath5::GFP reporter cells (4:1) stained for the presence of Otx2, Zpr1 and GFP by immunohistochemistry on day 9 (n=11 organoids in N=3 independent experiments) and day 11 (n=15 organoids in N=3 independent experiments). Otx2 expressing cell cluster are indicated by white arrow heads. Scale 100 µm.

2.2.6 Retinal clusters show tight association visible in ultrastructure

To examine the interaction and maturation of the cells within a cluster, electron microscopy images of retinal cell clusters were obtained through a collaboration with the group of Rasmus Schröder at Heidelberg University. In the ultrastructure of day 7 organoid, retinal cell clusters were identified by the integrity of cells and cellular organization (Figure 2.15 A, Figure 6.11). A representative cluster shown in Figure 6A consists of seven cells in direct contact with each other (Figure 2.15 B). The membranes of the cells are closely connected via tight junctions (Figure 2.15 C). Synaptic vesicles indicating the presence of synapses could not be observed. Even though the specific cell types are difficult to interpret based on the cellular ultrastructure, axonal projections were found in three of the 7 cells. Furthermore, cilia extending from the cell body were found in two cells (Figure 6.12). Both are characteristics of RGCs and PRs. The maturation of PR is characterized by the formation of outer segments. The sensory cilium with membrane folds displays a characteristic architecture. Within the acquired data sets, no structural components resembling outer segments of PR could be detected.

The findings from the ultrastructural analysis suggest a strong association between retinal cells within a cluster, indicating their survival and maintenance as a unit. No evidence of cellular maturation or synapse formation could be detected; however, this could be connected to the z-resolution of the sections or the developmental stage of the organoid. To understand the patterning process involved in the formation of the retinal clusters, I investigated the onset of cluster formation at the tissue level.

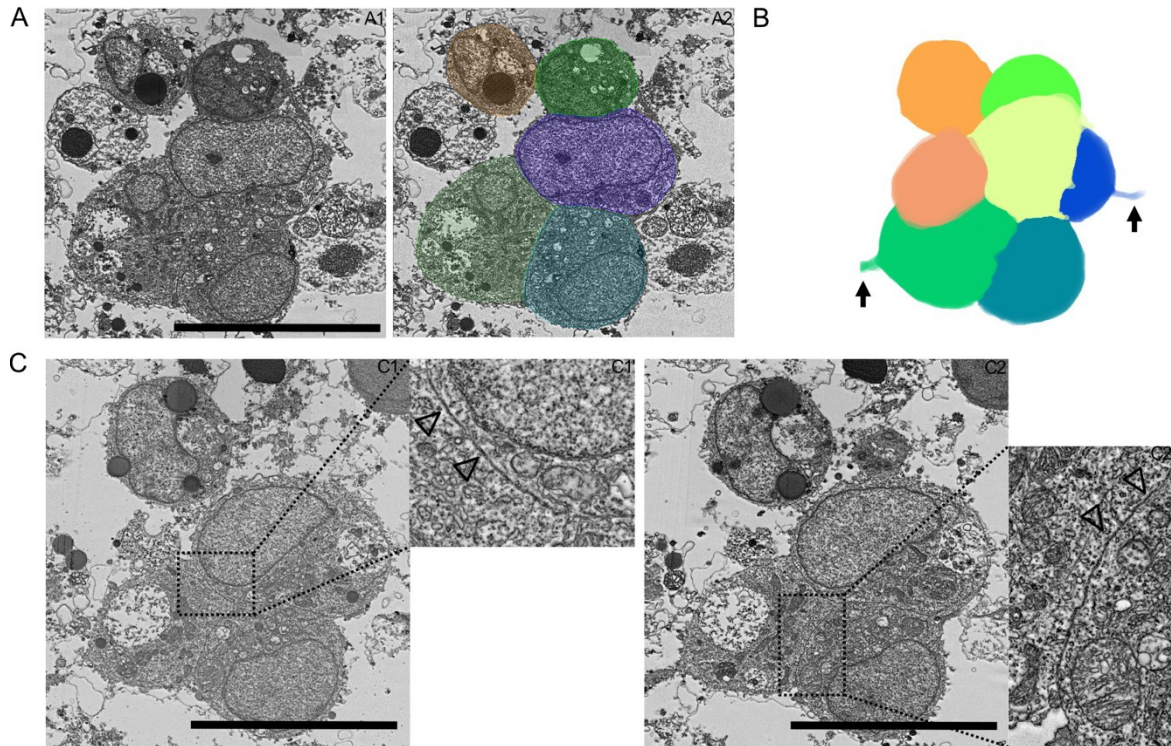
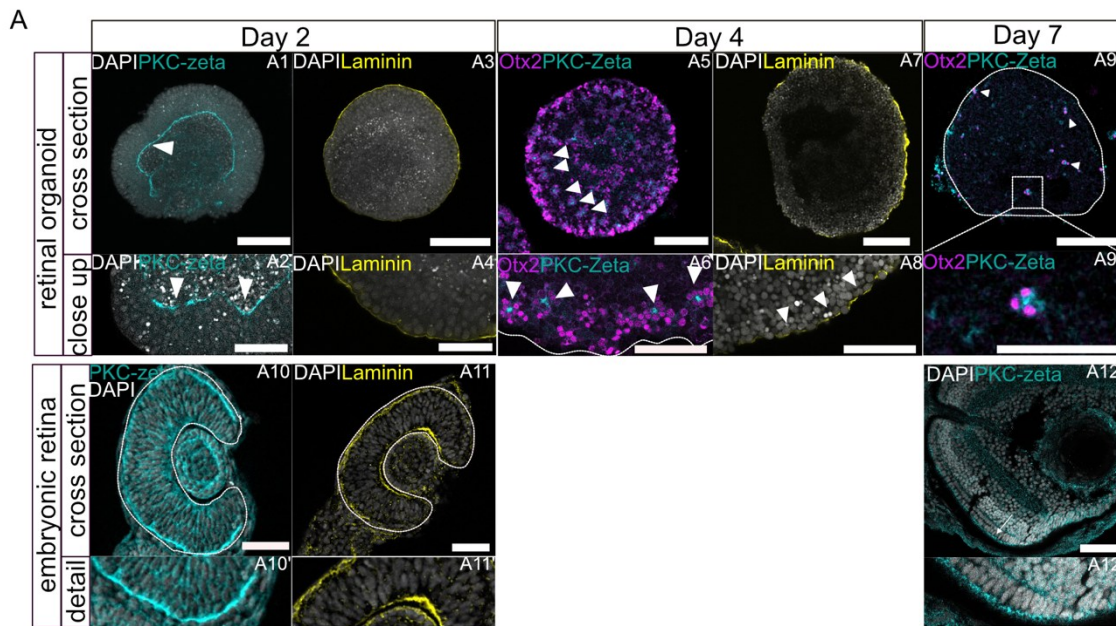


Figure 2.15: Ultrastructure of retinal cell clusters show tight association of cells. (A) Example of cell cluster in day 7 organoid imaged with electron microscopy. Single z-plane of cell cluster showing 5 of 7 tightly associated cells within the cluster. The same plane overlaid with segmentation markup using Amira. Scale 10 μ m. (B) 3D projection of seven segmented cells forming a cluster. Three cells show axonal projections. Two of those are visible in the displayed orientation (indicated by arrows). (C) Membrane association between neighbouring cells within cell cluster and close up. Unfilled arrow heads pointing at dense membrane regions indicating tight junctions. Scale 10 μ m.

2.2.7 Reorganization of neural retina going along with loss of global tissue polarity

The retinal cell clusters described in this study are not observed in the medaka retina, where stereotypic retinal layering is established by day 5 (stage 34) (Kitambi and Malicki, 2008). In contrast, organoid cultures exhibit a continuous retinal progenitor cell epithelium on day 2, which transitions to periodic retinal tissue in the form of clusters by day 4. To understand the transition from a neuroepithelial tissue layer to separate retinal clusters, I investigated the epithelial structure and polarity of the retinal organoid tissue over time.



B Polarity within embryonic retina vs. retinal organoid over time

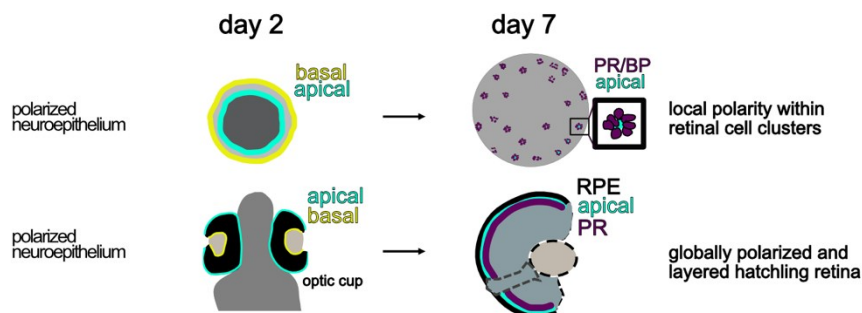


Figure 2.16: Loss of tissue polarity from within organoid development precedes cluster patterning process. (A) Polarity of retinal tissue retinal organoids in comparison to medaka embryos from day 2 to day 7. Optical cross sections of organoids and embryonic retina are shown. PKC-zeta marking apical cell polarity and Laminin marking basal pole of cells. Polarity of RPCs on day 2 in retinal organoids show a global structuring as an epithelium with the apical (PKC-zeta) marker on inner surface of epithelium (marked by arrow head), and basal marker (Laminin) on the periphery. In the embryo, the apical pole of the retinal tissue within the optic cup is facing the brain, while the basal side of the tissue is facing the lens. By day 4, Otx2-positive clusters are formed in the organoid with an apical pole towards the center of the cluster (marked by arrow heads). Laminin label on the outer rim of organoid is discontinuous (marked by arrow head). By day 7, the polarity is retained as the apical marker PKC-zeta can be found in the center of Otx2-cluster. In the retina of medaka fish at day 7 of development, the apical polarity in PR is still present at the interface to the RPE. Scale organoid cross sections 100 μ m. Scale organoid close up and embryonic retina 50 μ m. (B) Schematic of polarity in retinal organoids and the embryonic retina of medaka. The retinal organoid has a polarized epithelium on day 2 of culture with the apical pole facing the inside of the organoid, while the basal is on the outer rim of the organoid. In the optic cup of the embryonic retina, the apical pole is facing the outer rim of the retina, towards the head. The basal pole of the tissue is facing the lens. Therefore, the retinal organoid is polarized as the OC, but inverted. By day 7, retinal cell clusters are formed in the retinal organoid, with the apical pole of the Otx2-positive cells facing the center of the cluster. A local organization of the tissue has formed. In the embryo, the apical pole of the tissue remained at the outer rim of the retina facing the RPE, formed by the Otx2-positive PR cells. In the embryo, tissue polarity is kept over time and a layered retina is forming, while in the organoid, the retinal cells organize in localized structures with a tissue polarity.

On day 2 of culture, the continuous epithelium exhibits an apical-basal polarity, with the apical side (PKC-zeta) on the inner rim of the epithelium and basal (Laminin) on the surface of the organoid (Figure 2.16 A1-A4). This is similar to the apical and basal polarity in the optic cup of the medaka embryo at stage 24, which is positive for the apical marker on the proximal cup where the future PR layer will be localized and for the basal marker Laminin on the lens facing side (Figure 2.16 A10, A11).

Over the next two days, the epithelial structure of the organoid tissue is lost, and the cluster phenotype emerges (Figure 2.16 A5-A8). Each formed cluster establishes a separate polarity, with the apical side oriented towards the center of the cell cluster, while the Laminin label is still positioned on the organoid surface but in a less continuous pattern (Figure 2.16 A7, A8). This cluster polarity pattern is maintained over time, as seen by the same apical polarization towards the center of the clusters on day 7 of culture (Figure 2.16 A9, A9'). The basal marker Laminin could not be detected in day 7 organoids (data not shown). In contrast, the medaka retina maintains its epithelial polarization throughout development, with the apical rim on top of the PR layer and the basal side at the RGC layer (Figure 2.16 A12, A 12').

These findings suggest that the time point from which the alternative and substructure patterning is induced can be allocated to a time point between day 2 and day 4 (Figure 2.16 B). To understand the formation of clusters on a cellular level, I next investigated the clonal relationship within a cluster during this period.

2.2.8 Clusters are formed by several unrelated progenitors

During organoid maturation, the polarized epithelial tissue is replaced by retinal cell clusters with organized retinal cell composition. Within the retina, retinal cell types differentiate in a timely and spatially organized manner. To determine whether this organization arises from a single multipotent progenitor clone giving rise to all cell types or through the active attraction and clustering of specific precursors from different progenitor cells, I investigated the clonal relationships between cells within clusters. I employed a reporter line ubiquitously expressing GFP throughout all progeny.

For the experiment, I created a mixture containing 80% wild-type cells and 20% GFP-expressing cells, which I then subjected to standard retinal organoid culture protocols (Figure 2.17 A). By day 9, I fixed the organoids and used immunohistochemistry to detect GFP and Otx2 expression. With this approach, I identified Otx2-positive cell clusters composed of GFP-positive and GFP-negative cells next to non-labelled and fully-labelled clusters.

These findings suggest that the retinal cell clusters are not formed from one progenitor cell, but rather are composed of cells from different origins (Figure 2.17 B). Instead, the cells appear to actively group together to form retinal cell clusters with mixed cellular identity. To further understand the patterning process, I next addressed the impact of signaling pathways on the cluster-formation.

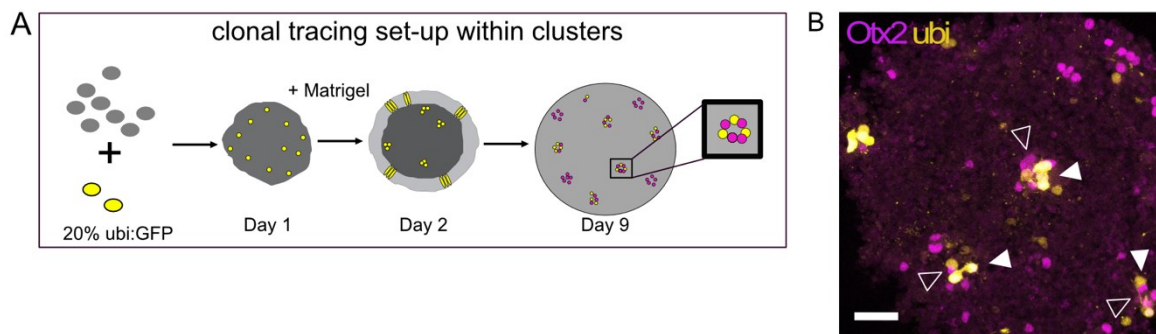


Figure 2.17: Cells contributing to Otx2-clusters from different clonal origin. (A) Scheme showing the experimental set-up of clonal tracing in the retinal organoid and a schematic representation of the outcome. Unlabeled wild type cells are mixed with GFP-labelled cells while seeding organoids on day 0. In the course of maturation GFP-positive clones are expanding. Analyzing GFP-labeled and unlabeled cells within Otx2-positive clusters allows to follow up on clonal relationship of cells within retinal cell cluster. (B) Otx2-cluster are made of cells of different clonal origin as seen in the mix of GFP-labelled cells (filled arrow head) and GFP-negative cells (empty arrow head). Scale 25 μ m.

2.2.9 Pattern formation is impacted by Notch-signaling

To understand the patterning mechanism underlying retinal cell organization in the organoids, I used chemical inhibitors to block factors known to be important for the periodic patterning in the *Drosophila* retina.

First, I targeted Notch-signaling by inhibiting of the gamma-secretase with DAPT, which blocks the cleavage of the Notch receptor. This treatment was applied prior to the onset of retinal cell type differentiation, as defined by the onset of Ath5::GFP

reporter expression, which is happening in the night from day 2 to day 3 (Figure 2.18 A). Following DAPT-treatment, Otx2-positive clusters exhibit two different morphologies: small clusters of up to 25 cells that were spaced apart in the day 4 organoid (Figure 2.18 B5, B6, B9), and large clusters of Otx2-positive cells with up to over 100 cells that formed long stretches along a common apical pole (Figure 2.18 B4, B7, B8). The smaller clusters seem to form more on the organoid surface while the bigger clusters form more centrally. In contrast, the untreated group showed, as seen before, the formation of clusters more centrally but on the rim a less organized and broader Otx2-positive cellular organization (Figure 2.18 B1, B2, B3). Across two independent experiments with a total number of N=14 organoids treated with DAPT, 71% (n=10) show a patterning phenotype and 28% (n=4) show no alteration in patterning.

Previous studies have demonstrated that Notch-inhibition by DAPT affects retinal cell differentiation. Specifically in the post-embryonic retina, Notch-inhibition at the retinal progenitor stage has been found to impact the ratios of RGCs and other retinal progenitors by an increase of RGCs upon DAPT- treatment (Perez et al., 2018). To ensure that retinal cell differentiation was not globally affected by Notch-inhibition, I compared RGC counts in treated and untreated samples. No significant difference in RGC number was observed, indicating that the DAPT treatment did not cause a major shift in retinal cell type differentiation (Figure 2.18 C).

Supplementation of BMP- and Shh antagonists, factors involved in the patterning process defining the retina in drosophila, and periodic pattern formation, prior to the onset of NR differentiation did not result in a patterning phenotype (Figure 6.13).

Taken together, Notch signaling plays a role in cluster formation, leading to both reduced separation and more regular spacing of clusters on day 4 of culture. Having approached a basic patterning process involved in forming the cluster-phenotype, the question remained of which factor is missing to allow for a layered retinal structure.

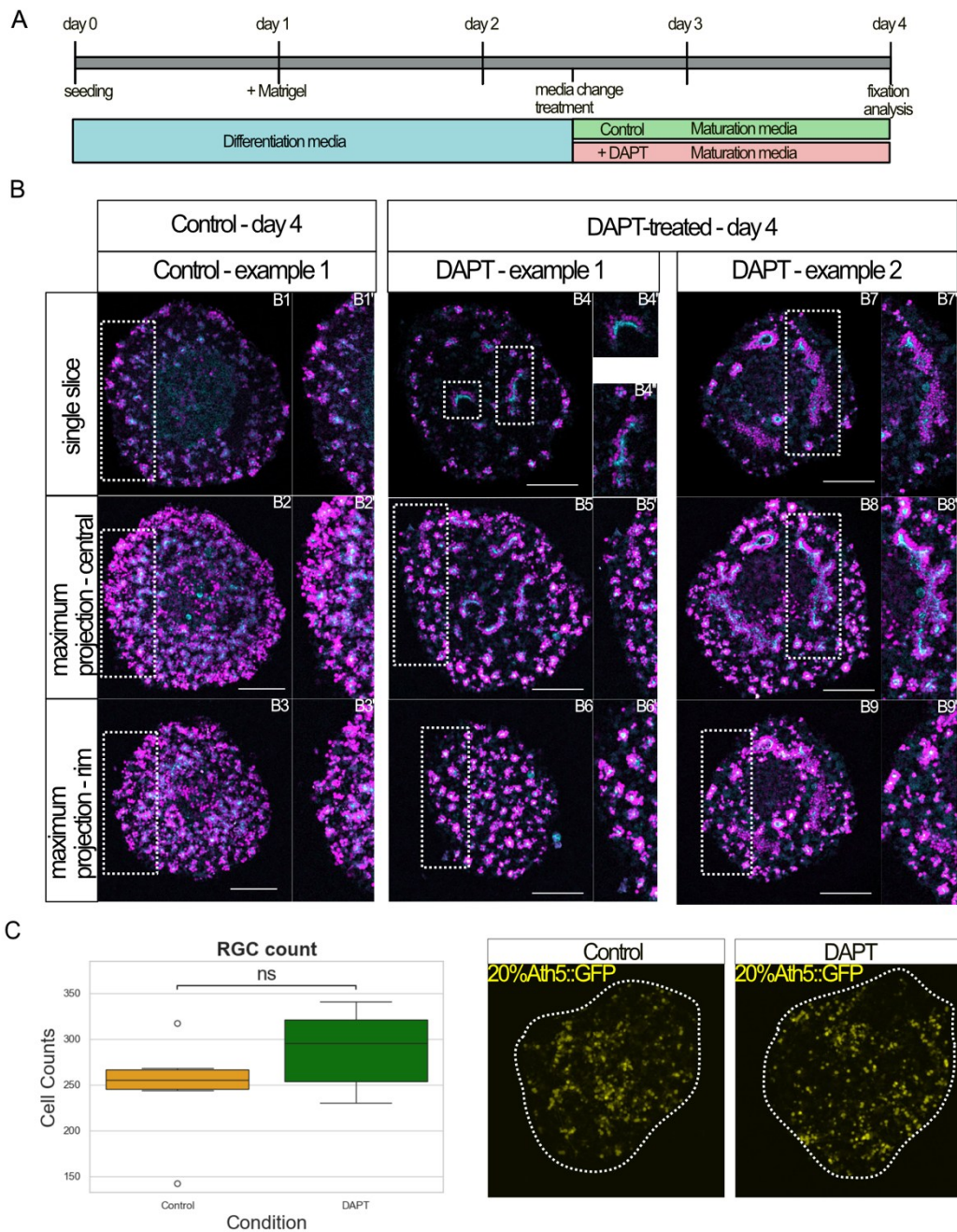


Figure 2.18: Notch-signaling is involved in cluster formation. (A) Experimental outline of treatment with Notch-inhibitor DAPT. Organoids were grown until late day 2 under standard conditions in differentiation media and addition of 2% Matrigel on day 1. From day 2, pre-onset of retinal cell differentiation, organoids were treated with 10 μ M DAPT in maturation media or cultured in maturation media only (control). Organoids were incubated until day 4. Afterwards the samples were fixed, immune stained and imaged. (B) Organoids treated on day 2 with DAPT show two sizes of Otx2-positive cell cluster forming. Panel shows examples for control (n=1) and DAPT-treated (n=2) organoids and a single central slice, as well as maximum z-projections of the outermost slices (rim) and central slices (central) to display cluster morphology. Small clusters are forming on the organoid rim with a more distinct spacing compared to the Otx2-positive cell clusters in the untreated control. Elongated clusters of Otx2-positive cells are forming, which include many cells from more centrally. Clusters show polarization with apical polarity towards center of cluster. The untreated control shows beginning cluster formation, but denser compared to the DAPT-treated samples. Across two independent experiments with a total number of N=14 organoids, n=7 show strong phenotype, n=3 show a less strong phenotype and n=4 show no altered phenotype. Scale 100 μ m. (C)

Quantification of Ath5::GFP-positive cells within control and DAPT-treated samples show no significant change in the overall numbers (n=6 organoids for each condition, independent two-sample t-test). SUM Projection of Ath5::GFP DAPT treated and untreated organoids.

2.2.10 Layering of cell types in presence of Laminin

While the neuronal cells in the retinal organoid are locally organized into small structures, the developing retina of the embryo maintains a stable polarization and tissue layering throughout development. In the organoids, an epithelialized tissue containing RPC is formed by day 2, similar to the polarized tissue in the optic cup of the medaka embryo at stage 24. However, as the culture progresses the epithelial tissue is replaced by retinal clusters on day 4.

Retinal layering in the embryo is dependent on the epithelial and polarized tissue arrangement. Given the role of the extracellular matrix (ECM) in structuring the retina during embryonic development, I hypothesized that supplementation of the retinal culture with Laminin could support the maintenance of an epithelial organization from day 2 onwards.

Therefore, I performed organoid culture and supplemented Laminin on day 2, before the loss of epithelial layering, and analysed the cellular layering on day 4 (Figure 2.19 A).

The results showed that supplementing Laminin from day 2 indeed maintained epithelial structuring and horizontal layering (partial and complete) within the day 4 organoids (Figure 2.19 B). In five independent experiments, with a total number of N=28 organoids, 21% (n=6) of organoids showed that most of the retinal tissue was epithelialized and polarized, while 64% (n=18) showed partial stretches of polarized tissue. In 14% (n=4), no layer of Otx2-positive cells with common tissue polarity was seen comparable to the untreated control (Figure 2.19 B). Notably, the polarized epithelium was oriented with the apical side towards the inside of the organoid and was therefore inverted in comparison to the embryonic retina. On the level of cellular organization, the retinal cells are arranged in layers, with the RGCs positioned in the outermost layer and an Otx2-positive cell layer positioned more centrally adjacent to the RGC layer (Figure 2.19 B).

These findings show that Laminin has a key role for epithelial tissue structure and retinal patterning in the medaka retinal organoid culture. The inversion of the tissue orientation is likely caused by the initial tissue polarization on day 2. I next asked whether a non-inverted layering can be achieved in the retinal organoids when initial culture conditions are changed.

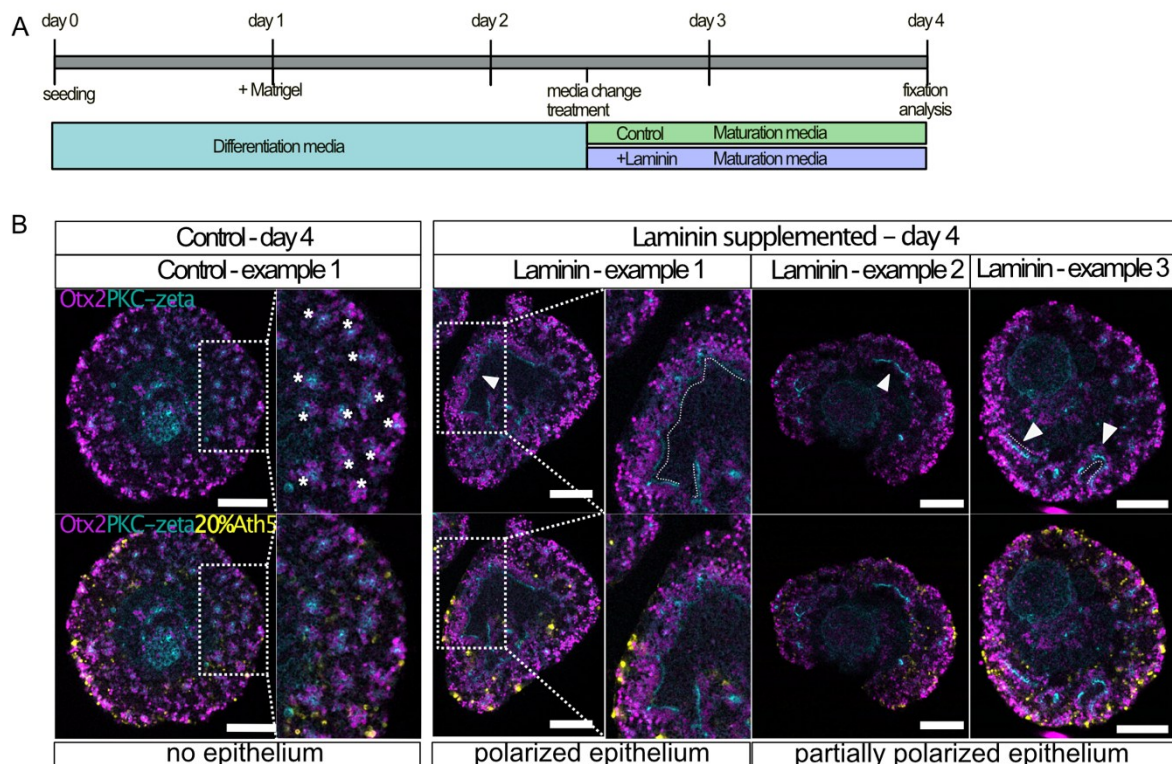


Figure 2.19: Supplementation of organoids with Laminin is sufficient to restore epithelial layering of neurons in retinal organoids. (A) Experimental outline of organoid culture supplemented with 25 μ g/ml Laminin from day 2 to day 4. Organoids were grown until late day 2 under standard conditions in differentiation media and addition of 2% Matrigel on day 1. Pre-ceeding the loss of tissue polarity, media was changed to maturation media and for Laminin-exposed samples, 25 μ g/ml Laminin was added to the well. Samples were incubated until day 4. Afterwards the samples were fixed, immune stained and imaged. (B) Loss of layering upon progression of organoid development after day 2 can be partially prevented by Laminin-supplementation by day 2. In Laminin-supplemented culture, tissue stretches stay polarized by day 4 and cluster formation is prevented. Otx2-positive cells line up with pical pole towards the center and RGC arrange in a layer adjacent facing the outer rim of the organoid. The layering is similar to the retinal layering only being inverted. In five independent experiments, with a total number of N=28 organoids, n=6 (21%) were majorly polarized, n=18 (64%) partially polarized and n=4 (14%) were as the untreated control. Scale 100 μ m.

2.2.11 Organoids cultured without Matrigel establish non-inverted epithelial tissue regions

The inverted polarization of the retinal tissue is a characteristic feature of standard retinal organoid culture, visible on day 2. However, I observed that the presence of Matrigel on day 1 is not required for the organoids to adopt retinal fate and form an epithelium with RPCs (see Figure 2.7; Figure 6.7). To investigate whether the presence of Matrigel affects the polarization of the retinal tissue and potentially also affect the pattern formation in consequence, I cultured organoids without Matrigel and analyzed their morphology on day 4. Additionally, I supplemented Laminin on day 2 to examine its influence on tissue patterning in this context (Figure 2.20 A).

Organoids cultured without Matrigel partially establish epithelial and layered retinal tissue with non-inverted polarization by day 4 (Figure 2.20 B). The polarized tissue regions were observed in the outermost layers of the organoid with the apical side oriented towards the surface of the organoid. Within these stretches, Otx2-positive cells form a dense layer of Otx2-positive cells underneath the PKC-zeta marked apical border, while RGCs layered more centrally within the organoid. Notably, some areas exhibited elongated Otx2-clusters, in which Otx2-positive cells were arranged on both sides of the apical marker, and RGCs were positioned adjacent to the Otx2-cell layer (Figure 2.20 B). However, in more central layers of the organoid, small circular Otx2-clusters are forming (Figure 2.20 B).

These results show that organoids cultured in the absence of Matrigel partially establish non-inverted retinal tissue with a layered organization. This suggests that the presence of Matrigel may be responsible for the inverted polarization observed in standard retinal culture. This tissue polarization, however, cannot be established within the entire retinal tissue. The small Otx2-cell clusters observed in the Matrigel-treated condition without Laminin-supplementation are also formed within the non-Matrigel condition in the more central layers of the organoid.

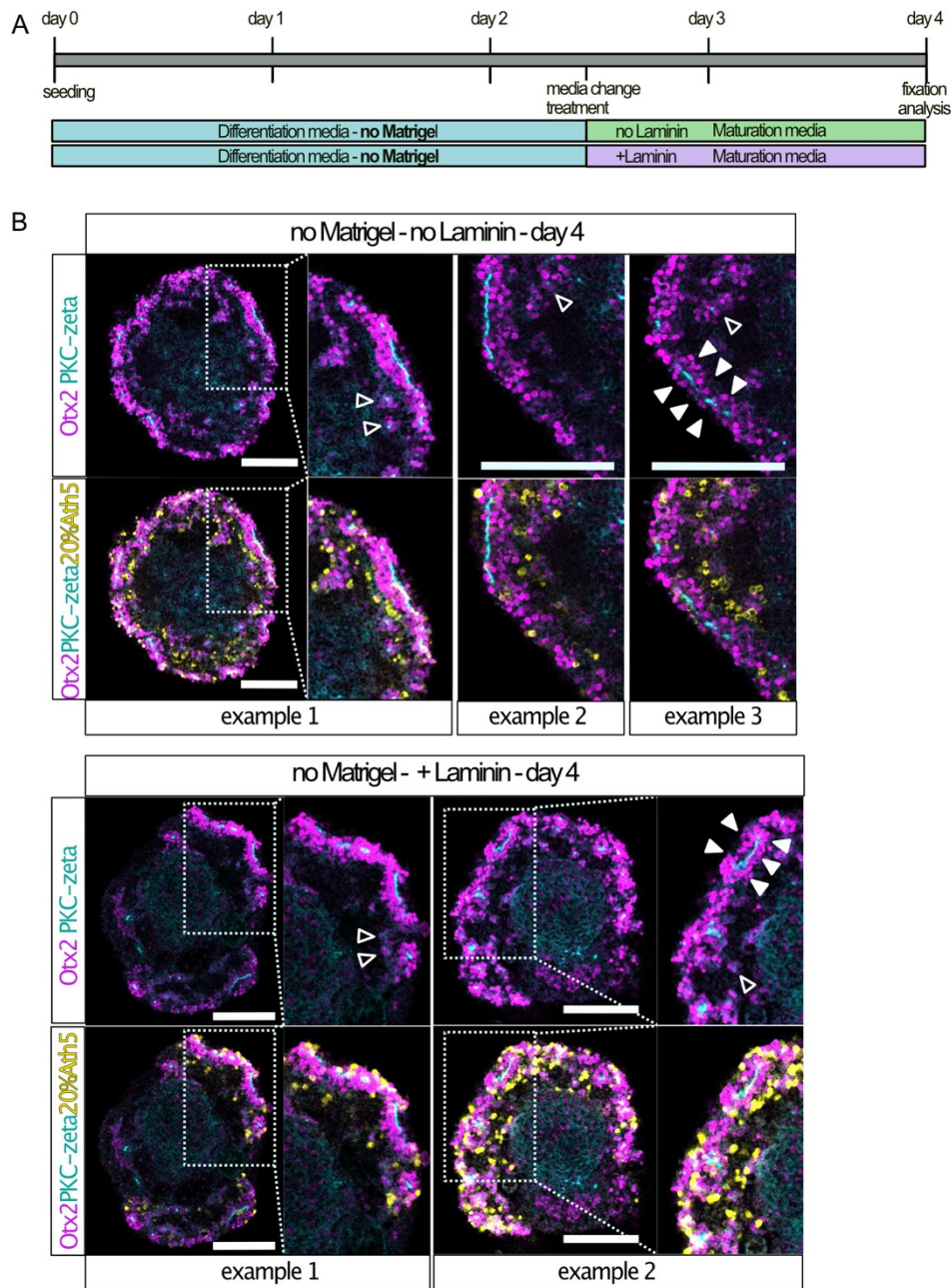


Figure 2.20: Retinal cells partially arrange in non-inverted epithelium when cultured without Matrigel from day 1 to day 2. (A) Experimental outline of organoid culture grown without Matrigel and supplemented with 25 μ g/ml Laminin from day 2 to day 4. Organoid culture is not supplemented with Matrigel on day 1. On late day 2, media was changed to maturation media and for Laminin-exposed samples, 25 μ g/ml Laminin was added to the well. Samples were incubated until day 4. Afterwards the samples were fixed, immune stained and imaged. (B) Optical sections of organoids stained for Otx2 (magenta), apical marker PKC-zeta (cyan) and for GFP (20% of cells with Ath5::GFP reporter). Organoids cultured without Matrigel and with or without Laminin as indicated in (A). Filled white arrow heads marking Otx2-cells arranging on both side of apical marker PKC-zeta. Unfilled white arrow heads point at small Otx2-cell clusters in the more central layer of the organoid. Scale 100 μ m.

Taken together, within medaka retinal organoids the majority of neuroretinal cell types is differentiating by day 7. The retinal cells form clusters with reproducible complexity, size and distribution when cultured in the standard conditions (Matrigel +; Laminin -). Although the cells within the clusters are tightly connected, maturation and synaptic connections could be shown. Notably, the establishment of the retinal culture is influenced by Notch-inhibition suggesting a role for this pathway in regulating cluster formation. When supplementing the organoid culture with Laminin from day 2, a polarized epithelial arrangement of retinal cells is established by day 4. Interestingly, omitting Matrigel from the culture allows for the formation of non-inverted retinal cell arrangements by day 4, but also in this condition Otx2-ell clusters are forming. This suggests that the presence of Matrigel during early stages of organoid development induces inverted retinal tissue polarization but for the cell layering more cues not to be provided.

3. Discussion

This study described different aspects of tissue self-organization in medaka retinal organoids and the processes involved in structuring the tissue in absence of the embryonic environment. Based on the alternative tissue pattern forming, I addressed questions towards single cues impacting on the tissue organization and tissue specification during organoid development. I tested the impact of tissue bending as a mechanical cue on the formation of the CMZ. Further, I characterized the cellular organization in the late retinal organoid by day 7 and presented the spontaneous formation of retinal cell clusters containing differentiated neuroretinal cell types. Along with the spontaneous tissue formation, I inspected the effect of the inhibition of the Notch signaling pathway and Laminin supplementation on retinal cell patterning. In the following, I will discuss the results obtained and the patterning principles, as well as the self-sufficiency of the system, to be deduced from this study. Finally, I will address how the organoid system, in which the cells organize detached from the embryonic constraints, could provide insight into evolutionary questions.

3.1 Epithelial bending and its impact on CMZ formation

In this study, I set out to test the impact of tissue morphology on the establishment of the CMZ within retinal organoids. The shape induction was performed at two developmental time points: pre-RPC establishment (day 1) and after RPCs were established and had formed a polarized epithelium (day 2). From the experimentally enforced tissue shape change, I could not conclude a causative connection of tissue morphology and CMZ-marker expression. While some experiments showed spontaneous CMZ-marker positive tissue formation in both the control and the treated condition, complex tissue composition including retinal and non-retinal tissue did not allow to conclude a shape-related impact on CMZ formation.

Since the experimental set-up aimed to simplify the morphological changes in OC formation and mainly impose a mechanical bending force onto the neuroepithelium, the approach covers a limited parameter space compared to the complex OC

morphogenesis. In the following I will discuss the impact that was generated on the retinal tissue by the shape-approach, the predominant importance of cell shape and the potential influence of the 3D environment on CMZ cell type induction.

3.1.1 Tissue polarization, mechanics, dimension and limitations within the experimental set-up

A key aspect of tissue bending during OC formation is epithelial polarization, which determines the specific side of the tissue that is affected. Between the experiments performed, the polarization of the tissue differed related to the time point of organoid transfer into the constricting shapes (day 1 and day 2).

Organoids treated on day 2 were exposed to Matrigel for more than 24h and obtained a polarized, RPC-containing tissue. In contrast, the organoids treated at day 1 experienced a shortened exposure to Matrigel of 6h and when tested on day 2, the tissue had not polarized. ECM components as Laminin have been shown to be indispensable for the establishment of the pseudostratified epithelium within the OV and for cell polarization (Ivanovitch, 2013). Therefore, the cells likely did not receive sufficient structural input by ECM to create a polarized epithelium when exposed only for a few hours to Matrigel. This difference in polarization results in differential impacts on the RPC-containing tissue. Although NR cell differentiation is initiated in unpolarized retinal tissue, the structural state of the tissue introduces an additional variable to the temporal difference in treatment between day 1 and day 2 to the experimental set-up. As a result, direct comparison between samples from different days can not be done.

For the polarized tissue in day 2 organoids, the intended 90° angle in the rectangular shape was impacting along the apical (inner) side of the epithelium. The actual bending angle induced along the apical side of the tissue could not be controlled due to the open and non-restrictive top and bottom of the mould and therefore varied between samples. During OC formation, the epithelial bending is occurring along the apical side of the tissue and the CMZ is established within the hinge domain (reviewed in Sokolova et al., 2023). Therefore, manipulation of the day 2 organoid targets the same tissue side as in the *in vivo* morphogenesis. Along with the bending of the

epithelium during OC formation, the NR acquires a convex curvature characterized by basal constriction and apical relaxation (Martinez-Morales et al., 2009). In the organoids exposed to the bi-axial bending, the originally convex basal side of the tissue sphere was forced to obtain a concave curvature with an opening angle of 120° . Within the more complex C-shape and X-shape therefore, apical bending of the epithelium, as happening in the CMZ, was enforced next to a tissue stretch forced to do basal tissue bending, which combines two major morphological steps during OC formation. Within the shape approach, key tissue morphologies can be enforced. The tissue angles induced, however, did not result in an instructive cue for CMZ formation.

In OC formation, a more drastic bending angle approaching 180° , as compared to the 120° in this study, is leading to the formation of the hinge domain. The question remains if a more extreme bending might be necessary to induce the CMZ. Although I did not observe bending-induced CMZ-specific gene expression, I could spot spontaneous emergence of Cndp1-positive tissue. The spontaneously emerging Cndp1-positive tissue regions obtained morphologies ranging from an arched shape to a more pronounced tissue curvature. This variation in the gross tissue morphology suggests a non-exclusive tissue morphology for the CMZ tissue in respect to the bending angle and that the extreme tissue angle is not inherently connected to CMZ tissue establishment. Within the OC, it might be forced to the degree of bending by the 3D environment.

While the time point of tissue bending, either before or after the establishment of RPCs, was considered in the experimental set-up, the possibility of a simultaneous process of shape and fate specification could not be simulated in the static shape format. Within crypt formation of intestinal organoids, it was found that tissue mechanics and cell fate induction are happening concurrently and are reinforcing each other (Pérez-González et al., 2021). A similar, iteratively reinforcing process could be connected to CMZ formation. However, the plasticity seen in the fate decisions among RPCs would suggest that cell fate determination towards either NR, RPE or CMZ fate can be impacted by external cues and even provide a window of trans-differentiation potential (Cai et al. 2010; Rowan et al. 2004; Sokolova, 2023). Ongoing research while this study was performed showed that CMZ fate can be induced within RPCs, independent of OC morphogenesis (Sokolova, 2023). Although morphogenesis is not

strictly required, tissue morphology appears to be closely linked to the CMZ-marker expressing tissue.

3.1.2 CMZ morphology and its connection to cell shape

The spontaneous emergence of Cndp1-positive tissue regions in the organoids suggests conditions for the tissue to form independently from externally applied signaling input or mechanical cues. Further, some tissue traits appear to be associated with CMZ identity. Next to the mentioned tissue curvature, a characteristic columnar cell-arrangement was established. The curvature of the tissue indicates that the cells underwent constriction of one cell side, likely the apical side. The polarity of the Cndp1-expressing tissue was not tested but due to the tissue polarization at day 2, the apical side of the tissue is expected to be on the inner side of the epithelium. This indicates that cellular constriction and the columnar cell shape are tightly connected to CMZ fate. The causality, however, could not be dissected in this study.

Bending within the hinge domain between the presumptive NR and RPE regions was assumed to be connected to apical cell constriction as the apical side of the tissue is folding (reviewed in Sokolova et al., 2023). A simulation based on mouse organoids proposed the relevance of lateral constriction for the formation of the hinge domain (Okuda et al., 2018). Irrespective of the type of constriction, these intracellular processes aiding the process of tissue bending are not targeted directly in the performed approach. It is unclear whether the bending of the epithelium on tissue-scale can induce the intracellular constriction, or whether the tissue bending can only be the result of apical, lateral or basal constriction. A study performed by Okuda et al. (2018) could show a lasting impact of mechanical pressure on intracellular tension within an epithelium even beyond the time frame of exposure. As the induced morphological change of the retinal tissue in my assay was rather gross relative to the cell size, cells were possibly able to evade the tissue constriction by rearrangement within the tissue. Especially, the non-epithelialized tissue on the surface of the organoids on day 1 could allow for a greater degree of evasion. Further the tissue stiffness is likely important for the mechanical impact on the cells when the tissue is bend. To assess the mechanical resistance on the tissue-level, mathematical simulation of the impact generated on the tissue would be instructive.

In the context of studying shape and fate, therefore the next step would be the transition from tissue shape to cell shape level. Intracellular shape changes need to be targeted with intracellular tools. Artificial induction of cellular shape changes was done utilizing the optogenetic construct OptoShroom3, which causes apical constriction upon light induction and resulted in epithelial bending (Martínez-Ara et al., 2022). In that study, Martínez-Ara et al. noticed that the polarization of OV in retinal organoid tissue with the apical side oriented to the inner surface of the epithelium, complicates the bending. The presence of the non-retinal cells in the central part of the medaka organoid could cause similar resistance as seen by Martínez-Ara et al. as the retinal tissue formed at the organoid rim is directly interfacing with non-retinal tissue more centrally in the organoid body. Mechanically, in the embryo, the OV is invaginating against the dorsal part of the OV and therefore bending against the epithelial tension of the tissue only and not against a non-retinal cell mass as in the organoid. Studying the effect of apical constriction on RPC cell fate with a tool like OptoShroom3 requires medaka retinal organoids forming OVs, which can be generated with a variation in cell seeding number (Zilova et al., 2021).

Interestingly, the CMZ-fated tissue spontaneously formed in my experiments exceeded the size of the CMZ domain seen in the embryonic retina. *In vitro*, bigger regions of CMZ-like tissue can be generated, which is interesting in respect to studies on regeneration. However, the emergence of Cndp1-positive tissue is not sufficient to conclude the establishment of retinal stem cells. The cellular characteristics and their potency to create RPCs and retinal cell types remain to be determined.

The spontaneous formation of the CMZ in medaka retinal organoids independent of external mechanical or chemical cues again raises the broader question of the necessary environment for the CMZ to form from the neuroepithelium in medaka. The 3D environment created by the neighboring tissues as the RPE and NR, but also the non-retinal tissue and the ECM can impact CMZ formation, not only on the mechanical level, but also on cell signaling and structural level. To consider the specifying roles of cellular interfaces for the medaka organoid patterning further, I will discuss aspects to be learned from the performed experiments on tissue-tissue and tissue-ECM context possibly necessary for the CMZ induction in the context of medaka.

3.1.3 Dependency of CMZ induction on tissue-tissue and tissue-ECM interactions

Within the assay, I restricted the analysis of CMZ induction on the experiments in which the control organoids obtained exclusively NR tissue, and neither non-NR tissue nor CMZ marker expression. This restriction was done to specifically read out the effect of tissue curvature on cell fate induction in the shape-restricted condition. However, the neighboring tissues could be necessary for tissue-tissue communication creating the proper pre-disposition of the cells to become CMZ-fated.

Within the spontaneously induced CMZ regions, no definitive environment posed by NR or RPE could be determined as a prerequisite for CMZ formation. Based on the experiments showing that Wnt-activation in day 2 RPCs can induce retinal stem cells as indicated by *Cndp1*-expression in retinal organoids (Zilova, unpublished), a source of Wnt/ β -catenin is likely acting as an inductive factor for CMZ fate. This could be provided extracellularly or produced and secreted by the cells themselves. It was reported in the mouse organoid culture that Wnt/ β -catenin is spontaneously expressed in the dorsal OV where it specifies RPE (Hasegawa et al., 2016). The interface with the non-retinal tissue could induce the spontaneous Wnt-expression in the organoids. Also, the mechanical induction of Wnt/ β -catenin was shown upon mechanical tension (Muncie et al., 2020). Potentially, a change in cellular morphology preceding the cell fate could induce the CMZ formation. With recent engineering approaches, a source for a Wnt-ligand can be placed into the organoids and create an artificial, localized Wnt-source for RPE induction (Afting et al., 2024). With such engineering approaches, tissue interfaces as well as signaling sources can be induced and could help to understand the pre-requisites for CMZ formation.

As a fundamental difference in the retinal organoid cultures of medaka, cells in mouse and human retinal organoids display a distinct morphogenesis of the OC. The absence of morphogenesis and the multipotent RPCs in the medaka organoid on day 2 formed the basis for my hypothesis to test the impact of mechanical tissue bending on CMZ induction.

Interestingly, for mouse retinal organoids, retinal morphogenesis can only happen when retinal and non-retinal tissue are interfacing. The separation of the OV from the

non-retinal neuroectodermal tissue interferes with the formation of an OC or RPE in the absence of the non-retinal tissue (Eiraku et al., 2011). However, the formation of the OC is independent of both, surface ectoderm or lens, and is therefore only dependent on the tissue interaction of retinal and brain tissue (Hasegawa, 2016). In human organoid culture, OC formation happens independently of non-retinal tissue, or the RPE, including the apical convex structure leading to tissue curvature (Nakano et al. 2012). Nakano et al. hypothesize that the thickness of the neuroepithelial layer is relevant for the process. This suggests that the retinal morphogenesis relies on different levels of autonomy and tissue-context in a species-specific manner.

Another aspect of this differential levels of autonomy encompasses the supply with ECM proteins. Several processes depending on ECM as for retinal tissue polarization and also, as discussed later in section 4.2. for proper retinal cell layering, appears not to be achieved independently by the cells.

Within the retinal organoid systems of mouse and human, Matrigel is applied until retinal marker expression (Rx) is induced (Eiraku et al., 2011; Nakano et. al, 2012). Within mouse and human systems, no external addition of ECM is required for OC formation and retinal differentiation. Dorgau et al. (2018) reported that retinal cells within human retinal organoids produce Laminins during organoid culture. This likely poses a difference to the retinal cells in the medaka retinal organoid system. From day 2 onwards, medaka retinal organoids depend on external supply of ECM to proceed with epithelialized retinal tissue formation. In zebrafish, Laminin interaction with the basal side of cells has been found to be important for cell migration involved in OC formation (Soans et al., 2022). Further, the absence of Laminin in the brain was found to cause failure of basal constriction and epithelial invagination (Gutzman et. al., 2008). This suggests that the presence of ECM, such as Laminin, could be instructive for apical or basal constriction processes, which are also connected to CMZ formation. Yet, when culturing organoids in presence of Laminin from day 2 to day 4, as done to test for layer formation, no OC formation was seen. Since the topology of the Laminin surrounding the forming OC seems to be of high relevance, the composition and porosity created by the ECM might not have suited OC induction (Soans et al., 2022).

The formation of the retina across species has found the adaptations necessary to meet features like developmental speed and spatial scales and seems to have evolved

with a degree of plasticity (Fuhrmann et al., 2020). The OC formation and retinal development within teleosts has been found to include specific processes as rim involution for the OC formation, which have not been described for mammalian systems (Heermann, et al., 2015) The non-autonomous process of OC formation and retinal cell layer specification for NR, CMZ and RPE in the medaka organoid could be related to a missing ECM component, or to a non-suitable or missing interface with non-retinal tissue on the organoid rim.

In conclusion, the applied change in tissue shape could not induce the formation of a CMZ. The possibility to test mechanical impact on cells and tissues in the organoid context creates a simplified platform in comparison to the embryo, but due to the complexity of these impacts, the tailored mechanical impact and read-out require further improvements. Supporting the experimental set-up with mathematical modeling and probing for the intracellular effect of cells affected by the shape change on tissue-level could help to understand the cellular mechanosensitivity better. It is very likely that a combination of several instructive signals is needed to instruct CMZ cell fate as signaling molecules, neighboring tissues and compartmentalization within the retina. The organoid system allows to apply cues iteratively and in combining as well as investigating them live, which opens further possibilities to study CMZ formation and mechanical cues in development.

3.2 Retinal patterning in late medaka organoids

The second objective of this study focused on another patterning process within the retinal tissue: the differentiation potential of neuroretinal cell types and tissue structure in late retinal organoids. Within the scope of this project, I focused on the cellular composition and arrangement in the organoid at 7 days of culture, which represents a time point at which the differentiation of all NR cell types and stratification are established in the embryo. I showed the establishment of retinal cell types in 7-day old organoids and the reproducible arrangement of the retinal cells in a cluster pattern. The clustered arrangement and regular spacing of these clusters are contrasting the retinal layering of medaka embryos. The regularity of clustering suggests a patterning mechanism driving a specific combination and a certain number of cells to come together and form a retinal cell cluster. I tested the impact of selected signaling pathways on the cluster formation and was able to achieve a layered retinal cell arrangements in 4-day old organoids when the culture was supplemented with Laminin. Following up on the pattern formation in the late retinal organoids upon Laminin treatment as well as exploring the ability of cell maturation beyond day 7 covering also the maturation of late born retinal cell types are intriguing to study in more detail in a follow up study.

In the following I will discuss the cellular composition and the patterning of the tissue in the late retinal organoid, as well as the possible modes of cluster formation and the importance of laminin for the epithelial tissue structure.

3.2.1 Neuroretinal cell types differentiation in late retinal organoids

The retinal cell clusters found in the late retinal organoid are composed of RGCs, BP, HC, cone and rod PR, therefore the majority of NR cell types found at day 7 in the embryo are present in the organoid. The reoccurring composition of clusters was assessed quantitatively based on the position of PR and BP. Cone PR were found within all clusters, while the presence of rod PR was varying between the organoids and averaged to 50% of clusters containing rod PR. Rod PR differentiate the latest among the neural cell types in the retina and only by 9 dpf (stage 39), rod PR are

established throughout the complete retina in the medaka embryo as seen by the expression of rod opsin (Kitambi and Malicki, 2008). Within the medaka retinal organoid culture, a close similarity in developmental time frames was seen with a delay of 3 hours in the initial stages of organoid development, likely due to the dissociation of cells (Zilova et al., 2021). Within retinal cell type differentiation, a delay of a few hours up to one day can be seen by the differentiation of RGCs beginning by 2.5-3 days of culture as compared to 2 days in the embryo and the detection of Zpr1-expression by day 6 of culture as compared to 4.5/5 days in the embryo (organoid data not shown, Kitambi and Malicki, 2008). This suggests a delay of one day in the retinal differentiation process, which needs to be considered for further analysis on functional aspects.

The ultrastructural analysis of the retinal clusters on day 7 showed some cells with a pair of extending cilia. The extension of processes has been reported in ultrastructural analysis of PR prior to outer segment (OS) formation and could therefore indicate an early stage of OS formation (Crespo and Knust, 2018). The establishment of OS is only achieved at embryonic stage 39 and gets more pronounced towards the adult stage (Kitambi and Malicki, 2008). The impact of light exposure on OS establishment is not clear, while no positive effect of light on outer segment establishment was seen in zebrafish or human, a positive effect was seen in mouse (Crespo and Knust, 2018; Contín et al., 2016; Bonezzi et al., 2023). With *in vitro* grown PR, the effect of light exposure on the maturation of PR could be explored independent of the effect on the whole organism (Koger et al., 1999).

The non-neural cell type of the retina, Müller glia (MG), was not specifically probed for within the characterization. In the medaka embryonic retina, Müller glia are described to be forming at later stages of development but it has not been precisely stated when (Centanin and Wittbrodt, 2014). Due to their requirement for a rather stiff environment to form and stretch properly, the disruption of epithelial structure early on could interfere with MG establishment (Prieto-Lopez et al., 2024). For the maintenance of the epithelial structure of the retina, the presence of MG is important and would especially be interesting to follow up on in Laminin supplemented, epithelialized organoids.

3.2.2 Retinal cell cluster as a minimal structural unit of retinal organization

The cell type composition within the clusters represents the main components of the retinal signaling axis and suggests the possibility of a functional connection within the clusters. In this study, the question towards the functional connection between the cells and their interaction is not covered and tests on neuronal activity and light sensitivity would be compelling next steps. However, I could show a tight association between the cells in the ultrastructural analysis, as well as the maintenance of the clustered organization until at least day 11. This supports the possibility of a reciprocal support of the cells within the cluster, which among neurons includes the need for neuronal activity (Meyer-Franke et al., 1998).

Diverse modes of retinal patterning can be seen across the animal kingdom and also between teleost species. A striking example in zebrafish and medaka retinal patterning is a difference in the PR mosaic pattern (Tohya et al., 2002). Irrespective of the patterning differences, the functional outcome and cellular layering in vertebrates are very similar. The described retinal cell clusters within this study drastically differ from the retinal cell arrangement in the medaka embryo. In disease states like retinitis pigmentosa, the formation of 'rosettes' within the ONL has been described which is connected to the loss of connection to the outer limiting membrane (reviewed in Hoon et al., 2014). These rosettes are formed from a layered retina and are represented by mainly PR forming loops within the ONL. Other retinal cell types are rarely involved. The rosette formation is a destructive process and does not resemble the clusters in the organoids. A clustering of the diverse retinal cells within vertebrates has to my knowledge not been reported. However, the arrangement of retinal cells in clusters is known for compound eyes in insects, like *Drosophila*. The circular arrangement of PR within the *Drosophila* retina together with pigment cells and interspaced by lattice cells creates a retina made of regularly spaced single units (reviewed in Warren and Kumar, 2023). The cellular composition within one of these so called ommatidia is sufficient to perform the visual signal transduction. Within the retinal organoids, a cellular composition reflecting the players in the vertebrate retinal signal transduction are forming separate clusters and potentially represent similar units as for the compound eye. To understand the process of retinal cluster formation, I took advantage of concepts of patterning processes described within teleosts and *Drosophila*.

3.2.3 Mechanism of retinal cluster formation

The establishment of the retinal cell clusters along with cellular differentiation suggests a process which is not destructive but constructive. But does it follow an energetically cheap regime or an active pattern formation?

The retinal organoid is a result of cell assembly and maturation void of factors present during *in vivo* retinal development like the adjacent embryonic tissues as well as the other retinal layers (RPE, CMZ). The way in which cells organize in this reduced context might hint towards an energy efficient patterning mechanism initiated upon the absence of organizing signals. The composition of the retinal cell clusters with respect to cell-cell ratios was found to be homogenous, with PR and BP having a 2:1 distribution that scaled with the overall number of cells within a cluster. The reproducible and regular distribution of different cell types within the organoid cell clusters suggests that such arrangement is a result of an (active) patterning process.

The composition of cell types within the retinal cell clusters hints at a patterning mode which could be connected to a functional aspect of combining cell types for the signal propagation across retinal cell types in adequate ratios. The conclusion drawn from the clonality-tracing, suggests that the cluster formation is orchestrated across different RPCs by either active grouping or local differentiation. Retinal neurogenesis in zebrafish embryos was proposed to result from coordinated differentiation of retinal cell types from different progenitor cells within a confined tissue region and subsequent migration to the appropriate layer (He et al., 2012; Almeida et al., 2014). A similar scenario might be happening in the medaka retinal organoids: due to the lack of a global tissue organization provided by an epithelium, the cells differentiate but fail to migrate towards a specific layer. However, If this process was happening only omitting the cell sorting into layers, differentiating retinal cells should cover as a result the whole organoid circumference in a continuous layer. Since this is not the case, a spacing mechanism needs to be involved in the patterning process, as well as the coordinated clustering of cell types of different cell fates.

Whether cells are defined to contribute to a cluster by their position and differentiate accordingly or whether cells obtain a specific cell fate and are then organizing together by active movement remains elusive. However, different ways of patterning can be

hypothesized based on cell type coordination events described, which I will outline in the following.

Initially, RPCs cover the organoid surface as a continuous tissue and only later, along cell differentiation, the spacing of the retinal cell clusters is established. Based on the stochastic stem cell model in the gut, RPCs could be multipotent and stochastically generate retinal cell types (Simons and Clevers, 2011; He et al., 2012). To coordinate such stochastic events to achieve the combination of different cell types, cell fates obtained in close vicinity need to be regulated. It was shown that retinal cells can influence the cell fate of their like-cell neighbors in cell culture experiments, as RGCs are inhibiting the fate of their neighbor to become RGC (chick) (Waid and McLoon, 1998) and AC inhibit their neighbor to become AC (rat) (Belliveau and Cepko, 1999). Therefore, it is likely that a similar negative feedback system within the retinal clusters is involved to achieve the diverse cellular composition.

The arrangement of retinal cells relative to another can be separated in the distance to like-cells and the relative position to unlike-cells. Within the same cell type (like-cells), the positioning of the retinal cells in the embryonic retina creates a mosaic, in the lateral view. Active migration of differentiating AC in mice was described to create a regular spacing to the already defined neighbor (Galli-Resta et al., 1997). Among the same cell types, autonomous, local regulators have been suggested to help the patterning of each cell type individually by inhibition (Stenkamp et al., 2002). While the spacing within the same cell type is highly ordered, the cellular spacing between different cell types (unlike-cells), does not follow a clear pattern. Across the cell layers (ONL, INL, RGC layer), the cells do not form columns of synaptically connected cells (Rockhill et al., 2000). The signaling of neighboring cell types could be potentially involved, but has not been reported yet.

For the cone PR mosaic in zebrafish, dual signaling to coordinate like and unlike-cells has been proposed: inhibition of a like-cell to occupy the nearby space and a permissive or inductive signal for unlike-cells to position closely (Stenkamp and Cameron, 2002). As the founder cell for this process, red cone PR have been suggested (Wan and Stenkamp, 2000). Within the organoid, the initiation of a retinal cell cluster could also be related to a founder cell which induces the organization of cell types around.

From regeneration studies in zebrafish it was concluded, that the formation of new retinal cell types requires a starting cell for organizational cues, which needs to be provided by a new born cells and not from a mature environment (Stenkamp and Cameron, 2002). For the role as a founder cell, an early differentiating cell type like RGCs or, as proposed for the zebrafish cone mosaic, cone PR are potential candidates.

To check whether a nucleation is happening around either cell type, knockout of RGC or cone PR and the subsequent patterning of the retinal cell types within the organoids will be instructive. Further, if initiation of cell type differentiation around the differentiating RGCs or cone PR were induced in wild type conditions, localized proliferation signals around forming RGCs or cone PR would hint at cluster nucleation initiated by these cell types. Generally, an increased proliferation in the cluster would hint at the induction of cell differentiation based on the position of the cells.

The second scenario, the attraction of differentiating cells by an organizing cell will be indicated by cellular movement towards those organizing centers as best analyzed by live imaging with appropriate cell markers. Following up on an cells labeled by an ubiquitous label or cell type specific label will display the mobility of the cells and whether they are actively migrating within the organoid to contribute to a cluster. Further, combination of reporters for different cell types, such as RGCs, cone PR and HC, would be instructive to follow up on cellular differentiation and pattern formation relative to another in space and time.

Interestingly, a gradual formation of Otx2-positive cell clusters from central to peripheral can be deduced from the label-positive cell distribution on day 4. Initially, Otx2-positive cells form clusters in the more central layers of the organoid while being less organized and more evenly dense in the outermost layers. By day 7, the clusters are also formed in the outermost layers. The change in Otx2-positive cell distribution from day 4 to day 7 indicates a reduction or rearrangement of these cells in the outer layers of the organoid. By day 4, the Otx2 expression marks progenitors for BP and PR and within this stage the cellular organization seems not to be fixed yet in the outermost layers. The formation of the Otx2-positive clusters over time suggests a selection process for cells to contribute to a cluster or, when out-selected, likely

undergoing apoptosis as indicated by a high degree of cell death amongst cells located between clusters.

Cell death within organoid cultures and also retinal development is not unusual. In retinal development of zebrafish and *Drosophila*, cell death is involved (Hoke and Fernald, 1998; Monserrare and Brachmann, 2006). In the absence of immune cells in the organoid cultures, dying or dead cells are not efficiently removed and eventually accumulate over time. While a high number of cells seems to undergo apoptosis, potentially also due to a lack of signaling activity for the neurons (Meyer-Franke et al., 1998), the cell death could also be connected to the cell cluster spacing. Out-selected cells not contributing to the retinal cell clusters might receive a death signal and consequently impact on the spacing between the retinal clusters. Such death signal could be provided by Notch signaling, known for inducing apoptosis in neural progenitor cells (Yang et al., 2004).

Notch-delta signaling has also been connected to local anti-clustering (Stenkamp and Cameron, 2002). This process is also involved in the formation of circular PR cluster in a periodic pattern in the *Drosophila* retina. The emergence of the clusters within the organoid and their relative positioning to each other likely requires such a local signal repressing direct neighboring cells to contribute to the cluster to create the spacing of the retinal clusters. To address the impact of Notch signaling on the patterning process of the retinal cell clusters, I employed chemical inhibition of Notch by DAPT before the onset of retinal cell differentiation. I analyzed the Otx2-positive cell distribution as a proxy for the effect of Notch on the cluster formation. Within the same organoids, big and long clusters of Otx2-positive cells formed more centrally in the organoid, while in the outermost layers small Otx2-clusters with pronounced spacing were formed. These two ways of cellular clustering seem to show a different effect of the Notch inhibition across the organoid depth. To better understand the effect of DAPT on the retinal cluster patterning, the concentration of DAPT and the timing of the treatment could be varied, as well as cell death within the organoids could be scored.

A known role for Notch signaling in the zebrafish retina is the induction of proliferation of RPCs at the apical side of the NR (Del Bene et al., 2008). The activity of Notch prevents differentiation, and its inhibition is thought to result in a higher number of differentiating RGCs, as seen in the postembryonic retina (Centanin and Wittbrodt,

2014; Saturnino et al., 2018). The effect of Notch is therefore also relevant for the cell type diversity within the NR. Since the number of RGCs is not affected in the organoid upon the DAPT treatment, the patterning effect is likely reflecting the cellular communication in respect to pattern formation and not due to a general shift in cell fate.

Although I could identify Notch signaling as a central pathway for the regulation of cluster formation and spacing, its inhibition does not show a uniform effect on the relative cell positioning across the tissue. This might reflect an uneven tissue organization across the organoid. This potential global structuring within the organoid could exist next to the local structure produced during cluster formation.

3.2.4 Higher-level of tissue organization in the organoids

Retinal maturation in the embryo is going along with a global temporal and spatial order of differentiation of cell types across the retina from central to peripheral. Whether a similar global tissue organization and a similar spatial and temporal gradient across the tissue is existing in the organoid is not clear and would require detailed analysis of the cell type distribution in the course of organoid development in space and time. However, a gradual formation of Otx2-positive cell clusters from central to peripheral can be deduced from the label-positive cell distribution on day 4 and day 7. This gradual progress of clustering across the tissue depth could be due to a difference in tissue structure or a temporal order of cellular organization.

A difference in tissue structure could be related to the polarization of the tissue across the tissue depth, as indicated by the relative longer maintenance of the basal marker (Laminin) on the organoid surface seen on day 4 compared to the apical label. While being less continuous than compared to day 2, the pattern suggests a maintained feature of the former epithelium. The organoid surface which is interfacing with Matrigel from day 1 to day 2 could still be impacted by its traces and affect cellular organization in the outer layers until day 4. Potentially, this structural difference in the outermost layers of the organoid causes the gradual cluster formation.

A temporal difference could be connected to the differentiation of the PR and BP from their common progenitors from day 4 to day 7. The cluster formation progressing from central to peripheral might reflect gradual differentiation of the cells and a connected separation into clusters in a temporal order across the tissue depth.

A spatio-temporal order of cell differentiation on the tissue-wide scale is also known for the NR (see Figure 1.4). The differentiation of cell types progresses from central to peripheral and causes a sequential appearance of cell type markers across the retina (Kitambi and Malicki, 2008). Additionally, across the embryonic retina, the distribution of the rod PR was suggested to be inhomogeneous based on varying intensity of the rod opsin label across the sectors of the retina (Kitambi and Malicki, 2008). The distribution of specific cell types as rod PR could also be inhomogeneous across the organoid as indicated by varying ratios of rod PR containing clusters. Within retinal development in *Drosophila*, such a spatio-temporal order of tissue formation is also occurring. The ommatidia formation is proceeding from posterior to anterior within the optic disc induced by the morphogenetic furrow (see Figure 1.4). Its progression is specifying cells from a non-differentiated epithelium to obtain specific cell fates in a space and time-dependent manner (reviewed in Warren and Kumar, 2023). Whether such a higher-level organizational component is present next to the local cluster formation in the organoids remains elusive. Investigating cell type distribution across the tissue or a temporal gradient of differentiation, e.g. by cell tracking, could resolve a global tissue organization on a whole-organoid level.

3.2.4 Impact of Laminin on retinal patterning

But how does the retinal tissue in the embryo organize in continuous layers rather than in retinal clusters? The layered tissue organization present in the embryonic retina is connected to its epithelial structure. In the context of retinal tissue structure, an ECM with a specific composition, particularly rich in Laminin, plays a crucial role. Indeed, the supplementation of Laminin to the organoid culture at day 2 was sufficient to maintain the epithelial organization and tissue polarization and the cluster-phenotype was replaced by retinal layering. On the organoid surface, facing the Laminin environment, the basal side of the NR tissue containing RGCs was established.

Interaction with Laminin was reported to be essential for RGC survival and retinal layering in chicken and in human retinal organoid culture (Dorgau et al., 2018; Halfter et al., 2005). A supporting function in retinal layering on the basal side of the tissue can be assumed in the medaka retinal organoid context. On the apical side of the tissue, facing the inner side of the organoid, Otx2-positive cells arranged in a layer below the RGCs. This result points towards the importance of a structural input for the cells to keep up the layered tissue organization. This finding suggests that the retinal cluster formation is the patterning mechanism employed in the absence of a structural component created by the ECM around the retinal tissue.

Interestingly, human retinal organoids produce laminins themselves to support the retinal cell structuring and cell survival and therefore do not need ECM supplementation (Dorgau et al., 2018). When blocking Laminin interaction by the application of a Laminin antibody at 45 days old cultured human retinal organoids, which marks the early stages of retinal cell type differentiation, retinal layering was disrupted, along with increased cell death and reduced expression of cell type markers (Dorgau et al., 2018). The disruption of layering, however, was not resulting in a cluster formation as seen in the medaka organoids. Comparing these systems, some aspects of cellular capacities can be noted. Human retinal organoids produce Laminins to support their survival and organization, but fail to properly differentiate the retinal cell types in their absence. Cells within the medaka organoids do not seem to produce sufficient ECM to support proper retinal layering but can, however, differentiate NR cell types independently.

Other than in the standard conditions, medaka retinal organoids achieve Otx2-positive cells (precursors for PR and BP) layering on the organoid surface and RGCs layering more centrally in the absence of Matrigel. However, in this condition not all retinal tissue in the organoid establishes this formation, but only regionally. The addition of Laminin neither leads to full polarization of the tissue. Potentially, the addition of a different scaffolding factor like Fibronectin or components of the complex interphotoreceptor matrix could support the cell layering and polarization in this non-inversed retinal tissue (Taylor et al., 2015; reviewed in Ishikawa et al., 2015). The interphotoreceptor matrix occupying the interface of the PR layer and their OS with the RPE is known to be important for the proper function and maintenance of the PR cells (Strauß, 2005). The absence of RPE poses as an apparent factor for the absence of

retinal layering. However, detachment of the NR from RPE was shown to not affect laminar stratification in mouse retinal organoid culture (Eiraku et al., 2011). Whether the same independency is true for the medaka retinal structure is not clear. Making use of recent engineering approaches enabling the formation of RPE and NR within the same organoid could allow to assess the support of retinal layering provided by adjacent RPE (Afting et al., 2024).

In the medaka retinal organoids, addition of an ECM component was sufficient to maintain the arrangement of the cells inside a common epithelial structure as opposed to the individual cluster formation in the absence of the ECM component.

3.2.5 Patterning transition from an array of clusters to a continuous epithelium as an evolutionary innovation

Within this study, I described the formation of retinal clusters with regular spacing and a retinal cell type arrangement comprising most neuroretinal cell types from vertebrate cells. The supplementation of Laminin maintained epithelial tissue structure and supported the inversed retinal cell layering. Within this discussion, I referred several times to patterning processes observed in the fish and in the fly to understand the pattern formation in the organoid. These species possess two different types of retinal structuring, termed the compound eye (fly) and the camera-type eye (fish). The eye has evolved in independent ways around 40 times in metazoan development and a variety of retinal structures have emerged in the animal kingdom (Schwab, 2017). The direct transition from a compound eye to a camera type eye, however, has not been described.

Could the observation made in the retinal organoid patterning process be valuable to understand how such a transition could have happened? A retinal structure which could be positioned in-between the compound eye and the camera-type eye are stemmata. Stemmata are single chamber eyes and are evolutionary related to the compound eyes. In several different instances, stemmata formed from ommatidial organization by fusion of multiple ommatidia units and through expansion of a single unit (Buschbeck, 2014). Whether ECM or the common cellular polarization was involved in the formation of stemmata has not yet been described. Polarization within

ommatidia is emerging during development and later, Laminins are important for the structural basal support of PR in ommatidia (Walther et al., 2024). Whether like in the case of the organoid patterning, an ECM component was helping the merge of ommatidia to form a spread retina as stemmata can only be speculated. As mentioned above in section 4.1, the medaka cells pose a special case in terms of self-sufficiency for retina formation compared to the mammalian retinal organoids. Within these systems, structural components enabling the retinal layering are produced by the cells themselves. Further, the retinal morphogenesis and patterning of neuroepithelium into NR, RPE and ciliary margin, are happening autonomously and are therefore more “hard-wired” than in the medaka retina. Learning these aspects of cellular capacities and tissue self-sufficiency can help to understand evolutionary robustness and species-specific adaptations of retinal development.

The medaka retinal organoids offer the opportunity to study different organizations of retinal tissue. The emergence of an inverted multilayered retina (Matrigel – Laminin), a multilayered retina (no Matrigel- no Laminin), and clustered retinal cells (Matrigel – no Laminin) from cells of an organism forming camera-type vertebrate eyes *in vivo*. Rockhill et al. (2000) phrased “The retina consists of an array of microcircuits arranged in a sheet.”, and this work contributes to the understanding of how specific factors can lead to this arrangement.

3.2.5 Organoids as a tool to study conservation, basic patterning principles and developmental robustness

The conservation of developmental processes between vertebrate species allows to study basic processes of embryonic development in more accessible organisms like fish. Organoid culture circumvents restrictions in accessibility, but the developmental processes happening in the organoid system display the structural complexity that can be independently generated by one tissue type in the absence of the embryonic environment only. Using this feature to advantage, organoid research can provide insight into basic patterning strategies employed in reduced environments.

Within the organoid system, conservation and independence of processes, e.g. pattern formations, can be addressed. Embryonic developmental processes have been widely studied across species and knowledge gained has been applied to understand similar pattern or organ formation in different species. Within this study, the possibility to study retinal patterning within the same species, the same cells, only in a different 'environment' was taken advantage of. Hereby, the most basic process of patterning achieved by the retinal cells in the culture context could be recapitulated. The comparison of differentiation and patterning mechanisms in *in vivo* organ formation with the processes observed in organoids can give insight into the importance of single factors, as shown here for the contribution of Laminin for the transition from a multi-unit tissue to a layered arrangement. It would be conceivable that cells fall "back" into an evolutionary more basic organizational state in case the scaffold, like ECM, is not provided, demonstrating the basic principles, that take over the patterning process as long as no stronger overwriting signal is given.

In the retina, fundamental differences in self-sustainable organ formation can be seen between medaka, mouse and human organoid cultures, which potentially reflect the extend of autonomous retinal development within each organism. This aspect of organoid research has not been used to its full potential, due to the focus on approaching the *in vivo* organ structure as much as possible. Only little has been extracted about fundamental principles within the organoid patterning.

Organoids develop along the plan of minimal input. Any cell fate induction apart from the 'main route', like NR fate in retinal organoids, needs to be applied externally in the medaka organoid. This feature was the basis of my objective asking for the mechanical impact of neuroepithelial tissue bending on CMZ induction. Basic principles can be more easily separated and single cues can be attempted to be addressed on a single input basis in the organoid system. However, a multi-cellular and potentially also multi-tissue structure inherently involves an interplay of different factors that can complicate the analysis of the applied cue. Analyzing the impact of tissue bending did not result in a conclusive result because several additional variations were introduced by the presence of non-retinal tissue and the unsuccessful polarization for the early developmental timepoint.

Within organoid culture, dependencies can be concluded based on the context the organoid tissue is in but alternative pathways may be used in the reduced environment a lead to different outcomes as compared to the organismal context. A pre-destined way within the embryo might be the energetically most advantageous in the context of the embryo but could be traced to a new state in free or supplemented surroundings.

4. Conclusion

The tissue complexity and patterning process in medaka retinal organoids provides insights into the self-sufficiency of the retinal cells in respect to organ formation. The curved and epithelialized tissue morphology appears to be tightly connected to CMZ fate and could not be induced by tissue bending alone. Neuroretinal cells differentiate in the late retinal organoids and the cells self-organize in clusters of recurrent cell type composition. To reinstate layering of retinal cells in the inversed conformation, ECM and especially Laminin have been presented to be sufficient. By investigating basic patterning processes, the functional integrity of the structures formed and the transition from single-unit to continuous tissue arrangements in organoids could help to understand the progress of tissue formation and evolution *in vivo*.

5. Materials and Methods

5.1 Materials

5.1.1 Organisms

Table 5.1: *Oryzias latipes* lines used in this study.

Stock	internal number	stock source	referred to as in thesis
Ath5::GFP	9900, 9965, 10689	Laboratory stock	Ath5::GFP
Cab	10346,10542,11057	Laboratory stock	Cab
Cndp1::oNTR_2A_mCherry	9684, 10015	Laboratory stock	Cndp1::mCherry Rx2::H2B_GFP
dsTrap#6	10793, 10863	Laboratory stock	ubi::GFP

5.1.2 Consumables

Table 5.2: Consumables employed in this study.

Consumable	Supplier
Aluminium	Roth
Cell saver tip 200 µl	Biozym, Cat#: 729055
Cell star dish 6 cm	Greiner bio one, Cat#: 664160
Cell star dish 10 cm	Greiner bio one, Cat#: 628160
Costar 24 Well Plate, Flat Bottom	CORNING, Cat#: 3473
Cover slips (glass)	Carl Roth, Cat#: HKE8.1

Filtropur V50, Vacuum filtration unit, 500 ml, PES, 0.45 µm	Sarstedt, Cat#: 83.3941
MatTek dish	Mattek, Cat#: P35G-1.5-10-C
Glas dish	Carl Roth
Latex gloves	semperguard
µ-Slide 8 well high Glass Bottom	Ibidi; Cat#: 80807
Microscopy slides	Roth
Microlance 3 (Needle)	BD, Cat#: 304000
Nitrile gloves	Starlab
Nunclon Sphera U-shaped Bottom Microplate	Thermo Fisher Scientific, Cat#: 174925
Parafilm	Thermo Fisher Scientific, Cat#: 13-374-10
PCR tubes	Eppendorf
Petri dishes 35mm, 60mm	Greiner
Petri dishes 92mm	Sarstedt
Pipette tips	Zisker
pluriStrainer Mini 40 µm	pluriSelect
Reaction tubes 1.5ml, 2ml, 5ml	Sarstedt
Resin – Clear V5	fromlabs
Resin – Black V5	fromlabs
Sandpaper 1000 grit	Bauhaus
Screw cap tubes 15 ml, 50ml	Sarstedt
Serological pipettes 2ml, 5ml, 10 ml, 25 ml	Sarstedt
Single well plate	VWR, Cat#: 734-2977

5.1.3 Chemicals, reagents and kits

Table 5.3: Chemicals, reagents and kits used in this study.

Chemical or Reagent	source	Catalogue number
Acetone	Sigma Aldrich	32201-2.5l
Agarose	VWR Avantor	35-1020
β-mercaptoethanol	Gibco (Thermo Fisher Scientific)	21985023
Benzyl dimethylamine	Serva	
Bovine serum albumin (BSA)	Sigma Aldrich	A9418-10G
Cyclopamine	Sigma Aldrich	239803-1MG
DAPI (4',6-Diamidino-2-Phenylindole, Dilactate)	Carl Roth	6335.1
DAPT	Sigma Aldrich	D5942-5MG
Dymethylamine	Serva	36975.01
DMSO (Dimethyl sulfoxide)	Sigma Aldrich	D4540-100ML
Dodecenylsuccinic acid anhydride	Serva	20755.01
Dorsomorphin	Sigma Aldrich	171260-1MG
D-sorbitol	Sigma Aldrich	V900390
Dulbecco's modified Eagle medium/Nutrient Mixture F-12 (DMEM/F12)	Gibco (Thermo Fisher Scientific)	21041025
EPON Mix	Serva	

Fetal Bovine Serum (FBS)	Sigma Aldrich	12103C
Glutaraldehyde Solution (25%)	Plano	R1010
Glycerol	Sigma Aldrich	V900122
Glycid ether 100	Serva	21045.01
HEPES (N-2-Hydroxyethylpiperazine-N'-2-ethansulfons.ure)	Carl Roth	7365-45-9
IP-polydimethylsiloxane (IP-PDMS)	Nanoscribe GmbH	
In Situ Cell Death Detection Kit, TMR red	Roche	12156792910
KnockOut™ Replacement Serum (KSR)	Gibco (Thermo Fisher Scientific)	10828028
Lead citrate Solution (3%)	Science Services	DM22410
Laminin	Roche	11243217001
Matrigel, Growth Factor Reduced (GFR) Basement Membrane Matrix	Corning	356230
MEM Non-Essential Amino Acid Solution (100X) (L-glutamine free)	Sigma Aldrich	M7145-100ML
Methyl nadic anhydride	Serva	29452.01
N2 supplement (100X)	Gibco (Thermo Fisher Scientific)	17502048
Noggin	Merck Millipore	GF173

Osmiumtetroxide (2% Solution)	Science Services	E19152
PBS, pH 7,4	Thermo Scientific	Fischer 10010023
Penicillin-Streptomycin (10,000 U/ml) (P/S)	Gibco (Thermo Fisher Scientific)	15140122
Paraformaldehyde (PFA)	Sigma Aldrich	P46148
Paraformaldehyde (16% Solution) – EM	Paro	R1026
PIPES (250g powder)	Carl Roth	9156.3
Potassium Chloride (KCl)	Merck	7447-40-7
Potassium ferricyanide		
Potassium hydroxide (KOH)	Merck	105033
Sheep serum	Sigma Aldrich	S2263
Sucrose	Sigma Aldrich	
Sodium chloride (NaCl)	Sigma Aldrich	7647-14-5
Sodium pyruvate (100 mM)	Sigma Aldrich	S8636-100ML
Taurine	Sigma Aldrich	T8691
Tissue Freezing Medium	Leica	1402018926
Tricaine	Sigma Aldrich	8886-86-2
Tris-hydrochloride (Tris-HCl)	Sigma Aldrich	10812846001
Tween 20	Sigma Aldrich	P7949
Uranylacetate (25g powder)	Science Services	E22400
Urea	Sigma Aldrich	V900119

5.1.4 Solutions and buffers

Table 5.4: Solutions and buffers used in this study.

Solutions or Buffer	Ingredients
Blocking solution	4% sheep serum, 1% BSA and 1% DMSO in PTW
Differentiation medium	DMEM/F12, 5% KSR, 0.1 mM MEM Non-Essential Amino Acids, 0.1 mM sodium pyruvate, 0.1 mM β -mercaptoethanol, 20 mM HEPES pH = 7.4, 100 U ml ⁻¹ penicillin–streptomycin
Embryo rearing medium (ERM)	17 mM NaCl, 40 mM KCl, 0.27 mM CaCl ₂ , 0.66 mM MgSO ₄ , 17 mM HEPES
EPON resin	42.4 g glycid ether 100, 29.6 g dodecenylsuccinic acid anhydride (DDSA), 18.4 g methyl nadic anhydride (MNA), 2.4 g benzyldimethylamine (BDMA) as initiator
Maturation medium	DMEM/F12, 10% FBS, 1 μ M N2 supplement, 1 mM taurine, 20 mM HEPES pH = 7.4, 100 U ml ⁻¹ penicillin–streptomycin
Optical clearing solution (Zhu et al., 2019)	20% (wt/vol) urea, 30% (wt/vol) D-sorbitol, 5% (wt/vol) glycerol dissolved in DMSO
PFA (4%)	4% paraformaldehyde in 1x PTW
PTW	0.05% Tween20 solved in 1x PBS

5.1.5 Antibodies

Table 5.5: Primary antibodies used in this study. Values in brackets indicate dilutions used for stainings performed in cryosections.

Target	Host	Dilution	Source
anti-Acetylated tubulin	mouse	1:300	Sigma Aldrich, Cat#: mA1-12717, Lot: 0000128058
anti-DsRed	rabbit	1:300	Clotech, Cat#: 632496, Lot: 2103116
anti-GFP	chicken	1:300	Thermo Fisher Scientific, Cat#: A10262; Lot: 2480084
anti-HuC/D	mouse	1:300 (1:500)	Thermo Fisher Scientific, Cat#: A21271; Lot: 2441512
anti-Laminin	rabbit	1:200	Sigma-Aldrich, Cat#: L9393, Lot: 67M4872V
anti-Otx2	goat	1:300 (1:500)	R&D systems, Cat#: AF1979; Lot: KNO1022091
anti-PKC-alpha (C-20)	rabbit	1:200 (1:500)	Santa Cruz, Cat#: sc-208
anti-PKC-zeta (C-20)	rabbit	1:200 (1:500)	Santa Cruz, Cat#: sc-216
anti-Prox1	rabbit	1:200 (1:500)	Millipore, Cat#: AB5475; Lot: 3811358
anti-Rhodopsin	mouse	1:300 (1:500)	Sigma-Aldrich, Cat#: MABN15
anti-Rx2	rabbit	1:300	Homemade, Lot: 2794/11#1
anti-Zpr1	mouse	1:300 (1:500)	Zebrafish International Resource Center

Table 5.6: Secondary antibodies used in this study. Dilutions apply for, both, whole mount staining and cryosections.

Target	Host	Dilution	Source
anti-chicken Alexa Fluor 488	donkey	1:500	Jackson ImmunoResearch Europe Ltd., Cat#: 703-545-155; Lot: 162189
anti-goat Alexa Fluor 488	chicken	1:500	Invitrogen, Cat#: A-21467
anti-goat Alexa Fluor 594	donkey	1:500	Thermo Fisher Scientific, Cat#: A-11058; Lot: 714270
anti-goat Alexa Fluor 647	donkey	1:500	Thermo Fisher Scientific, Cat#: A-21447; Lot: 2273668
anti-mouse Alexa Fluor 488	goat	1:500	Life Technologies, Cat#: A11029
anti-mouse Alexa Fluor 647	donkey	1:500	Jackson ImmunoResearch Europe Ltd., Cat#: 715-605-151; Lot: 105869
anti-rabbit Alexa Fluor Plus 488	donkey	1:500	Thermo Fisher Scientific, Cat#: A32790; Lot: VC296619
anti-rabbit Alexa Fluor 594	donkey	1:500	Thermo Fisher Scientific, Cat#: A21207, Lot: 2747441
anti-rabbit Alexa Fluor 647	donkey	1:500	Thermo Fisher Scientific, Cat#: A31573, Lot: 2083195

5.1.6 Equipment and Instruments

Table 5.7: Equipment and instruments used in this study.

Equipment or Instrument	Source
ACQUIFER Imaging Machine (timelapse	ACQUIFER Imaging GmbH

widefield microscopy)	
Centrifuges 5417C, 5425, 5430R, 5810R	Eppendorf
Field Emission Scanning Electron Microscope	Ultra 55, Carl Zeiss Microscopy
Forceps 110 mm, straight	NeoLab
Freezer -20°C / -80°C	Freezer -20°C / -80°C
Incubator (cell culture)	Thermo Fisher Scientific, HERAcell 150 I, RUMED
Incubator (fish embryos, reagents and others)	Heraeus instruments, RUMED, Liebherr, Binder
Jumbo 35° diamond knife	Diatome, Switzerland
Laminar Flow Hood	Thermo Fisher Scientific, Model: 51022734
Leica Dmi8 (epifluorescence microscopy)	Leica
Leica TCS Sp8 (confocal laser scanning microscopy)	Leica
Nikon SMZ18 with a Digital Sight DSRI1 camera (stereomicroscopy)	Nikon
Olympus MVX10 (epifluorescence stereomicroscopy)	Olympus
Olympus SZX7	Olympus
Photonic Professional GT2	Nanoscribe GmbH
Pipettes 2.5 µl, 10 µl, 20 µl, 200 µl, 1000 µl	Gilson
PowerTome Ultramicrotome	RMC Boeckeler

Laminar Flow Box FBS 75 – SuSi	SPETEC
Form 3+ - 3D printer	formlabs
Vortex Genie 2	Scientific Industries

5.1.7 Software

Table 5.8: Software used in this study.

Software	Source
Affinity Designer	v. 1.10.5
Amira	Thermo Fisher Scientific
Atlas 5	Carl Zeiss Microscopy
Copilot	Microsoft
Fiji (ImageJ2)	v. 2.16.0/1.54m – plugins: Acquirer
Jupyter lab	v. 4.4.0a1 – packages used: statannotiations, seaborn, pandas, matplotlib, numpy,
LasX	Leica
Perplexity	v. 3.2.0
Mendeley Reference Manager	v. 2.130.2
Microsoft Office	v. 16.78
YoKi	v. Meta-llama/Meta-Llama-3.1-70B-Instruct

‘YoKi’ (accessed March 2025) run by Heidelberg University was exclusively used for language and proofreading suggestions. No original content was generated by it. Microsoft Co-pilot was used for suggestions on python code used for data plotting. Perplexity was used to retrieve original literature.

5.2 Methods

5.2.1 Fish husbandry

Medaka (*Oryzias latipes*) stocks were kept as previously described (Koster et al., 1997) at the Centre for Organismal Studies at Heidelberg University. Fish were maintained at 28°C in closed stocks with a 14 h light and 10 h dark cycle. Husbandry of the fish (permit number: AZ35-9185.64/BH; experiment permit: 35–9185.81/G-145/15 Wittbrodt) was performed according to the EU directive 2010/63/EU guidelines and the German animal welfare laws (Tierschutzgesetz §11, Abs. 1, Nr.1).

5.2.2 Medaka retinal organoid generation

For the generation of medaka organoids, cells of embryos of late blastula stage (stage 11, 1000-2000 cells; Iwamatsu, 2004) were extracted similar as described in Zilova et al. (2021). Medaka embryos were collected shortly after fertilization and incubated at 32°C for about 4h in Embryo Rearing Media (ERM) until stage 10 was reached (Iwamatsu, 2004). Embryos were processed starting from stage 10 to extract primary pluripotent embryonic cells. Embryos were dechorionated using hatching enzyme and washed in sterile 1x ERM. To detach the cell body from the yolk, the yolk was punctured using a needle (microlance 3). Cell bodies were washed carefully in 1x PBS and cells were dissociated in 200 µl PBS by pipetting. The suspension was transferred to a cell strainer (pluriStrainer) in a 1.5 ml reaction tube and spun for 3 min at 180*g. The cell pellet was re-suspended in differentiation media. Cells were seeded at a density of about 1500 cells/100 µl. In this step, cells of different genetic background were combined in the ratios mentioned (15%/20% Ath5::GFP with 80/85% Cab cells; 20% dsTrap#6 with 80% Cab cells). The cells were seeded by pipetting 100 µl of the cell suspension into a low binding U-bottom-shaped 96-well plate and placed for aggregation at 26°C without CO₂ control over night (o.n.). On day 1, organoids were washed in fresh differentiation medium and 2% Matrigel were added to each well in standard conditions. Matrigel addition was omitted for non-Matrigel condition. Organoids were incubated at 26°C with CO₂ control. Organoids were transferred into

maturation medium on day 2 and onwards incubated at 26°C with CO₂ control. Media was changed on day 4 and day 7 for fresh maturation media.

For supplementation of organoids with Laminin from day 2, Laminin was added to a final concentration of 25 µg/ml to one organoid per well. For the control condition, standard culture was performed as described above. Organoids were incubated at 26°C with CO₂ control until day 4.

For treatment with chemical inhibitors, organoids were exposed to 10µM DAPT, 1µM cyclopamine, 100ng/µl dorsomorphin and 100ng/µl Noggin in maturation media. Compounds were dissolved in DMSO and control condition was supplemented with highest DMSO concentration reached within treated condition (1:1000) in maturation media. Organoids were treated starting from day 2 (18h) and cultured until day 4 (26°C with CO₂ control).

Organoids incubated in agarose mould were transferred to the moulds either 6h after Matrigel addition on day 1 or on day 2. The moulds were covered with differentiation media (day 1) or maturation media (day 2) and organoids were inserted into imprinted shapes by gentle pushing using a needle. Media was changed on day 2 for maturation for organoids transferred on day 1. Organoids in moulds were incubated until day 4 (26°C with CO₂ control). For autofluorescence control, 3-5 organoids of wild type cells (Cab) without a reporter were mounted and cultured as well.

5.2.3 Stamp and mould fabrication

Stamps and shapes for mould preparation were 3D printed by multi-photon 3D laser printing (Photonic Professional GT2; performed by Philip Mainik) for C- and X-shapes or low force stereolithography (Form3+; performed by Gero Hofmann) for rectangular and round shapes and stamps. Stamp for mounting nano-printed forms were fabricated from acrylic glass (96 olymethylmethacrylate) by Gero Hofmann. Schematics of printed shapes are displayed in in Figure 6.1 and Figure 6.5.

Agarose moulds were prepared from 2% agarose (sterile) in 1x PBS (sterile) in the Laminar Flow Box (SPETEC). Agarose was heated to liquid phase and poured into 1-well plates and 6cm dishes for full coverage of the dish bottom or pipetted into 8-well

ibidi slides (100 µl per well). Stamps were inserted until solidification. After solidification, stamps were carefully removed and agarose was washed with DMEM/F12 media by covering the gel and resting for 15 min. DMEM/F12 wash was removed and media was added to the wells.

5.2.4 Whole mount staining of medaka organoids and medaka embryos

For sample preservation, organoids/embryos were washed in 1x PBS/1xERM and fixed in 4% PFA (paraformaldehyde) in 1x PTW for 48h at 4°C. After washing organoids/embryos with 1x PTW (3x), the embryos were dechorionized and dissected from the yolk with forceps. Organoids/embryos were permeabilized with ice cold Aceton at -20°C for 15 min. Samples were washed in 1xPTW (3x) and transferred to a fresh PCR tube. The organoids were blocked in 10% BSA in 1xPTW for 2h at r.t., embryos were incubated in blocking solution for 2h at r.t.. Primary antibodies (Abs) (see Table 5.5) were applied in 1% BSA in 1x PTW/blocking solution and incubated for 48h at 4°C. Samples were in 1x PTW (3x) and the secondary Abs (see Table 5.6) and DAPI (1:500) were applied in 1% BSA in 1x PTW /blocking solution o.n. at 4°C in darkness. Afterwards, samples were washed in 1x PTW (3x). TUNEL (Terminal deoxynucleotidyl transferase dUTP nick end labeling) staining was, if performed, done subsequently by, first, incubating organoids in Acteone:EtOH (1:2) at -20°C for 20 min and, second, by incubating in labelling solution + enzyme solution (9:1) at 37°C for 2h. Samples were washed in 1x PTW (3x).

For confocal microscopy, organoids/embryos were mounted in optical clearing solution (Zhu et al., 2019) on matec-dishes.

5.2.5 Cryosectioning

Embryos or hatchlings (anesthetized in 1x tricaine in 1x ERM) were fixed in 4% PFA in PTW for 48h at 4°C and heads were manually dissected using forceps. For cryopreservation, samples were transferred into 30% (w/w) sucrose and incubated at 4°C o.n.. Next, samples were transferred into a 1:1 mix of Tissue Freezing Medium

and 30% sucrose and incubated at 4°C o.n.. For sectioning, fish heads were placed at the bottom of the cryo mould with the snout facing the bottom and all liquid was removed. The mould was filled with Tissue Freezing media and snap frozen in liquid nitrogen. Sections of 16 µm were cut, placed on glass slides and dried at 4°C o.n.. Sections on slides were rehydrated with 1x PTW for 10 min. Blocking was done with 10% BSA in 1x PTW for 2 h in a humidified chamber. After washing in 1x PTW (2x), primary Abs (see Table 5.5) were applied in 1% BSA o/n at 4°C in a humidified chamber. Sections on slides were washed in 1x PTW (3x) and secondary Abs (see Table 5.6) and DAPI were applied in 1% BSA in 1x PTW for 2 h at 37°C in a humidified chamber. Afterwards, samples were washed 1x PTW (3x) and mounted by adding 70 µl 60% glycerol onto sections and covering them with a coverslip. Edges were sealed with nail polish. Sections were analysed under the confocal microscope.

5.2.6 Light microscopy imaging and image processing

Confocal imaging of fixed organoid and embryo samples were performed using a Leica TCS Sp8 Dmi8 inverted confocal microscope (20x and 63x oil immersion objective). Samples were mounted in tissue clearing media. Live imaging of organoids mounted in shapes was done using a Leica Dmi8 microscope or a ACQUIFER imaging machine. Data acquired at the ACQUIFER Imaging Machine cover 10-slices in 50µm steps. For display, confocal images were subjected to rolling ball background subtraction of 25 or 50 pixels and median filtering (1.2 pixels). Within one condition, all images were treated the same way.

Image stacks obtained from live imaging of organoids in agarose moulds (ACQUIFER imaging machine) were processed by sum-projection of stacks (10 z-slices) of day 4 organoids and cropping to a rectangle covering the organoid in rectangular or round shape with minimal background. Images processed the same way of Cab organoid samples (non-fluorescent control) were measured for signal intensity in red channel to estimate the background fluorescence. The average of 3-4 Cab samples per experiment was subtracted from cropped sum-projections carrying the reporter (Cndp1::mCherry). The following background average values were calculated and subtracted from images: experiment day 1-A background average 608 (n=3 Cab

samples), experiment day 1-B background average 642 (n=4 Cab samples), experiment day 2 background average 730 (n=3 Cab samples). Cropped organoids from the same experiments were morphed to similar size, overlaid and sum-projected.

Quantification of cell type ratios and cell numbers within late retinal organoids was done manually using Fiji. Counting of cells within a cluster was done by using the cell counter tool. A cluster was defined as a group of Otx2-positive cell with two or more cells, which are located in close vicinity. Counting of cell types within clusters was done using the cell counter and scoring the double positive cells for the respective cell type specific label (Rx2-Otx2 – PR; Zpr1-Otx2 – cone PR) within an Otx2-positive cell cluster. Otx2-only cells in the Rx2-Otx2-double labeling were counted as BP cells. Quantification of the qualitative presence of rod PR in Otx2-cell clusters was done by scoring rhodopsin-expression per cluster based on maximum intensity projections. Distance measurements between organoids was done by defining the center of each cluster in a defined z-stack (sub-stack; up to 30 clusters per stack) and documenting the position in 3D by recording the coordinates (measuring tool). Vector length between all coordinates within one sub-stack were calculated (n=159 clusters in n=10 organoids; 2-3 sub-stacks per organoid). The data sets ('all distances') include the distances between not directly neighboring clusters, which were removed as outliers. To filter for the distances of direct neighboring clusters only (remove outliers), a range of values was defined by the average and 3x standard variation (+/-) of the smallest distance value within the distance data of each sub-stack. This range was used as boundaries within the 'all distances' data and the values were displayed using a kde plot. Schematic of nearest neighbor calculation in Figure 6.10. RGC number between control and DAPT-treated organoids was done by counting RGC number in Fiji using sum projections of 60 z-slices per organoid (5 per condition, equal z-distance) and using the analyze particles tool. For improving cell counting, sum projections were processed as: despeckle > subtract background 25 pixels > auto local watershed after Bernsen with radius 10, parameter 1:30 > watershedding, prior to particles (size= 10-infinity, circularity: 0.2-1, overlay). Graphs were plotted and statistical analysis done in Python (Jupyter lab interface).

5.2.8 Electron microscopy Sample Preparation and Ultramicrotomy

Day 7 organoids were fixed for several days in a solution containing 1.25% glutaraldehyde and 2% PFA in 0.1 M PIPES buffer, pH 6.8. After thorough washing with the buffer, the samples were incubated for 1 hour in a solution of 1% osmium tetroxide (OsO_4) and 0.8% potassium ferricyanide ($\text{K}_3[\text{Fe}(\text{CN})_6]$) on ice. Subsequently, the samples were stained o.n. with 2% uranyl acetate in 25% ethanol/water.

Following staining, the samples were subjected to a graded ethanol dehydration series (25%, 50%, 70%, 90%, and 100% ethanol/water), followed by ethanol/acetone (1:1) and 100% acetone, with each step lasting 15 minutes. The samples were then infiltrated with Epon resin in acetone in two stages: 30% and 70% Epon for 2 hours each. The samples were finally embedded in 100% Epon resin. Polymerization was carried out at 60°C for 2 days.

Ultrathin serial sections (100 nm thickness) were prepared using a PowerTome Ultramicrotome equipped with a Jumbo 35° diamond knife. The sections were transferred onto silicon wafer substrates for further analysis. Post-staining was performed by immersing the sections in a solution of 3% uranyl acetate in water for 10 minutes followed – after washing – by a solution of 3% lead citrate in water for 5 minutes.

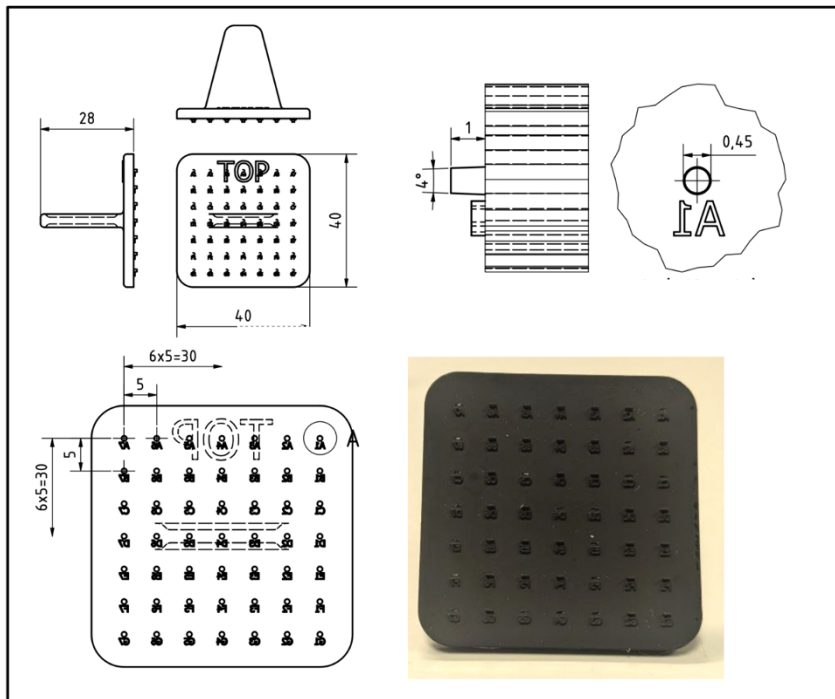
5.2.9 Electron Microscopy and Image Processing

The ultrathin sections were imaged using a field emission scanning electron microscope operated at a primary electron energy of 1.5 keV. Both, secondary electron (SE2) and backscattered electron (ESB) detectors were used to capture the images. Automated acquisition of large scan fields was performed using the Atlas 5 software to target regions of interest. The resulting image stacks were aligned and processed using the TrakEM module in Fiji (Cardona et al., 2012).

Z-Stack of ultrastructural images (6nm pixel size in x-y and 100nm in z) was cropped and reduced in scale by half using Fiji and contrast was enhanced automatically. Cells were segmented using the Amira software (voxel size of 1-2-8.3). Using the segmentation tool, cells within the cell cluster were outlined separately in x-y plane and interpolated. Segmented labels were visualized using Volren display option.

6. Appendix

A



B

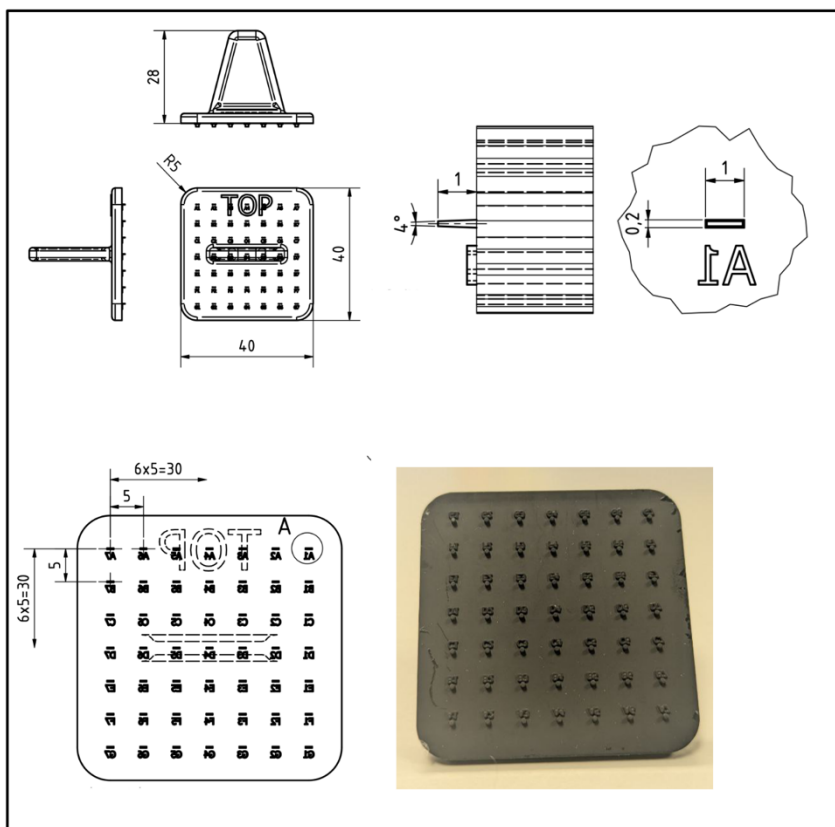


Figure 6.1: Stamps with rectangular and round shapes for imprinting into agarose. (A) Scheme and image of printed stamp with round shapes. (B) Scheme and image of printed stamp with rectangular shapes.

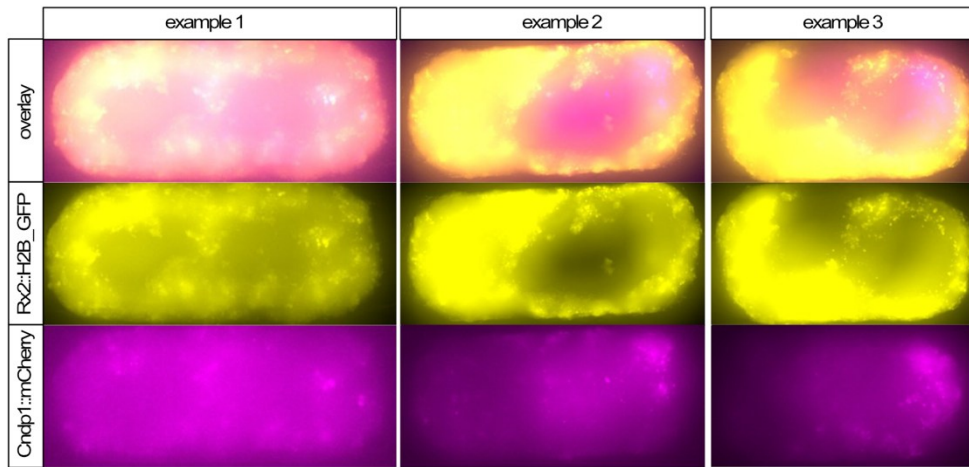


Figure 6.2: Organoids transferred on day 1 show in 2 experiments complex tissue composition and are not considered for shape induction analysis. Maximum projection of z-slices of single organoids of Rx2::H2B_GFP and Cndp1::mCherry fluorescent signal and their overlay. Examples from two different experiments show organoids transferred on day 1 to rectangular shapes with retinal and non-retinal tissue. The organoids from these experiments were not considered for shape induction analysis.

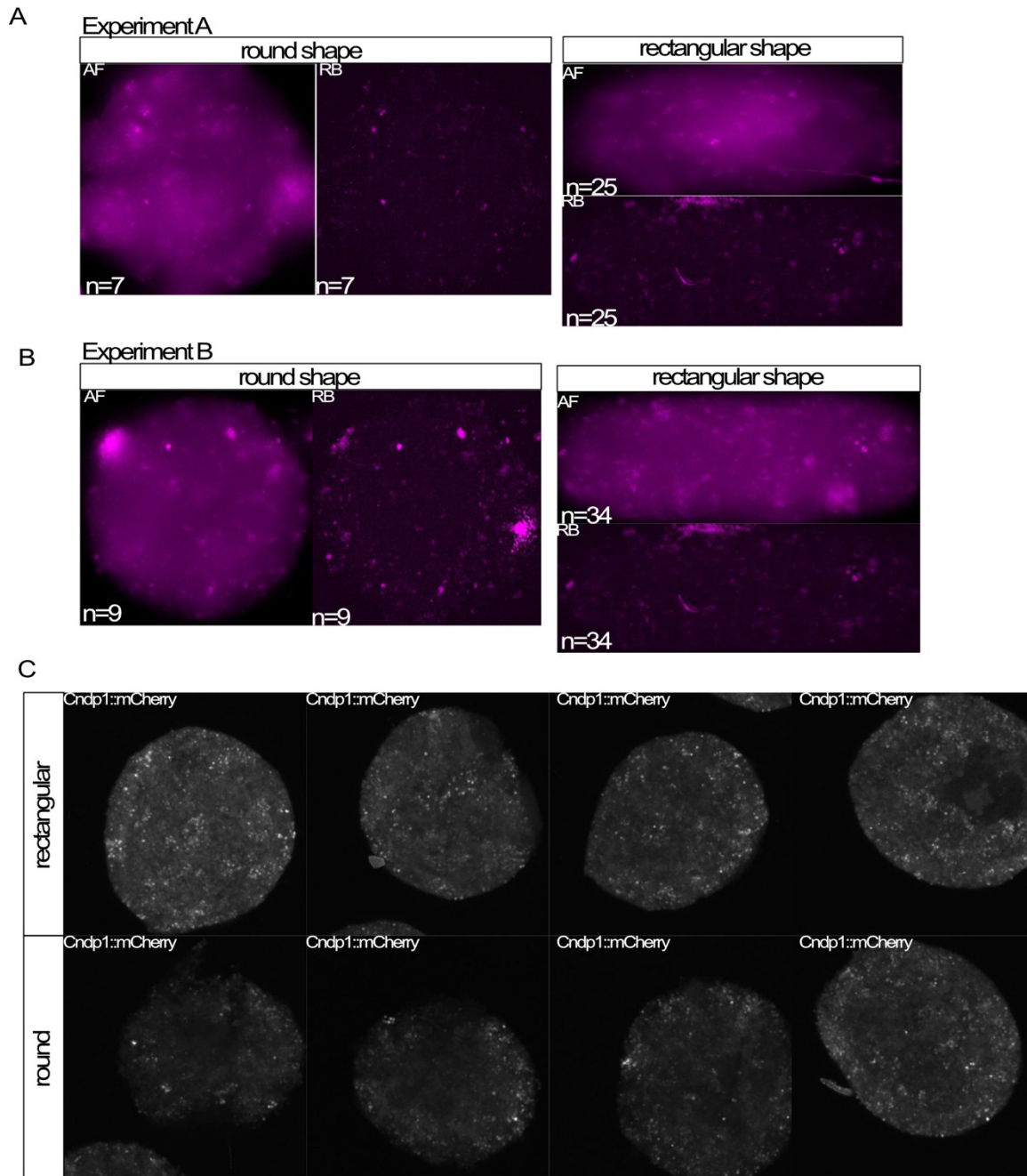


Figure 6.3: Organoids transferred on day 1 to rectangular shape show no Cndp1 expression in 2 independent experiments in live and immune stained. (A) Overlay of maximum projections of all samples of experiment A analyzed for Cndp1::mCherry expression within control (round shape) and shape-induced (rectangular shape) organoids. Fluorescent images acquired by live imaging at Acquirer imaging machine on day 4. Signal in maximum projections normalized by autofluorescence background (AF) reduction or rolling ball background subtraction (RB). For round shape, images of 7 organoids were overlaid, for rectangular shape, images of 25 organoids were overlaid. (B) Overlay of maximum projections of all samples of experiment B analyzed for Cndp1::mCherry expression within control and shape-induced organoids. Fluorescent images acquired by live imaging at Acquirer imaging machine on day 4. Signal in maximum projections normalized by autofluorescence background (AF) reduction or rolling ball background subtraction (RB). For round shape, images of 9 organoids were overlaid, for rectangular shape, images of 34 organoids were overlaid. (C) Maximum projections of Cndp1::mCherry channel of fixed,

demounted and immune stained organoids after culturing in mounted in shapes (day 1- day 4). Side view of organoids shapes as coins (rectangular shape) or spherical (round shape) after treatment.

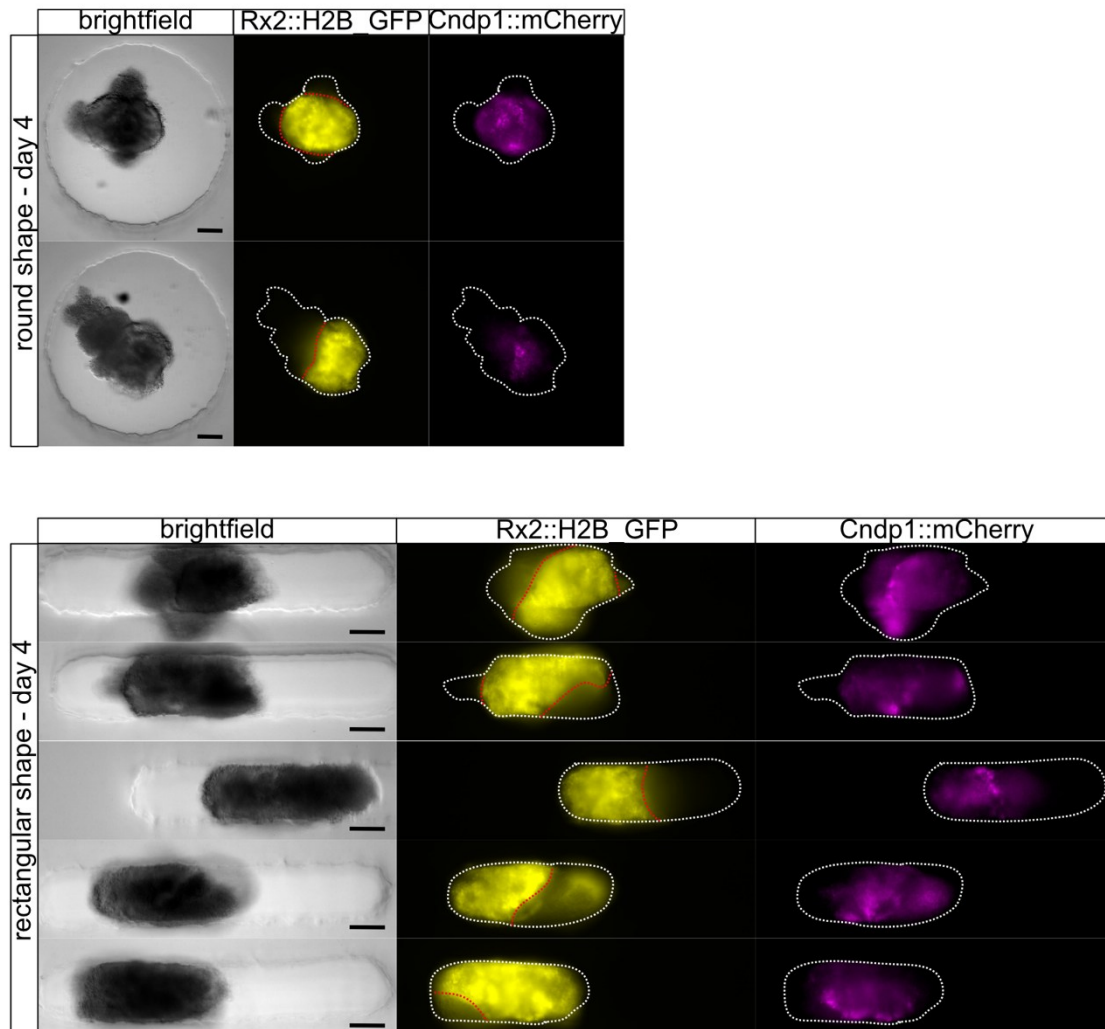


Figure 6.4: Organoids mounted in rectangular moulds on day 2 with complex tissue composition and CMZ tissue. Fluorescent reporter signals overlaid with brightfield of organoids mounted in shapes (round or rectangular) on day 4 imaged with Acquirer imaging machine. White dashed lines outlining organoid shape. Red dashed lines outlining Rx2::H2B_GFP reporter positive areas vs. reporter negative areas. Scale 100 μ m.

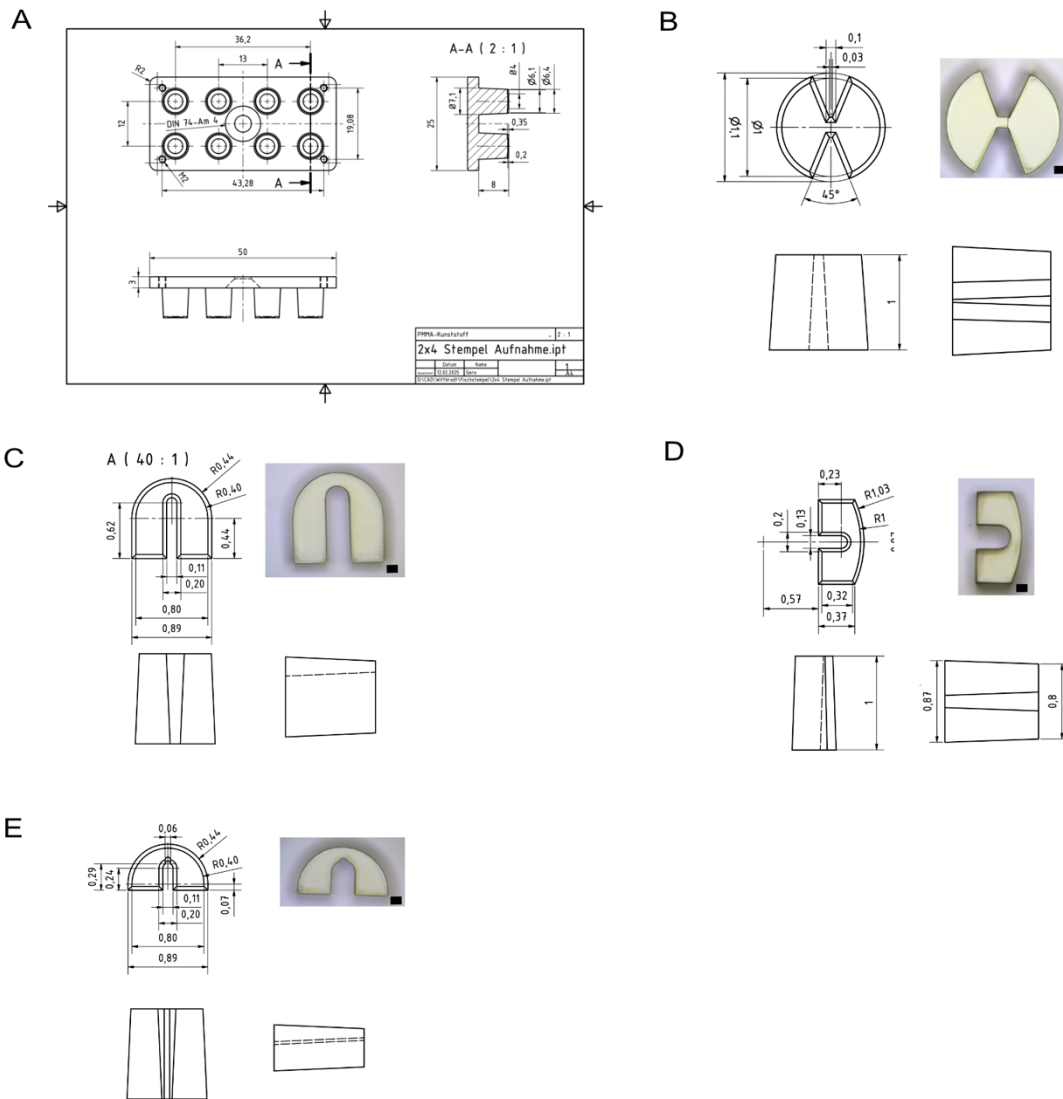


Figure 6.5: Schemes and dimensions of nano-printed rectangular shapes. (A) Scheme of stamp for shape-mounting. Design of stamp adapted to fit multi-well coverslip. (B) Design and 3D printed X-shape. Scale 100 μm . (C) Design and 3D printed C-shape1. Scale 100 μm . (D) Design and 3D printed C-shape2. Scale 100 μm . (E) Design and 3D printed C-shape3. Scale 100 μm .

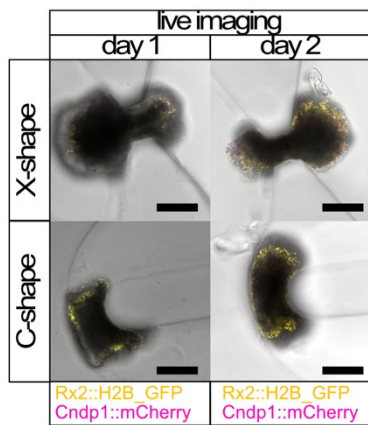


Figure 6.6: Organoids in C-shape and X-shape mounted on day 1 or day 2 imaged live. Overlay of brightfield, Rx2::H2B_GFP (yellow) and Cndp1::mCherry (magenta) signal in single z-slices. Scale 100µm.

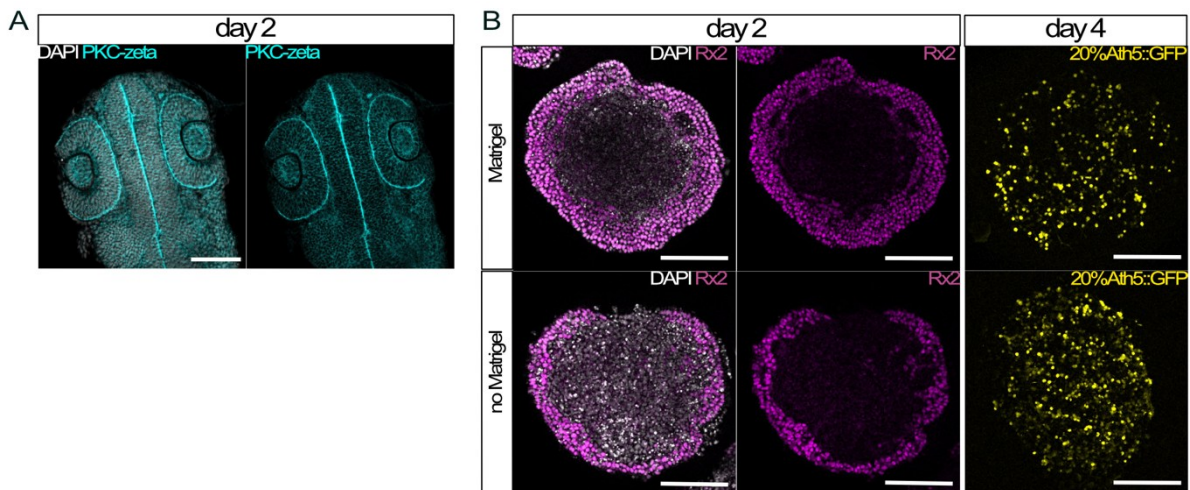


Figure 6.7: PKC-zeta serves as apical polarity marker staining proximal rim of OC tissue in day 2 embryo and organoids establish retinal identity independent of Matrigel exposure. (A) Polarity marker PKC-zeta in day 2 Medaka embryo. Scale 100 µm. (B) Immune staining for Rx2 in day 2 organoids treated with Matrigel and cultured without. Maximum projection of Ath5::GFP label of day 4 organoids treated with Matrigel and cultured without. Scale 100 µm.

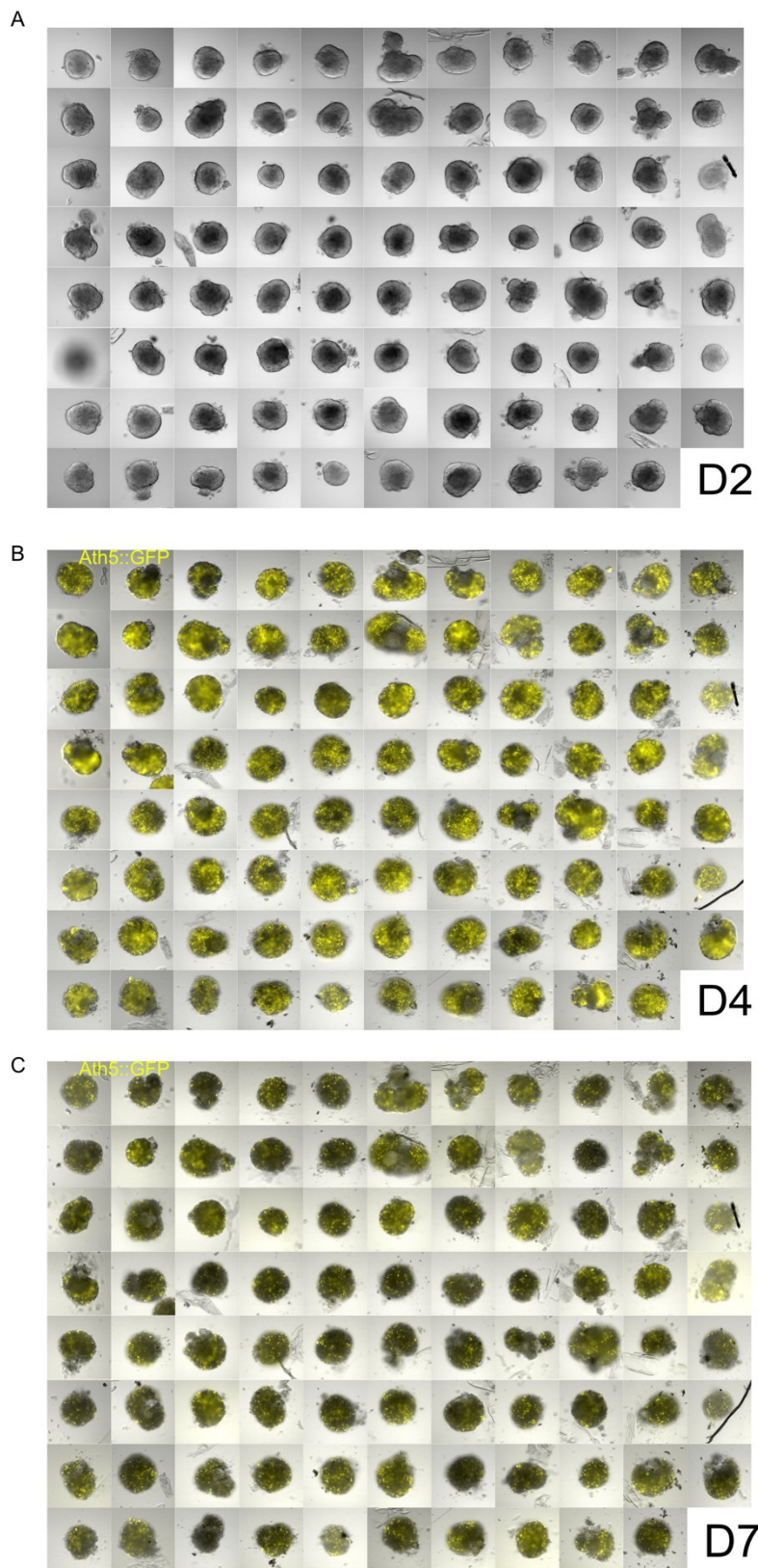


Figure 6.8: Differentiation of retinal organoids containing RGCs is robust and reproducible. Retinal organoids grown on one 96 well plate imaged with the Acquirer imaging machine on day 2 (A), day 4 (B) and day 7 (C). GFP signal of Ath5::GFP reporter shown in overlay with brightfield images.

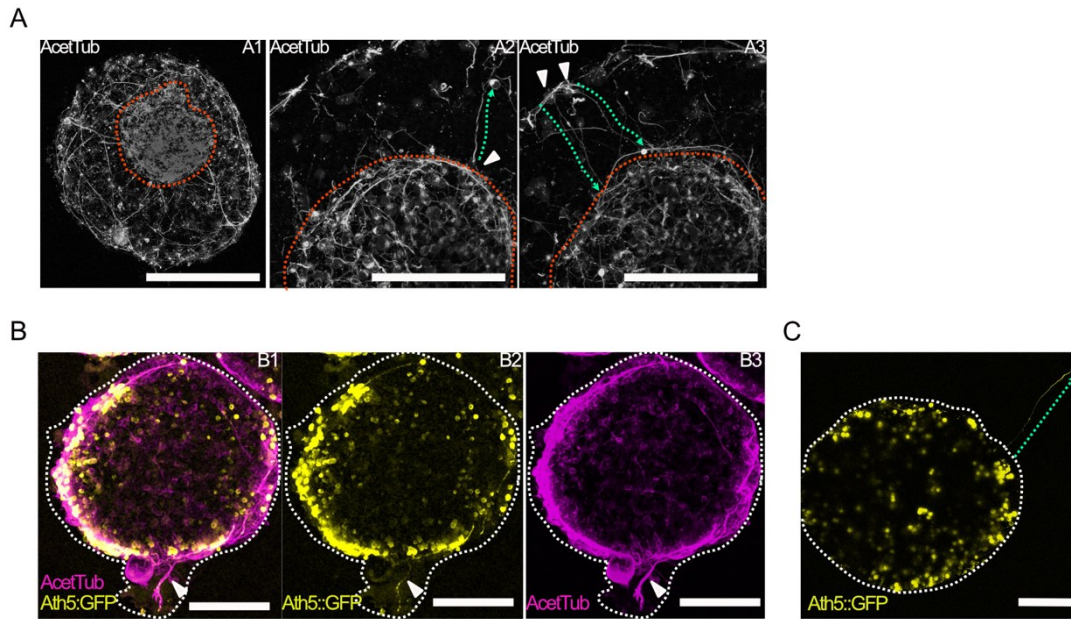


Figure 6.9: Complex neuronal projections in late retinal organoids. (A) Immune staining for acetylated tubulin shows axonal projections on day 7 organoid surface and a neuronal core structure (outlined with red dashed line) within in the organoid (A1). Axons are found to reach from the organoid rim to the central core (A2) and from the core to the rim (A3). Core structure detected in 4 out of 28 organoids. Scale bar is 50 μ m. (B) Organoid with nerve-like bundle of axons distancing from the retinal to GFP-negative part of the organoid. Nerve bundle contains RGC axons as marked by the overlapping Ath5::GFP signal. Scale 100 μ m. (C) RGC axon leaving organoid (d7) when organoid is mounted in ECM environment (100% Matrigel). Scale 100 μ m.

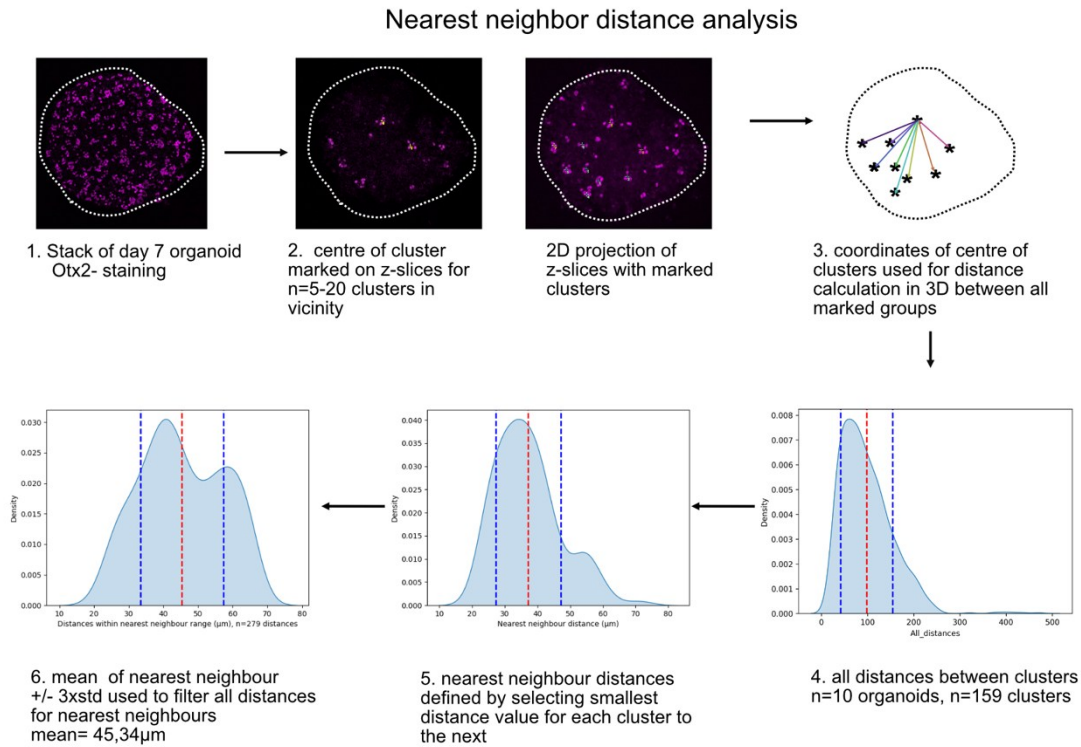


Figure 6.10: Scheme of distance measurement between clusters and assessment of the nearest neighbor distances.

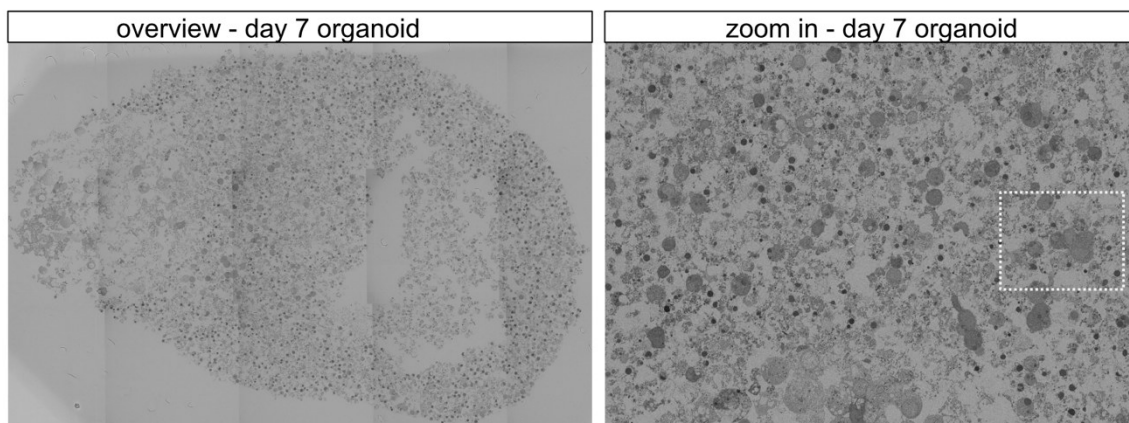


Figure 6.11: Ultrastructure of day 7 retinal organoid. Overview of ultrastructure in central organoid cross section. Close-up on cross section showing clusters of cells surrounded by cell debris.

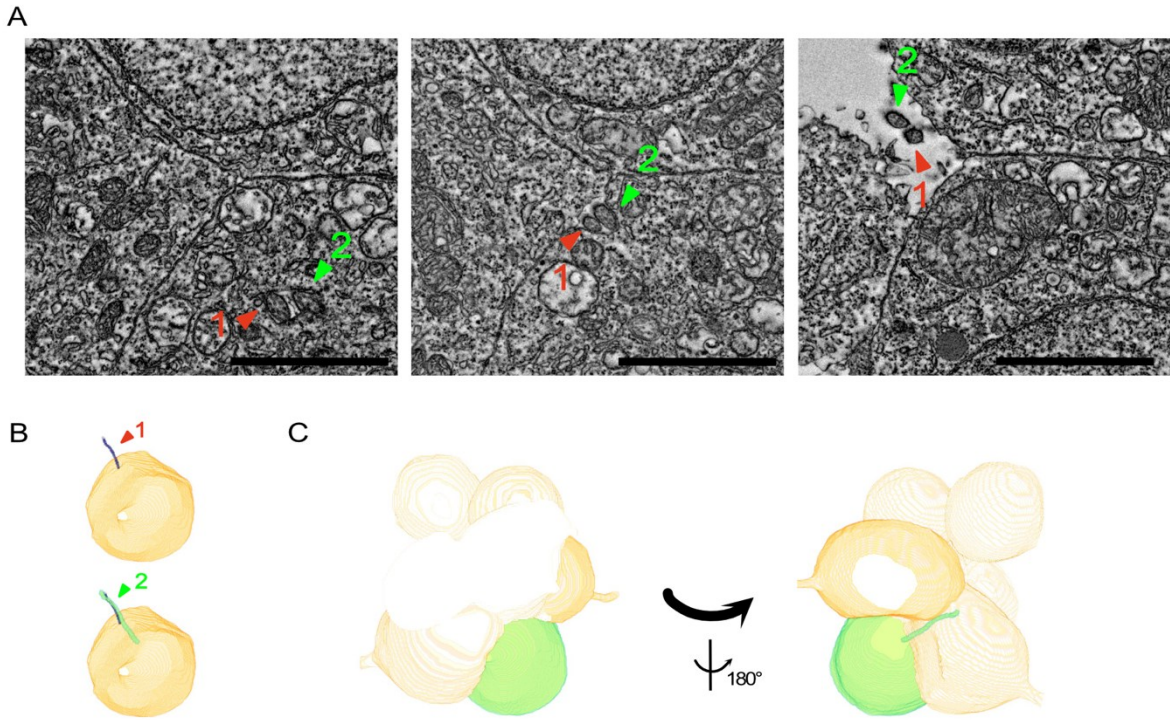


Figure 6.12: Two cells within cluster contain cilia projecting out of cells. (A) Cell with two cilia projecting into the same direction and out of cell. Cilia grow out along neighboring cells. Cilia marked by arrows and numbers. Scale $2\mu\text{m}$. (B) 3D volume of segmented cell in (B) with cilia 1 only and both cilia 1 and 2. (C) Cell with cilia (green) in context with whole cell cluster shown in cell segmentation. Shown in same orientation as single cell display in (C) and turned by 180° on the vertical axis.

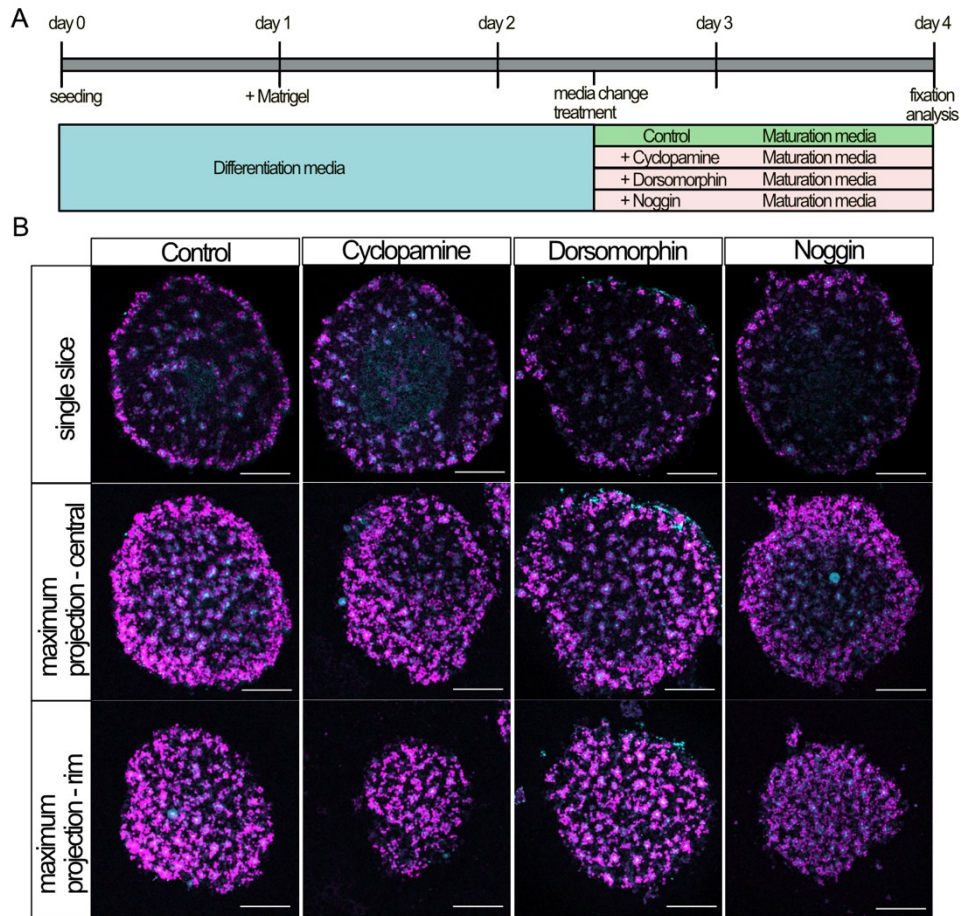


Figure 6.13: Antagonist treatments against Sonic hedgehog or BMP signaling do not show patterning effect by day 4. (A) Experimental outline of treatment with Notch-inhibitor DAPT. Organoids were grown until late day 2 under standard conditions in Differentiation media and addition of 2% Matrigel on day 1. Pre-onset of retinal cell differentiation, organoids were treated with $1\mu\text{M}$ cyclopamine, $100\text{ng}/\mu\text{l}$ dorsomorphin, or $100\text{ng}/\mu\text{l}$ Noggin in maturation media or the control was only transferred to maturation media. Samples were incubated until day 4. Afterwards the samples were fixed, immune stained and imaged. (B) Cluster patterning impacted by blocking sonic hedgehog by cyclopamine and BMP signaling by Dorsomorphin and Noggin. Organoids treated on day 2 with antagonists show no patterning effect when comparing Otx2-pattern. $N=6$ for each condition, experiment performed one time. Scale $100\mu\text{m}$.

References

- Afting, C., Walther, T., Drozdowski, O. M., Schlagheck, C., Schwarz, U. S., Wittbrodt, J., & Göpfrich, K. (2024). DNA microbeads for spatio-temporally controlled morphogen release within organoids. *Nature Nanotechnology*. <https://doi.org/10.1038/s41565-024-01779-y>
- Almeida, A. D., Boije, H., Chow, R. W., He, J., Tham, J., Suzuki, S. C., & Harris, W. A. (2014). Spectrum of Fates: a new approach to the study of the developing zebrafish retina. *Development (Cambridge)*, *141*(14), 1971–1980. <https://doi.org/10.1242/dev.114108>
- Avanesov, A., & Malicki, J. (2010). Analysis of the retina in the zebrafish model. *Methods in Cell Biology*, *100*, 153–204. <https://doi.org/10.1016/B978-0-12-384892-5.00006-2>
- Bachleda, A. R., Pevny, L. H., & Weiss, E. R. (2016). Sox2-Deficient Müller glia disrupt the structural and functional maturation of the mammalian retina. *Investigative Ophthalmology and Visual Science*, *57*(3), 1488–1499. <https://doi.org/10.1167/iovs.15-17994>
- Bao, S. (2014). Notch Controls Cell Adhesion in the Drosophila Eye. *PLoS Genetics*, *10*(1). <https://doi.org/10.1371/journal.pgen.1004087>
- Barton, A., & Fendrik, A. J. (2015). Retinogenesis: Stochasticity and the competency model. *Journal of Theoretical Biology*, *373*, 73–81. <https://doi.org/10.1016/j.jtbi.2015.03.015>
- Belliveau, M. J., & Cepko, C. L. (1999). Extrinsic and intrinsic factors control the genesis of amacrine and cone cells in the rat retina. *Development*, *126*(3), 555–566. <https://doi.org/10.1242/dev.126.3.555>
- Bernardos, R. L., Barthel, L. K., Meyers, J. R., & Raymond, P. A. (2007). Late-stage neuronal progenitors in the retina are radial Müller glia that function as retinal stem cells. *Journal of Neuroscience*, *27*(26), 7028–7040. <https://doi.org/10.1523/JNEUROSCI.1624-07.2007>

Bernardos, R. L., Lentz, S. I., Wolfe, M. S., & Raymond, P. A. (2005). Notch-Delta signaling is required for spatial patterning and Müller glia differentiation in the zebrafish retina. *Developmental Biology*, 278(2), 381–395. <https://doi.org/10.1016/j.ydbio.2004.11.018>

Biehlmaier, O., Neuhauss, S. C. F., & Kohler, K. (2001). Onset and time course of apoptosis in the developing zebrafish retina. *Cell and Tissue Research*, 306(2), 199–207. <https://doi.org/10.1007/s004410100447>

Bogdanović, O., Delfino-Machín, M., Nicolás-Pérez, M., Gavilán, M. P., Gago-Rodrigues, I., Fernández-Miñán, A., Lillo, C., Ríos, R. M., Wittbrodt, J., & Martínez-Morales, J. R. (2012). Numb/Numbl-Opo Antagonism Controls Retinal Epithelium Morphogenesis by Regulating Integrin Endocytosis. *Developmental Cell*, 23(4), 782–795. <https://doi.org/10.1016/j.devcel.2012.09.004>

Bonezzi, P. J., Tarchick, M. J., Moore, B. D., & Renna, J. M. (2023). Light drives the developmental progression of outer retinal function. *Journal of General Physiology*, 155(9). <https://doi.org/10.1085/jgp.202213262>

Brachmann, C. B., & Cagan, R. (2003). Patterning the fly eye: the role of apoptosis. *TRENDS in Genetics*, 19(2), 91–96. DOI: 10.1016/S0168-9525(02)00041-0

Buschbeck, E. K. (2014). Escaping compound eye ancestry: The evolution of single-chamber eyes in holometabolous larvae. *Journal of Experimental Biology*, 217(16), 2818–2824. <https://doi.org/10.1242/jeb.085365>

Cai, Z., Feng, G. S., & Zhang, X. (2010). Temporal requirement of the protein tyrosine phosphatase Shp2 in establishing the neuronal fate in early retinal development. *Journal of Neuroscience*, 30(11), 4110–4119. <https://doi.org/10.1523/JNEUROSCI.4364-09.2010>

Cardona, A., Saalfeld, S., Schindelin, J., Arganda-Carreras, I., Preibisch, S., Longair, M., Tomancak, P., Hartenstein, V., & Douglas, R. J. (2012). TrakEM2 software for neural circuit reconstruction. *PloS ONE*, 7(6). <https://doi.org/10.1371/journal.pone.0038011>

Centanin, L., Hoeckendorf, B., & Wittbrodt, J. (2011). Fate restriction and multipotency in retinal stem cells. *Cell Stem Cell*, 9(6), 553–562. <https://doi.org/10.1016/j.stem.2011.11.004>

Centanin, L., & Wittbrodt, J. (2014). Retinal neurogenesis. *Development (Cambridge)*, 141(2), 241–244. <https://doi.org/10.1242/dev.083642>

Chakrabarty, K., Nayak, D., Debnath, J., Das, D., Shetty, R., & Ghosh, A. (2024). Retinal organoids in disease modeling and drug discovery: Opportunities and challenges. *Survey of Ophthalmology*, 69(2), 179–189. <https://doi.org/10.1016/j.survophthal.2023.09.003>

Chow, R. L., & Lang, R. A. (2001). EARLY EYE DEVELOPMENT IN VERTEBRATES. *Annu. Rev. Cell. Dev. Biol.*, 17, 255–296. www.annualreviews.org.

Contín, M. A., Benedetto, M. M., Quinteros-Quintana, M. L., & Guido, M. E. (2016). Light pollution: The possible consequences of excessive illumination on retina. In *Eye (Basingstoke)* (Vol. 30, Issue 2, pp. 255–263). Nature Publishing Group. <https://doi.org/10.1038/eye.2015.221>

Cordero, J., Jassim, O., Bao, S., & Cagan, R. (2004). A role for wingless in an early pupal cell death event that contributes to patterning the *Drosophila* eye. *Mechanisms of Development*, 121(12), 1523–1530. <https://doi.org/10.1016/j.mod.2004.07.004>

Cowan, C. S., Renner, M., de Gennaro, M., Gross-Scherf, B., Goldblum, D., Hou, Y., Munz, M., Rodrigues, T. M., Krol, J., Szikra, T., Cuttat, R., Waldt, A., Papasaikas, P., Diggelmann, R., Patino-Alvarez, C. P., Galliker, P., Spirig, S. E., Pavlinic, D., Gerber-Hollbach, N., ... Roska, B. (2020). Cell Types of the Human Retina and Its Organoids at Single-Cell Resolution. *Cell*, 182(6), 1623-1640.e34. <https://doi.org/10.1016/j.cell.2020.08.013>

Crespo, C., & Knust, E. (2018). Characterisation of maturation of photoreceptor cell subtypes during zebrafish retinal development. *Biology Open*, 7(11). <https://doi.org/10.1242/bio.036632>

del Bene, F., Wehman, A. M., Link, B. A., & Baier, H. (2008). Regulation of Neurogenesis by Interkinetic Nuclear Migration through an Apical-Basal Notch Gradient. *Cell*, *134*(6), 1055–1065. <https://doi.org/10.1016/j.cell.2008.07.017>

di Meglio, I., Trushko, A., Guillamat, P., Blanch-Mercader, C., Abuhattum, S., & Roux, A. (2022). Pressure and curvature control of the cell cycle in epithelia growing under spherical confinement. *Cell Reports*, *40*(8). <https://doi.org/10.1016/j.celrep.2022.111227>

Dorgau, B., Felemban, M., Sharpe, A., Bauer, R., Hallam, D., Steel, D. H., Lindsay, S., Mellough, C., & Lako, M. (2018). Laminin γ 3 plays an important role in retinal lamination, photoreceptor organisation and ganglion cell differentiation. *Cell Death and Disease*, *9*(6). <https://doi.org/10.1038/s41419-018-0648-0>

Dyer, M. A., Livesey, F. J., Cepko, C. L., & Oliver, G. (2003). Prox1 function controls progenitor cell proliferation and horizontal cell genesis in the mammalian retina. *Nature Genetics*, *34*(1), 53–58. <https://doi.org/10.1038/ng1144>

Eiraku, M., & Sasai, Y. (2012). Mouse embryonic stem cell culture for generation of three-dimensional retinal and cortical tissues. *Nature Protocols*, *7*(1), 69–79. <https://doi.org/10.1038/nprot.2011.429>

Eiraku, M., Takata, N., Ishibashi, H., Kawada, M., Sakakura, E., Okuda, S., Sekiguchi, K., Adachi, T., & Sasai, Y. (2011). Self-organizing optic-cup morphogenesis in three-dimensional culture. *Nature*, *472*(7341), 51–58. <https://doi.org/10.1038/nature09941>

Ekström, P., & Johansson, K. (2003). Differentiation of ganglion cells and amacrine cells in the rat retina: Correlation with expression of HuC/D and GAP-43 proteins. *Developmental Brain Research*, *145*(1), 1–8. [https://doi.org/10.1016/S0165-3806\(03\)00170-6](https://doi.org/10.1016/S0165-3806(03)00170-6)

Fanto, M., & Mlodzik, M. (1999). Asymmetric Notch activation specifies photoreceptors R3 and R4 and planar polarity in the *Drosophila* eye. *Nature*, *397*, 523–526. DOI: 10.1038/17389

Fossat, N., le Greneur, C., Béby, F., Vincent, S., Godement, P., Chatelain, G., & Lamonerie, T. (2007). A new GFP-tagged line reveals unexpected Otx2 protein localization in retinal photoreceptors. *BMC Developmental Biology*, 7. <https://doi.org/10.1186/1471-213X-7-122>

Frantz, C., Stewart, K. M., & Weaver, V. M. (2010). The extracellular matrix at a glance. *Journal of Cell Science*, 123(24), 4195–4200. <https://doi.org/10.1242/jcs.023820>

Galli-Resta, L., & Ensini, M. (1996). An Intrinsic Time Limit between Genesis and Death of Individual Neurons in the Developing Retinal Ganglion Cell Layer. *The Journal of Neuroscience*, 16(7), 2318–2324. DOI: 10.1523/JNEUROSCI.16-07-02318.1996

Galli-Resta, L., Resta, G., Tan, S.-S., & Reese, B. E. (1997). Mosaics of Islet-1-Expressing Amacrine Cells Assembled by Short-Range Cellular Interactions. *The Journal of Neuroscience*, 17(20), 7831–7838. DOI: 10.1523/JNEUROSCI.17-20-07831.1997

Glubrecht, D. D., Kim, J. H., Russell, L., Bamforth, J. S., & Godbout, R. (2009). Differential CRX and OTX2 expression in human retina and retinoblastoma. *Journal of Neurochemistry*, 111(1), 250–263. <https://doi.org/10.1111/j.1471-4159.2009.06322.x>

Greferath, U., Grünert, U., & Wässle, H. (1990). Rod bipolar cells in the mammalian retina show protein kinase C-like immunoreactivity. *Journal of Comparative Neurology*, 301(3), 433–442. <https://doi.org/10.1002/cne.903010308>

Halfter, W., Willem, M., & Mayer, U. (2005). Basement membrane-dependent survival of retinal ganglion cells. *Investigative Ophthalmology and Visual Science*, 46(3), 1000–1009. <https://doi.org/10.1167/iovs.04-1185>

Hasegawa, Y., Takata, N., Okuda, S., Kawada, M., Eiraku, M., & Sasai, Y. (2016). Emergence of dorsal-ventral polarity in ESC-derived retinal tissue. *Development (Cambridge)*, 143(21), 3895–3906. <https://doi.org/10.1242/dev.134601>

He, J., Zhang, G., Almeida, A. D., Cayouette, M., Simons, B. D., & Harris, W. A. (2012). How Variable Clones Build an Invariant Retina. *Neuron*, 75(5), 786–798. <https://doi.org/10.1016/j.neuron.2012.06.033>

Heavner, W., & Pevny, L. (2012). Eye development and retinogenesis. *Cold Spring Harbor Perspectives in Biology*, 4(12). <https://doi.org/10.1101/cshperspect.a008391>

Heermann, S., Schütz, L., Lemke, S., Kriegelstein, K., & Wittbrodt, J. (2015). Eye morphogenesis driven by epithelial flow into the optic cup facilitated by modulation of bone morphogenetic protein. *Elife*, 4:e05216. <https://doi.org/DOI:10.7554/eLife.05216>

Heller, E., & Fuchs, E. (2015). Tissue patterning and cellular mechanics. *Journal of Cell Biology*, 211(2), 219–231. <https://doi.org/10.1083/jcb.201506106>

Herder, C., Swiercz, J. M., Müller, C., Peravali, R., Quiring, R., Offermanns, S., Wittbrodt, J., & Loosli, F. (2013). ArhGEF18 regulates RhoA-Rock2 signaling to maintain neuro-epithelial apico-basal polarity and proliferation. *Development (Cambridge)*, 140(13), 2787–2797. <https://doi.org/10.1242/dev.096487>

Hofmann L, Palczewski K. The G protein-coupled receptor rhodopsin: a historical perspective. *Methods Mol Biol*. 2015;1271:3-18. Doi: 10.1007/978-1-4939-2330-4_1.

Hoke, K. L., & Fernald, R. D. (1998). Cell death precedes rod neurogenesis in embryonic teleost retinal development. *Developmental Brain Research*, 111, 143–146. DOI: 10.1016/s0165-3806(98)00131-x

Holt, C. E., Bertsch, T. W., Ellis, H. M., & Harris, W. A. (1988). Cellular Determination in the Xenopus Retina Is Independent of Lineage and Birth Date. *Neuron*, 1, 15–26. DOI: 10.1016/0896-6273(88)90205-x

Hoon, M., Okawa, H., della Santina, L., & Wong, R. O. L. (2014). Functional architecture of the retina: Development and disease. *Progress in Retinal and Eye Research*, 42, 44–84. <https://doi.org/10.1016/j.preteyeres.2014.06.003>

Ishikawa, M., Sawada, Y., & Yoshitomi, T. (2015). Structure and function of the interphotoreceptor matrix surrounding retinal photoreceptor cells. *Experimental Eye Research*, 133, 3–18. <https://doi.org/10.1016/j.exer.2015.02.017>

Ivanovitch, K., Cavodeassi, F., & Wilson, S. W. (2013). Precocious Acquisition of Neuroepithelial Character in the Eye Field Underlies the Onset of Eye Morphogenesis. *Developmental Cell*, 27(3), 293–305. <https://doi.org/10.1016/j.devcel.2013.09.023>

Iwamatsu, T. (2004). Stages of normal development in the medaka *Oryzias latipes*. *Mechanisms of Development*, 121(7–8), 605–618. <https://doi.org/10.1016/j.mod.2004.03.012>

Jensen, K. B., & Little, M. H. (2023). Organoids are not organs: Sources of variation and misinformation in organoid biology. *Stem Cell Reports*, 18(6), 1255–1270. <https://doi.org/10.1016/j.stemcr.2023.05.009>

Kay, J. N., Finger-Baier, K. C., Roeser, T., Staub, W., & Baier, H. (2001). Retinal Ganglion Cell Genesis Requires *lakritz*, a Zebrafish atonal Homolog. *Neuron*, 30, 725–736. DOI: 10.1016/s0896-6273(01)00312-9

Kitambi, S. S., & Malicki, J. J. (2008). Spatiotemporal features of neurogenesis in the retina of medaka, *Oryzias latipes*. *Developmental Dynamics*, 237(12), 3870–3881. <https://doi.org/10.1002/dvdy.21797>

Koger, C. S., I, S. J., & Hinton, D. E. (1999). Variations of Light and Temperature Regimes and Resulting Effects on Reproductive Parameters in Medaka (*Oryzias latipes*) 1. *BIOLOGY OF REPRODUCTION*, 61, 1287–1293. DOI: 10.1095/biolreprod61.5.1287

Koike, C., Nishida, A., Ueno, S., Saito, H., Sanuki, R., Sato, S., Furukawa, A., Aizawa, S., Matsuo, I., Suzuki, N., Kondo, M., & Furukawa, T. (2007). Functional Roles of Otx2 Transcription Factor in Postnatal Mouse Retinal Development. *Molecular and Cellular Biology*, 27(23), 8318–8329. <https://doi.org/10.1128/mcb.01209-07>

Kwan, K. M., Otsuna, H., Kidokoro, H., Carney, K. R., Saijoh, Y., & Chien, C. bin. (2012). A complex choreography of cell movements shapes the vertebrate eye. *Development*, 139(2), 359–372. <https://doi.org/10.1242/dev.071407>

Lan, X., Jiang, H., Wang, Q., Shiqi, Q., & Xiong, Y. (2024). The application of retinal organoids in ophthalmic regenerative medicine: A mini-review. *Regenerative Therapy*, 26, 382–386. <https://doi.org/10.1016/j.reth.2024.06.013>

Li, Z., Joseph, N. M., & Easter, S. S. (2000). The morphogenesis of the zebrafish eye, including a fate map of the optic vesicle. *Developmental Dynamics*, 218(1), 175–188. DOI: 10.1002/(SICI)1097-0177(200005)218:1<175::AID-DVDY15>3.0.CO;2-K

Liu, H., Xu, S., Wang, Y., Mazerolle, C., Thurig, S., Coles, B. L. K., Ren, J. C., Taketo, M. M., van der Kooy, D., & Wallace, V. A. (2007). Ciliary margin transdifferentiation from neural retina is controlled by canonical Wnt signaling. *Developmental Biology*, 308(1), 54–67. <https://doi.org/10.1016/j.ydbio.2007.04.052>

Livesey, F. J., & Cepko, C. L. (2001). VERTEBRATE NEURAL CELL-FATE DETERMINATION: LESSONS FROM THE RETINA. *Nature Reviews*, 2, 109–118. DOI: 10.1038/35053522

Lust, K., & Wittbrodt, J. (2018). Activating the regenerative potential of Müller glia cells in a regeneration-deficient retina. *Elife*, e32319. <https://doi.org/https://doi.org/10.7554/eLife.32319>

Lyu, P., Iribarne, M., Serjanov, D., Zhai, Y., Hoang, T., Campbell, L. J., Boyd, P., Palazzo, I., Nagashima, M., Silva, N. J., Hitchcock, P. F., Qian, J., Hyde, D. R., & Blackshaw, S. (2023). Common and divergent gene regulatory networks control injury-induced and developmental neurogenesis in zebrafish retina. *Nature Communications*, 14(1). <https://doi.org/10.1038/s41467-023-44142-w>

Ma, W., Yan, R. T., Xie, W., & Wang, S. Z. (2004). A role of ath5 in inducing neuroD and the photoreceptor pathway. *Journal of Neuroscience*, 24(32), 7150–7158. <https://doi.org/10.1523/JNEUROSCI.2266-04.2004>

Malicki, J., Neuhauss, S. C. F., Schier, A. F., Sonica-Krezel, L., Stemple, D. L., Stainier, D. Y. R., Abdelilah, S., Zwartkruis, F., Rangini, Z., & Driever, W. (1996). Mutations affecting development of the zebrafish retina. *Development*, *123*, 263273. <https://doi.org/10.1242/dev.123.1.263>

Martínez-Ara, G., Taberner, N., Takayama, M., Sandaltzopoulou, E., Villava, C. E., Bosch-Padrós, M., Takata, N., Trepát, X., Eiraku, M., & Ebisuya, M. (2022). Optogenetic control of apical constriction induces synthetic morphogenesis in mammalian tissues. *Nature Communications*, *13*(1). <https://doi.org/10.1038/s41467-022-33115-0>

Martinez-Morales, J. R., del Bene, F., Nica, G., Hammerschmidt, M., Bovolenta, P., & Wittbrodt, J. (2005). Differentiation of the vertebrate retina is coordinated by an FGF signaling center. *Developmental Cell*, *8*(4), 565–574. <https://doi.org/10.1016/j.devcel.2005.01.022>

Martinez-Morales, J. R., Rembold, M., Greger, K., Simpson, J. C., Brown, K. E., Quiring, R., Pepperkok, R., Martin-Bermudo, M. D., Himmelbauer, H., & Wittbrodt, J. (2009). Ojoplano-mediated basal constriction is essential for optic cup morphogenesis. *Development*, *136*(13), 2165–2175. <https://doi.org/10.1242/dev.033563>

Masai, I., Yamaguchi, M., Tonou-Fujimori, N., Komori, A., & Okamoto, H. (2005). The hedgehog-PKA pathway regulates two distinct steps of the differentiation of retinal ganglion cells: The cell-cycle exit of retinoblasts and their neuronal maturation. *Development*, *132*(7), 1539–1553. <https://doi.org/10.1242/dev.01714>

Meister, M., & Berry, M. J. (1999). The Neural Code of the Retina Review A Sample Problem. *Neuron*, *22*, 435–450. [https://doi.org/10.1016/S0896-6273\(00\)80700-X](https://doi.org/10.1016/S0896-6273(00)80700-X)

Meyer-Franke, A., Wilkinson, G. A., Kruttgen, A., Hu, M., Munro, E., Hanson Jr, M. G., Reichardt, L. F., & Barres, B. A. (1998). Depolarization and cAMP Elevation Rapidly Recruit TrkB to the Plasma Membrane of CNS Neurons. *Neuron*, *21*(4), 681–693. DOI: 10.1016/s0896-6273(00)80586-3

Mikula Mrstakova, S., & Kozmik, Z. (2024). Genetic analysis of medaka fish illuminates conserved and divergent roles of Pax6 in vertebrate eye development. *Frontiers in Cell and Developmental Biology*, 12. <https://doi.org/10.3389/fcell.2024.1448773>

Miles, A., & Tropepe, V. (2021). Retinal stem cell 'retirement plans': Growth, regulation and species adaptations in the retinal ciliary marginal zone. *International Journal of Molecular Sciences*, 22(12). <https://doi.org/10.3390/ijms22126528>

Miller, C. G., Budoff, G., Prenner, J. L., & Schwarzbauer, J. E. (2017). Minireview: Fibronectin in retinal disease. *Experimental Biology and Medicine*, 242(1), 1–7. <https://doi.org/10.1177/1535370216675245>

Mills, E. A., & Goldman, D. (2017). The Regulation of Notch Signaling in Retinal Development and Regeneration. *Current Pathobiology Reports*, 5(4), 323–331. <https://doi.org/10.1007/s40139-017-0153-7>

Monserrate, J. P., & Baker Brachmann, C. (2007). Identification of the death zone: A spatially restricted region for programmed cell death that sculpts the fly eye. *Cell Death and Differentiation*, 14(2), 209–217. <https://doi.org/10.1038/sj.cdd.4401947>

Moreno-Mármol, T., Ledesma-Terrón, M., Tabanera, N., Jesús Martin-Bermejo, M., Cardozo, M. J., Cavodeassi, F., & Bovolenta, P. (2021). *Stretching of the retinal pigment epithelium contributes to zebrafish optic cup morphogenesis*. 10, 63396. <https://doi.org/10.7554/eLife>

Muncie, J. M., Ayad, N. M. E., Lakins, J. N., Xue, X., Fu, J., & Weaver, V. M. (2020). Mechanical Tension Promotes Formation of Gastrulation-like Nodes and Patterns Mesoderm Specification in Human Embryonic Stem Cells. *Developmental Cell*, 55(6), 679–694.e11. <https://doi.org/10.1016/j.devcel.2020.10.015>

Nakano, T., Ando, S., Takata, N., Kawada, M., Mugeruma, K., Sekiguchi, K., Saito, K., Yonemura, S., Eiraku, M., & Sasai, Y. (2012). Self-formation of optic cups and storable stratified neural retina from human ESCs. *Cell Stem Cell*, 10(6), 771–785. <https://doi.org/10.1016/j.stem.2012.05.009>

Nicolás-Pérez, M., Kuchling, F., Letelier, J., Polvillo, R., Wittbrodt, J., & Martínez-Morales, J. R. (2016). Analysis of cellular behavior and cytoskeletal dynamics reveal a constriction mechanism driving optic cup morphogenesis. *Elife*, 5(e15797). <https://doi.org/10.7554/eLife.15797.001>

Nishida, A., Furukawa, A., Koike, C., Tano, Y., Aizawa, S., Matsuo, I., & Furukawa, T. (2003). Otx2 homeobox gene controls retinal photoreceptor cell fate and pineal gland development. *Nature Neuroscience*, 6(12), 1255–1263. <https://doi.org/10.1038/nn1155>

O'Hara-Wright, M., & Gonzalez-Cordero, A. (2020). Retinal organoids: A window into human retinal development. *Development (Cambridge)*, 147(24). <https://doi.org/10.1242/dev.189746>

Okuda, S., Takata, N., Hasegawa, Y., Kawada, M., Inoue, Y., Adachi, T., Sasai, Y., & Eiraku, M. (2018). Strain-triggered mechanical feedback in self-organizing optic-cup morphogenesis. *Science Advances*, 4(11). <https://doi.org/DOI:10.1126/sciadv.aau1354>

Pan, F. C., Evans, T., & Chen, S. (2020). Modeling endodermal organ development and diseases using human pluripotent stem cell-derived organoids. *Journal of Molecular Cell Biology*, 12(8), 580–592. <https://doi.org/10.1093/jmcb/mjaa031>

Park, H. C., Kim, C. H., Bae, Y. K., Yeo, S. Y., Kim, S. H., Hong, S. K., Shin, J., Yoo, K. W., Hibi, M., Hirano, T., Miki, N., Chitnis, A. B., & Huh, T. L. (2000). Analysis of upstream elements in the HuC promoter leads to the establishment of transgenic Zebrafish with fluorescent neurons. *Developmental Biology*, 227(2), 279–293. <https://doi.org/10.1006/dbio.2000.9898>

Pérez-González, C., Ceada, G., Greco, F., Matejčić, M., Gómez-González, M., Castro, N., Menendez, A., Kale, S., Krndija, D., Clark, A. G., Gannavarapu, V. R., Álvarez-Varela, A., Roca-Cusachs, P., Batlle, E., Vignjevic, D. M., Arroyo, M., & Trepats, X. (2021). Mechanical compartmentalization of the intestinal organoid enables crypt folding and collective cell migration. *Nature Cell Biology*, 23(7), 745–757. <https://doi.org/10.1038/s41556-021-00699-6>

Picker, A., & Brand, M. (2005). Fgf signals from a novel signaling center determine axial patterning of the prospective neural retina. *Development*, 132(22), 4951–4962. <https://doi.org/10.1242/dev.02071>

Prieto-López, L., Pereiro, X., & Vecino, E. (2024). The mechanics of the retina: Müller glia role on retinal extracellular matrix and modelling. *Frontiers in Medicine*, *11*. <https://doi.org/10.3389/fmed.2024.1393057>

Provis, J. M., van Driel, D., Billson, F. A., & Russell, P. (1985). Development of the human retina: Patterns of cell distribution and redistribution in the ganglion cell layer. *Journal of Comparative Neurology*, *233*(4), 429–451. <https://doi.org/10.1002/cne.902330403>

Raymond, P. A., Barthel, L. K., Bernardos, R. L., & Perkowski, J. J. (2006). Molecular characterization of retinal stem cells and their niches in adult zebrafish. *BMC Developmental Biology*, *6*. <https://doi.org/10.1186/1471-213X-6-36>

Reinhard, J., Joachim, S. C., & Faissner, A. (2015). Extracellular matrix remodeling during retinal development. *Experimental Eye Research*, *133*, 132–140. <https://doi.org/10.1016/j.exer.2014.07.001>

Rockhill, R. L., Euler, T., Masland, R. H., & Baylor, D. (2000). Spatial order within but not between types of retinal neurons. *PNAS*, *97*(5), 2303–2307. DOI: 10.1073/pnas.030413497

Rowan, S., Chen, C. M. A., Young, T. L., Fisher, D. E., & Cepko, C. L. (2004). Transdifferentiation of the retina into pigmented cells in ocular retardation mice defines a new function of the homeodomain gene *Chx10*. *Development*, *131*(20), 5139–5152. <https://doi.org/10.1242/dev.01300>

Saturnino, A. P., Lust, K., & Wittbrodt, J. (2018). Notch signalling patterns retinal composition by regulating *atoh7* during post-embryonic growth. *Development (Cambridge)*, *145*(21). <https://doi.org/10.1242/dev.169698>

Schiller, P. H. (2010). Parallel information processing channels created in the retina. *Proceedings of the National Academy of Sciences of the United States of America*, *107*(40), 17087–17094. <https://doi.org/10.1073/pnas.1011782107>

Schmitt, E. A., & Dowling, J. E. (1994). Early-eye morphogenesis in the zebrafish, *Brachydanio rerio*. *Journal of Comparative Neurology*, 344(4), 532–542. <https://doi.org/10.1002/cne.903440404>

Schwab, I. R. (2018). The evolution of eyes: Major steps. The Keeler lecture 2017: Centenary of Keeler Ltd. *Eye (Basingstoke)*, 32(2), 302–313. <https://doi.org/10.1038/eye.2017.226>

Sidhaye, J., & Norden, C. (2017). Concerted action of neuroepithelial basal shrinkage and active epithelial migration ensures efficient optic cup morphogenesis. *Elife*, 6:e22689. <https://doi.org/DOI:10.7554/eLife.22689>

Simons, B. D., & Clevers, H. (2011). Strategies for homeostatic stem cell self-renewal in adult tissues. In *Cell* (Vol. 145, Issue 6, pp. 851–862). Elsevier B.V. <https://doi.org/10.1016/j.cell.2011.05.033>

Sinn, R., & Wittbrodt, J. (2013). An eye on eye development. *Mechanisms of Development*, 130(6–8), 347–358. <https://doi.org/10.1016/j.mod.2013.05.001>

Sokolova, N. (2019). *Neuroepithelial flow and BMP signaling shape the optic cup in medaka*.

Sokolova, N. (2023). *From progenitors to stem cells: emergence and characterization of adult retinal stem cells in medaka*.

Sokolova, N., Zilova, L., & Wittbrodt, J. (2023). Unravelling the link between embryogenesis and adult stem cell potential in the ciliary marginal zone: A comparative study between mammals and teleost fish. *Cells and Development*, 174. <https://doi.org/10.1016/j.cdev.2023.203848>

Song, Y., Overmass, M., Fan, J., Hodge, C., Sutton, G., Lovicu, F. J., & You, J. (2021). Application of Collagen I and IV in Bioengineering Transparent Ocular Tissues. *Frontiers in Surgery*, 8. <https://doi.org/10.3389/fsurg.2021.639500>

Stenkamp, D. L. (2007). Neurogenesis in the Fish Retina. In *International Review of Cytology* (Vol. 259, pp. 173–224). [https://doi.org/10.1016/S0074-7696\(06\)59005-9](https://doi.org/10.1016/S0074-7696(06)59005-9)

Stenkamp, D. L., & Cameron, D. A. (2002). Cellular pattern formation in the retina: retinal regeneration as a model system. *Molecular Vision*, 8, 280–293. PMID: 12181523

Strauss, O. (2005). The Retinal Pigment Epithelium in Visual Function. *Physiol. Rev.*, 85, 845–881. <https://doi.org/10.1152/physrev.00021.2004>.

Sutlive, J., Xiu, H., Chen, Y., Gou, K., Xiong, F., Guo, M., & Chen, Z. (2022). Generation, Transmission, and Regulation of Mechanical Forces in Embryonic Morphogenesis. *Small*, 18(6). <https://doi.org/10.1002/smll.202103466>

Tang, X. Y., Wu, S., Wang, D., Chu, C., Hong, Y., Tao, M., Hu, H., Xu, M., Guo, X., & Liu, Y. (2022). Human organoids in basic research and clinical applications. *Signal Transduction and Targeted Therapy*, 7(1). <https://doi.org/10.1038/s41392-022-01024-9>

Taylor, L., Arnér, K., Engelsberg, K., & Ghosh, F. (2015). Scaffolding the retina: The interstitial extracellular matrix during rat retinal development. *International Journal of Developmental Neuroscience*, 42, 46–58. <https://doi.org/10.1016/j.ijdevneu.2015.03.002>

Tohya, S., Mochizuki, A., & Iwasa, Y. (2003). Difference in the retinal cone mosaic pattern between zebrafish and medaka: Cell-rearrangement model. *Journal of Theoretical Biology*, 221(2), 289–300. <https://doi.org/10.1006/jtbi.2003.3192>

Turner, D. L., & Cepko, C. L. (1987). A common progenitor for neurons and glia persists in rat retina late in development. *Nature*, 328. <https://doi.org/10.1038/328131a0>

Tworig, J. M., & Feller, M. B. (2022). Müller Glia in Retinal Development: From Specification to Circuit Integration. *Frontiers in Neural Circuits*, 15. <https://doi.org/10.3389/fncir.2021.815923>

Varshney, S., Hunter, D. D., & Brunken, W. J. (2015). Extracellular Matrix components regulate cellular polarity and tissue structure in the developing and mature Retina. *Journal of Ophthalmic and Vision Research*, 10(3), 329–339. <https://doi.org/10.4103/2008-322X.170354>

Villeneuve, C., Hashmi, A., Ylivinkka, I., Lawson-Keister, E., Miroshnikova, Y. A., Pérez-González, C., Myllymäki, S. M., Bertillot, F., Yadav, B., Zhang, T., Matic Vignjevic, D., Mikkola, M. L., Manning, M. L., & Wickström, S. A. (2024). Mechanical forces across compartments coordinate cell shape and fate transitions to generate tissue architecture. *Nature Cell Biology*, 26(2), 207–218. <https://doi.org/10.1038/s41556-023-01332-4>

Vogel, M., & Möller, K. (1980). Cellular Decay in the Rat Retina During Normal Postnatal Development: A Preliminary Quantitative Analysis of the Basic Endogenous Rhythm *. *Albrecht v. Graefes Arch. Klin. Exp. Ophthalm.*, 212, 243–260. DOI: 10.1007/BF00410519

Völkner, M., Zschätzsch, M., Rostovskaya, M., Overall, R. W., Buskamp, V., Anastassiadis, K., & Karl, M. O. (2016). Retinal Organoids from Pluripotent Stem Cells Efficiently Recapitulate Retinogenesis. *Stem Cell Reports*, 6(4), 525–538. <https://doi.org/10.1016/j.stemcr.2016.03.001>

von Erlach, T. C., Bertazzo, S., Wozniak, M. A., Horejs, C. M., Maynard, S. A., Attwood, S., Robinson, B. K., Autefage, H., Kallepitis, C., del Río Hernández, A., Chen, C. S., Goldoni, S., & Stevens, M. M. (2018). Cell-geometry-dependent changes in plasma membrane order direct stem cell signalling and fate. *Nature Materials*, 17(3), 237–242. <https://doi.org/10.1038/s41563-017-0014-0>

Wahle, P., Brancati, G., Harmel, C., He, Z., Gut, G., del Castillo, J. S., Xavier da Silveira dos Santos, A., Yu, Q., Noser, P., Fleck, J. S., Gjeta, B., Pavlinić, D., Picelli, S., Hess, M., Schmidt, G. W., Lummen, T. T. A., Hou, Y., Galliker, P., Goldblum, D., ... Camp, J. G. (2023). Multimodal spatiotemporal phenotyping of human retinal organoid development. *Nature Biotechnology*, 41(12), 1765–1775. <https://doi.org/10.1038/s41587-023-01747-2>

Waid, D. K., & McLoon, S. C. (1998). Ganglion cells influence the fate of dividing retinal cells in culture. *Development*, 125(6), 1059–1066. <https://doi.org/10.1242/dev.125.6.1059>

Walther, R. F., Lancaster, C., Burden, J. J., & Pichaud, F. (2024). A dystroglycan-laminin-integrin axis coordinates cell shape remodeling in the developing *Drosophila* retina. *PLoS Biology*, 22(9 September). <https://doi.org/10.1371/journal.pbio.3002783>

Wan, J., & Stenkamp, D. L. (2000). Cone mosaic development in the goldfish retina is independent of rod neurogenesis and differentiation. *Journal of Comparative Neurology*, 423(2), 227–242. [https://doi.org/10.1002/1096-9861\(20000724\)423:2<227::AID-CNE4>3.0.CO;2-Z](https://doi.org/10.1002/1096-9861(20000724)423:2<227::AID-CNE4>3.0.CO;2-Z)

Wang, S., Li, W., Chen, M., Cao, Y., Lu, W., & Li, X. (2023). The retinal pigment epithelium: functions and roles in ocular diseases. *Fundamental Research*. <https://doi.org/10.1016/j.fmre.2023.08.011>

Wang, Y., Stonehouse-Smith, D., Cobourne, M. T., Green, J. B. A., & Seppala, M. (2022). Cellular mechanisms of reverse epithelial curvature in tissue morphogenesis. *Frontiers in Cell and Developmental Biology*, 10. <https://doi.org/10.3389/fcell.2022.1066399>

Warren, J., & Kumar, J. P. (2023). Patterning of the *Drosophila* retina by the morphogenetic furrow. *Frontiers in Cell and Developmental Biology*, 11. <https://doi.org/10.3389/fcell.2023.1151348>

Wetts, R., & Fraser, S. E. (1988). Multipotent Precursors Can Give Rise to All Major Types of the Frog Retina. *Science*, 239. DOI: 10.1126/science.2449732

Wohl, S. G., Jorstad, N. L., Levine, E. M., & Reh, T. A. (2017). Müller glial microRNAs are required for the maintenance of glial homeostasis and retinal architecture. *Nature Communications*, 8(1). <https://doi.org/10.1038/s41467-017-01624-y>

Xu, J., Zhao, C., & Kang, Y. (2024). The Formation and Renewal of Photoreceptor Outer Segments. *Cells*, 13(16). <https://doi.org/10.3390/cells13161357>

Yang, X., Klein, R., Tian, X., Cheng, H. T., Kopan, R., & Shen, J. (2004). Notch activation induces apoptosis in neural progenitor cells through a p53-dependent pathway. *Developmental Biology*, 269(1), 81–94. <https://doi.org/10.1016/j.ydbio.2004.01.014>

Yi, B., Xu, Q., & Liu, W. (2022). An overview of substrate stiffness guided cellular response and its applications in tissue regeneration. *Bioactive Materials*, *15*, 82–102. <https://doi.org/10.1016/j.bioactmat.2021.12.005>

Zhao, H., & Yan, F. (2024). Retinal Organoids: A Next-Generation Platform for High-Throughput Drug Discovery. *Stem Cell Reviews and Reports*, *20*(2), 495–508. <https://doi.org/10.1007/s12015-023-10661-8>

Zilova, L., Weinhardt, V., Tavhelidse, T., Schlagheck, C., Thumberger, T., & Wittbrodt, J. (2021). Fish primary embryonic pluripotent cells assemble into retinal tissue mirroring in vivo early eye development. *Elife*, *10*. <https://doi.org/10.7554/eLife.66998>

Publications during PhD

Afting C*, Walther, T*, Drozdowski OM, Schlagheck C, Schwarz US, Wittbrodt J, Göpfrich K (*equal contribution). *DNA microbeads for spatio-temporally controlled morphogen release within organoids*. Nat Nanotechnol (2024)

Kariss K, Sokolova N, Zilova L, Schlagheck C, Reinhardt R, Baumbach T, Farago F, van de Kamp T, Wittbrodt J & Weinhardt V. Visualisation of gene expression within the context of tissues using an X-ray computed tomography-based multimodal approach. Sci Rep 14, 8543 (2024).

Colombo F, Taale M, Taheri F, Villiou M, Debatin T, Dulatahu G, Kollenz P, Schmidt M, Schlagheck C, Wittbrodt J, Selhuber-Unkel C. Two-Photon Laser Printing to Mechanically Stimulate Multicellular Systems in 3D. Adv. Funct. Mater., 2303601 (2024).

Zilova L, Weinhardt V, Tavhelidse T, Schlagheck C, Thumberger T, Wittbrodt J. Fish primary embryonic pluripotent cells assemble into retinal tissue mirroring early eye development. eLife 10:e66998. (2021).

Manuscripts in peer review

Munding N, Schlagheck C, Wittbrodt J, Ho AD, Takashima Y, Tanaka M. One-Step Surface Functionalization of Hydrogel-Based, Stimulus Responsive 3D Microscaffolds for Human Stem Cells. manuscript in review (04/2025)

Afting C, Bhatti N, Schlagheck C, Sánchez Salvador E, Herrera-Astorga L, Agarwal R, Suzuki R, Hackert N, Lorenz HM, Zilova L, Wittbrodt J, Exner T. Deep learning predicts tissue outcomes in retinal organoids. bioRxiv 2025.02.19.639061; doi: <https://doi.org/10.1101/2025.02.19.639061>

Acknowledgements

A big thank you to Jochen, whose joy for a challenge and talent to (re-)spark motivation are truly inspiring. My PhD project(s) involved several phases of reorientation, which made the goal and hence the sense of purpose quite blurry at times. Your encouragement to think out of the box, along with your confidence placed in both the process and in me, motivated me to keep searching for my own niche. While I enjoy to explore broadly and employ the “lawn mower” approach – collecting all treasures to be found in the garden – your guidance helped me to eventually focus on one of the curiosities: the fascinating process of self-organization. Thank you, Jochen, for going through all ups and downs together and for your caring and enthusiastic support.

Thank you also to Steffen, who accompanied me throughout the journey – whether in TAC meetings, hallway talks or extended brain storming sessions. Your openness to explore any line of thought and to question different perspectives was very helpful. Thank you also to Prof. Dr. Ana Martín-Villalba and Prof. Dr. Gáspár Jékely for joining my defence committee and hereby going the last step in the PhD journey together.

How can one begin to express gratitude for the environment created by the members of the 5th and the -1st floors? You guys build a space that holds enthusiasm, pragmatism, creativity, dedication, comfort, comedy, a hands-on-attitude, open ears, helping hands, sports partners, board game lovers and big warm hugs. Thanks for all the shared thoughts, laughter, support, wisdom, meals and coffees. The support during the writing process provided in form of proofreading – Eva, Joergen, Lucie, Cassian, Venera and Jasmin-, technical upgrades – Gero -, ‘active’ distraction as sports and walks – Kaisa, Rashi, Bettina and Katha– or by a soothing talk in the hallway – all of you – made it more than bearable. Despite the setbacks and occasional frustrations, going to the lab was a real pleasure because of colleagues like you, who embrace any quirk and always share a smile.

Ein riesengroßes Danke auch an meine Freunde, die von nah und fern an diesem Weg beteiligt waren. Ihr habt immer dafür gesorgt, dass die „Realität“ nicht zu kurz kommt und ihr bereitet mir einfach ganz viel Freude. Michael, du machst jeden Tag besser. Du fängst mich auf und schenkst mir Fürsorge und Freiraum – Danke.

Ein ganz besonderer Dank gilt meiner Familie: ihr habt meinen Weg von klein auf geprägt. Auch wenn manche von euch heute nicht mehr dabei sein können, bin ich euch allen von Herzen dankbar - für eure Unterstützung und dafür, dass ihr mir immer ein Vorbild wart und seid.

Declaration

Herewith I declare that I prepared the PhD thesis “Organoid-based studies on the fundamental rules of retinal tissue self-organization and patterning“ on my own and with no other sources and aids than quoted.

Heidelberg, 2025

List of figures

Figure 1.1: Medaka retinal architecture.....	4
Figure 1.2: Morphogenetic steps in retinal development.	7
Figure 1.3: Medaka retinal organoid maintain spherical morphology throughout differentiation progress.	10
Figure 1.4: Current understanding of retinal patterning process in teleosts and <i>Drosophila melanogaster</i>	16
Figure 2.1: Retinal organoids display a reduced tissue complexity in comparison to the embryonic.	22
Figure 2.2: Fluorescent reporter line allows for live tissue recognition in embryo and organoid.....	23
Figure 2.3: Mould design and expected bending impact on tissue.....	25
Figure 2.4: Mould design and shape expectation preparation for morphological shape induction for organoids.....	27
Figure 2.5: Organoids mounted in rectangular moulds on day 1 show no CMZ induction by day 4.....	29
Figure 2.6: Organoids mounted in rectangular moulds on day 2 with complex tissue composition cannot be scored for shape-induction causality.	31
Figure 2.7: Tissue bending along two axes on day 1 and day 2 does not instruct CMZ formation.	33

Figure 2.8: Spontaneous CMZ formation shows epithelial and curved morphology for reporter-positive tissue stretches.....	35
Figure 2.9: Organoids with shortened Matrigel exposure show altered epithelial make-up and polarity.....	37
Figure 2.10: Retinal ganglion cells and long axonal projections in 7 days old retinal organoids.....	39
Figure 2.11: Otx2-positive cells are present in day 7 retinal organoids and form morphologically distinct clusters as the organoid matures.....	41
Figure 2.12: Differentiated neuroretinal cell types in late retinal organoid organize in clusters.....	43
Figure 2.13: Quantification of cellular ratios and cluster distribution in day 7 retinal organoid.....	46
Figure 2.14: Cells between retinal clusters are dying while retinal clusters are stable until at least day 11.....	48
Figure 2.15: Ultrastructure of retinal cell clusters show tight association of cells.....	50
Figure 2.16: Loss of tissue polarity from within organoid development precedes cluster patterning process.....	51
Figure 2.17: Cells contributing to Otx2-clusters from different clonal origin.....	53
Figure 2.18: Notch-signaling is involved in cluster formation.....	55

Figure 2.19: Supplementation of organoids with Laminin is sufficient to restore epithelial layering of neurons in retinal organoids.....	57
Figure 2.20: Retinal cells partially arrange in non-inverted epithelium when cultured without Matrigel from day 1 to day 2.....	59
Figure 6.1: Stamps with rectangular and round shapes for imprinting into agarose.....	101
Figure 6.2: Organoids transferred on day 1 show in 2 experiments complex tissue composition and are not considered for shape induction analysis.....	102
Figure 6.3: Organoids transferred on day 1 to rectangular shape show no Cndp1 expression in 2 independent experiments in live and immune stained.....	103
Figure 6.4: Organoids mounted in rectangular moulds on day 2 with complex tissue composition and CMZ tissue.....	104
Figure 6.5: Schemes and dimensions of nano-printed rectangular shapes.....	105
Figure 6.6: Organoids in C-shape and X-shape mounted on day 1 or day 2 imaged live.....	106
Figure 6.7: PKC-zeta serves as apical polarity marker staining proximal rim of OC tissue in day 2 embryo and organoids establish retinal identity independent of Matrigel exposure.....	106
Figure 6.8: Differentiation of retinal organoids containing RGCs is robust and reproducible.....	107
Figure 6.9: Complex neuronal projections in late retinal organoids.....	108
Figure 6.10: Scheme of distance measurement between clusters and assessment of the nearest neighbour distances.....	109

Figure 6.11: Ultrastructure of day 7 retinal organoid.....109

Figure 6.12: Two cells within cluster contain cilia projecting out of cells.....110

Figure 6.13: Antagonist treatments against Sonic hedgehog or BMP signaling do not show patterning effect by day 4.....111

List of tables

Table 5.1: <i>Oryzias latipes</i> lines used in this study.....	85
Table 5.2: Consumables employed in this study.....	85
Table 5.3: Chemicals, reagents and kits used in this study.	87
Table 5.4: Solutions and buffers used in this study.....	90
Table 5.5: Primary antibodies used in this study.....	91
Table 5.6: Secondary antibodies used in this study.....	92
Table 5.7: Equipment and instruments used in this study.....	92
Table 5.8: Software used in this study.....	94